Conceptual Design of Adaptive Structural Control Systems

by

Michael Cusack

B.S. Civil Engineering
Rensselaer Polytechnic Institute, 1998

Submitted to the Department of Civil and Environmental Engineering
in partial fulfillment of the requirements for the degree of
Master of Science in Civil and Environmental Engineering
at the
MASSACHUSETTS INSTITUTE OF TECHNOLOGY
September 1999

Author.....

Department of Civil and Environmental Engineering
August 6, 1999

Certified by.....

Jerome J. Connor
Professor
Thesis Supervisor

Accepted by.....

Daniele Veneziano
Chairman, Departmental Committee of Graduate Students

Conceptual Design of Adaptive Structural Control Systems

by

Michael Cusack

Submitted to the Department of Civil and Environmental Engineering
on August 6, 1999, in partial fulfillment of the
requirements for the degree of
Master of Science in Civil and Environmental Engineering

Abstract

Civil engineering structures have long been at the mercy of extreme events, such as earthquakes and high winds. But recently the process of structural control has allowed engineers to affect how structures behave during extreme events, improving the performance of the structures under these conditions. Passive structural control systems are effective at limiting the response to a narrow spectrum of excitations, but they can do little to control the response outside of this spectrum. Active structural control differs from passive structural control in that it relies on external energy to achieve a higher level of control. Active structural control systems allow a structure to analyze its current state, decide on the appropriate corrective actions, and implement these actions through control forces, which translates to improved performance over a wider range of excitations. Although practical applications of active structural control have been demonstrated in actual structures, their use has been limited because of the large energy requirements of the system.

This thesis explores the concept of adaptive structural control, a special type of active structural control. By controlling a system adaptively, one changes the stiffness and damping of the system, as well as the gain of the control algorithm, to affect the response. This varying of parameters, combined with the use of smaller actuator forces, can result in a better overall performance of the structure, while using much less energy.

Three different proposed systems of control force-generating actuators are presented. In addition, a simulation of non-adaptive active structural control and adaptive structural control on a single degree of freedom system is presented. The intent is not only to show the superior performance of the controlled system over the uncontrolled system, but also to demonstrate the appropriateness of adaptive structural control as an alternative to non-adaptive active structural control.

Thesis Supervisor: Jerome J. Connor
Title: Professor of Civil and Environmental Engineering

Acknowledgements

First, many thanks go to my advisor, Jerome Connor, who has taught me more in the last year than I could have thought possible. After having access to his vast knowledge, I am a little wiser going into the real world and have a newfound appreciation for the opportunities that lie ahead. His guidance and patience in helping me complete my thesis was immeasurable.

Secondly, I thank my sister Eileen, and my brothers Patrick, Timothy and Kevin. They are some of the best friends I have ever known and it has been very rewarding to watch them grow up. Because of them, life on Hickory Road has always been unpredictable and fun.

Finally, and most importantly, I thank my parents, who truly made all of this possible. They have been there for me my whole life, and they always believed in me, even the times when I didn't believe in myself. Thanks to them, and everything they have ever given me, I finally made it.

Contents

Actuator Technologies

Algorithms

List of Figures

List of Tables

1 Introduction

1.1 Definition of Active Structural Control

Active structural control is the process of altering the response of a structure by application of external forces. The intent in altering the response of the structure is to limit the structure's response to a prescribed level. Applications of active structural control exist in areas of high seismic activity, where large ground accelerations can literally shake buildings to pieces, and areas of high winds, where tall buildings are subjected to significant dynamic loads. By applying control forces, one can limit the effect that the excitations have on the structure. This has come of interest in recent years, as the concept of performance of structures has taken on new importance. Whereas in the past buildings were designed so that they would not collapse during an earthquake, oftentimes now it is required that they remain operational after an earthquake, with minimal damage to critical components. Such needs merit having structures that can *react* to the loads they undergo, so that they can survive and remain functional.

1.2 Components of Active Structural Control System

In general terms, an active structural control system consists of components that measure the state of the system, decide on a course of action to take, and implement that course of action. Sensors capable of recording displacement, velocity, or acceleration at a given time measure the state of the system. How many of these sensors are installed and where they are placed will affect the degree of measurement of the current state. A central computer acting as a cognitive unit for the control system typically carries out decision-making processes. By examining the current state of the system, it decides what forces to apply to minimize the response. Implementation of these control forces is done by force actuators, which are capable of producing large forces through mechanical, magnetic, hydraulic or other processes.

1.3 Active Control and Adaptive Control

An active structural control system is one that uses external energy to affect the response of the system. This is in contrast to passive structural control, which requires no external energy. Adaptive structural control is a form of active structural control, where the structural system changes its stiffness and damping to adjust its response. This self-adjusting of stiffness and damping leads to a control algorithm that varies with time; in other words, the gain of the control algorithm is no longer constant. With non-adaptive active control, there is no change in the gain of the control algorithm. In order for adaptive control to be considered an effective alternative to non-adaptive active control however, it must be shown that a similar magnitude of control can be achieved using either method.

1.4 Scope of Thesis

This thesis presents the conceptual design of three high-force actuator systems to implement active structural control in civil engineering structures. Additionally, it presents a detailed breakdown of the theory behind active and adaptive structural control, and summarizes a computer simulation of active and adaptive control on a single degree of freedom system. The objective of these simulations is to demonstrate the effectiveness of adaptive structural control as an alternative to active structural control.

Chapter 1 introduced the idea of structural control, and the basic definitions of active and adaptive structural control. Chapter 2 presents a conceptual system of high-force actuators that use large pliers-like elements to magnify actuator forces going into the system. Chapter 3 shows a similar type of system where actuator forces are generated by superconducting electromagnets. Chapter 4 details a high-force actuator system using large cables to control motion. Chapter 5 discusses the theory behind active structural control. Chapter 6 summarizes the active control and adaptive control simulations and presents the theoretical basis for the adaptive control algorithm. Finally, the conclusions are presented in Chapter 7.

2 Mechanical Leveraging System

2.1 Theory

As its name implies, this system operates on the principle of mechanical leverage. The concept is to use actuators to create small forces that can then be translated into larger actuating forces through plier or scissor action to generate the necessary effect on the structure. The unit is intended to be packaged so that it will fit inside a single column or a single wall and could be mass-produced in predetermined sizes and force ratios, unless it appears to be more economical to design the leveraging elements on an individual basis. The basic mechanical principle is as follows:

$$P_{in} \times r_{in} = P_{out} \times r_{out}, \tag{2.1}$$

where P_{in} is the force input to the system from the actuator, r_{in} is the lever arm from the input force to the pivot point of the system, and similarly P_{out} is the output force, and r_{out} is the lever arm associated with the output force. One can rearrange (2.1) to solve for the output force:

$$P_{out} = P_{in} \times \left(\frac{r_{in}}{r_{out}} \right). \tag{2.2}$$

Assuming one wants to keep the actuator (input) forces as small as possible, which will result in energy savings, the way to increase the output force is to increase the length of the lever arm of the input force relative to the lever arm of the output force. If this mechanism is installed vertically in a typical story of a typical building, one can expect to achieve a maximum ratio of r_{in}/r_{out} of about 10:1. Furthermore, if this output force can be coupled to another identical leveraging mechanism and used as input, called P_{int} (for intermediate force), then additional magnification of the original input force can be realized, along with greater energy savings. The final output force is now

$$P_{out} = P_{\text{int}} \times \left(\frac{r_{\text{int}2}}{r_{out}} \right) = P_{in} \times \left(\frac{r_{in}}{r_{\text{int}1}} \right) \times \left(\frac{r_{\text{int}2}}{r_{out}} \right), \tag{2.3}$$

where

$$P_{\text{int}} = P_{in} \times \left(\frac{r_{in}}{r_{\text{int}1}} \right). \tag{2.4}$$

Since for every iteration it is possible to achieve force magnifications on the order of 10:1, it may be possible to get total magnifications on the order of 100:1, a substantial increase in force. This would allow for the use of conventional force actuators and small linear motors to provide input forces, whereas previously these actuators would not have had the capacity to be effective in controlling civil engineering structures.

2.2 Components of Leveraging System

2.2.1 Column Assembly

The column itself will be designed somewhat like a space truss, and will be required to resist all gravity loads and lateral loads. (See Figure 2.1.) Incorporation of the leveraging system will require that as much as possible of the interior column space remain open, hence the space truss concept (Fig. 2.1a). The system components will essentially look like a large pair of pliers inside the column (Fig. 2.1b), with the long lever arms coupled with the input forces and the shorter arms coupled with the output forces. It will not be the function of the pliers to resist any "normal" loads on the column; their sole purpose will be for providing control forces.

Depending on how many of these pliers are coupled together, the input force actuators will either be located at the top or bottom of the column assembly. They will apply forces to the long arms in the transverse direction, which will cause the arms to open or close, depending on the direction of the input force. The subsequent moment action around the pivot point in the assembly and through the short arms on the opposite end of the assembly will provide a magnification of the force. Although originally applied in the transverse direction, the force can easily be converted to an axial force (Fig. 2.1c). As the longer lever arms close, the smaller lever arms will rotate and push against a rigid plate welded to the top of the space truss. This plate will transmit axial forces to the column.

In addition to damping out the structure's response to dynamic excitation, the column actuator assemblies will also have the capacity to resist short-term gravity loads applied to the structure

which are in excess of the structural capacity of the passive column elements. Depending on the use of the structure, this feature may or may not be advantageous. If for example, these column actuators were installed in a warehouse, then it would be possible to occasionally permit heavy equipment or other such large loads to occupy the floor area for short periods of time at non-regular intervals. This type of adaptive prestressing would enable the columns to resist compression by inducing tension. Ordinarily it would be prohibitively expensive to design a structure to resist extreme loads such as this, but by making use of actuator technology, it would be possible to do this on occasion. Such an operation, however, would require a failsafe system and necessitate severe precautions to insure the safety of all those in the area. If such operations were to take place, it would require a very high degree of robustness in the system, an issue to be discussed later.

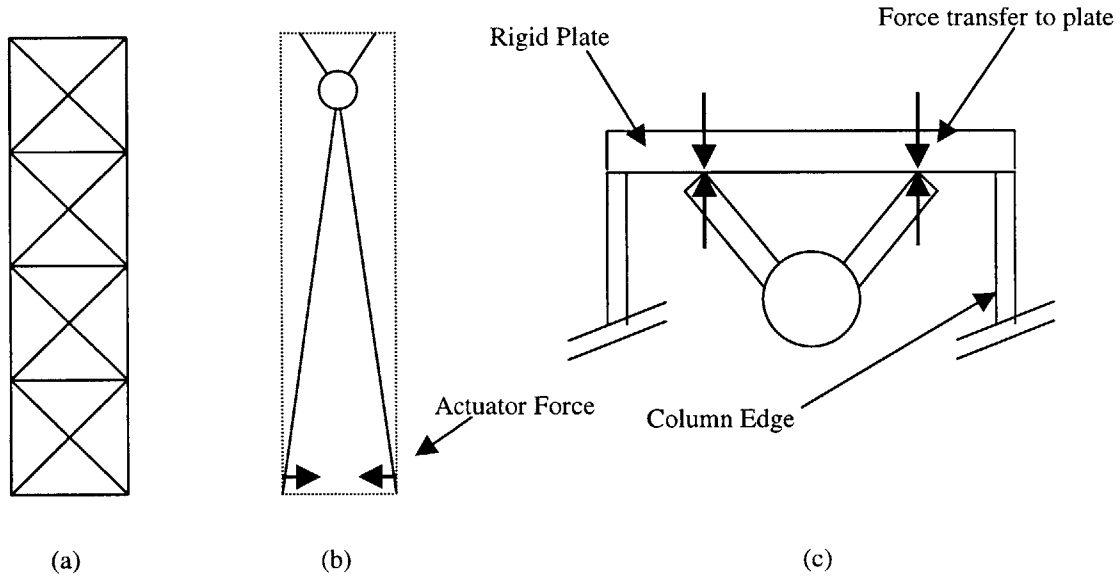

Figure 2.1 - Column Assembly Actuator – (a) Space truss-like structural frame, (b) lever components inside column, (c) close-up of top of column-plate interface

2.2.2 Wall Assembly

Another method of implementing control forces is through an assembly within an entire wall section between two column lines. The principles behind this setup and the column assembly are exactly the same, with the exception that force magnification within the wall system is done

mostly within the horizontal plane, instead of the vertical plane, and is done through more simple lever action, rather than scissor or plier action. By using the spacing between two adjacent column lines, it could be possible to achieve force magnifications greater than the 10:1 ratio predicted for the column assembly, depending on the size of the bay. Also, this system may allow for more instances of force coupling and force magnification, due to the availability of vertical space, out of the plane of the lever action.

Ideally, the output force will be tied into an exterior column, where it will be most efficient. The final stage lever can be welded, or preferably bolted, to the top of the column through a plate or brackets positioned near the top of the column. Bolted connections are preferred to welded connections because bolted connections would prevent any moments from being imparted to the column. There may be, however, transmission of lateral forces to the top of the column, if the lever motion is not completely vertical. This can be minimized by keeping the upper lever arm as horizontal as possible, as shown in the figure below.

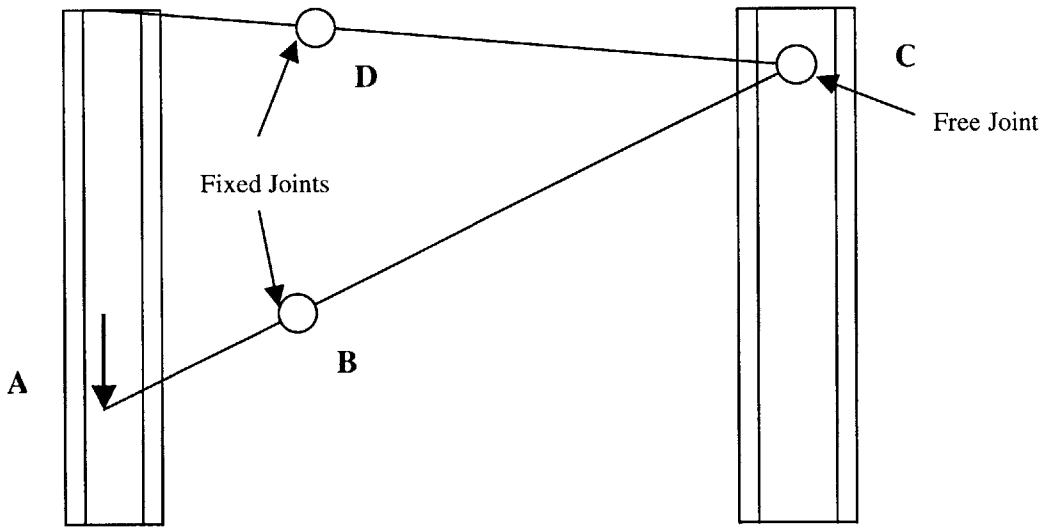

Figure 2.2 – Lever Assemblage Inside Wall Panel

The system works as follows. (Refer to Figure 2.2.) An input force is provided at point A, which causes the lower lever arm to rotate around point B, which is fixed in space. Point C is a freely moving hinge that transmits forces from the lower lever to the upper lever. The motion of

the lower lever arm causes point C to move upwards, rotating the upper lever arm around point D, which is fixed in space. This transmits a compressive load to the column.

Much like the column assembly, this mechanism could be used to provide resistance to extreme static gravity loads as discussed in the previous section. The issue of robustness again becomes central, as this procedure should not be carried out if the performance of the system cannot be guaranteed.

Another option, to control shear deformation with a wall assembly, is to position the elements in a typical story as shown below.

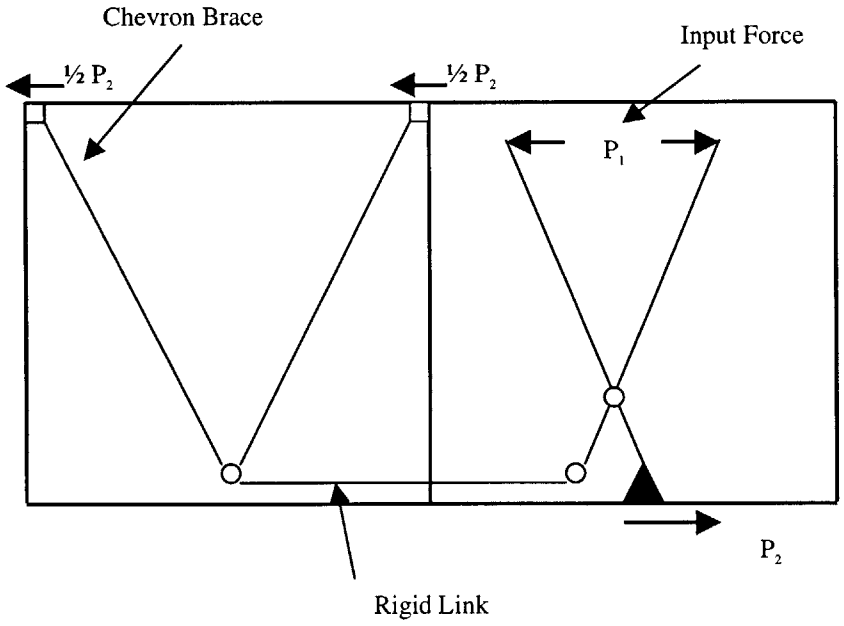

Figure 2.3 – Lever Assemblage Inside Wall Panel (Shear Control)

An input force P_1 is applied to the top lever arms of the pliers in the right bay. The reaction in the lower right lever arm, P_2, is transmitted to a pin connection at the base. The reaction in the lower left lever arm (also P_2) is transmitted to a rigid link that is attached to a Chevron brace in the left bay. The Chevron brace then transmits the lateral force in the rigid link to the top of the bay as a shear force.

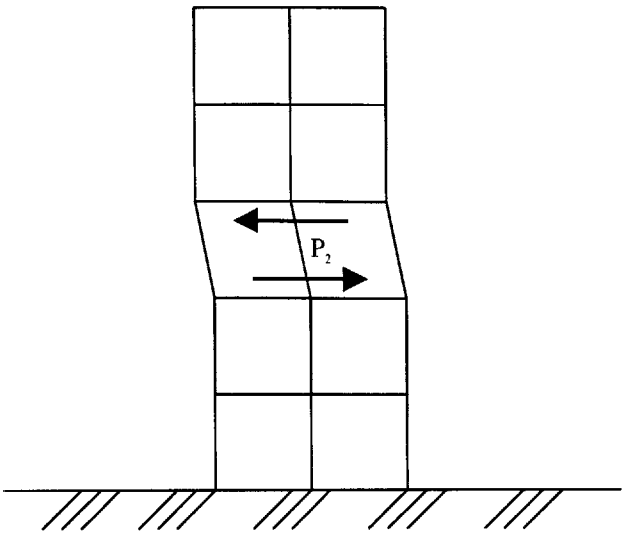

Figure 2.4 – Shear Lever Assemblage Acting on Building

2.2.3 Diagonal Assembly

In addition to the previous proposal, another option for controlling shear deformation is configuring the system so that forces are generated along the diagonals of a bay, as shown:

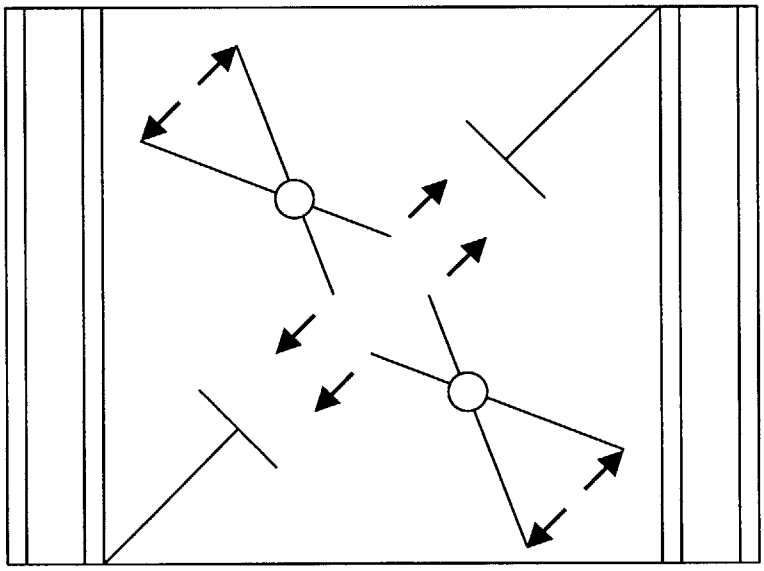

Figure 2.5 – Diagonal Actuating Assembly

Conceptually, this arrangement is no different than the previous, except for the orientation of the pliers. Instead of being tied to a Chevron brace, the pliers can push or pull against the T-shaped brace elements along the diagonals to generate shear forces. Because of symmetry, the same output force can be supplied by applying half the same input force in each pair of pliers, which will allow for use of smaller, cheaper actuators. An offset to this advantage however, is the somewhat limited space in the diagonals of the bay, which may force the lever arms to be smaller than desired. This will require an increase in the actuator forces, as well as stiffening of the lever arms.

2.2.4 Multi-Story Assembly

In order to increase lever arm ratios to maximize force magnification, it is prudent to explore the possibility of extending lever components through multiple stories. With this arrangement will come some loss of the dispersed control offered by many smaller elements, but a greater range of control forces will be gained, which will allow for control of the structure over a larger range of applied loads. In addition, because fewer elements will need to be manufactured for the structure, there exists the potential for cost savings. There are actually two separate ways in which output forces applied to the structure can be increased with a multi-story system. One is that the lever arm ratio can be made much higher, due to the increase in available space. The other is that because a larger system will be inherently stronger, it will be able to handle larger input forces, which lead to larger output forces. In order to work properly however, this system will need to make use of a Chevron brace similar to the one in Figure 2.3.

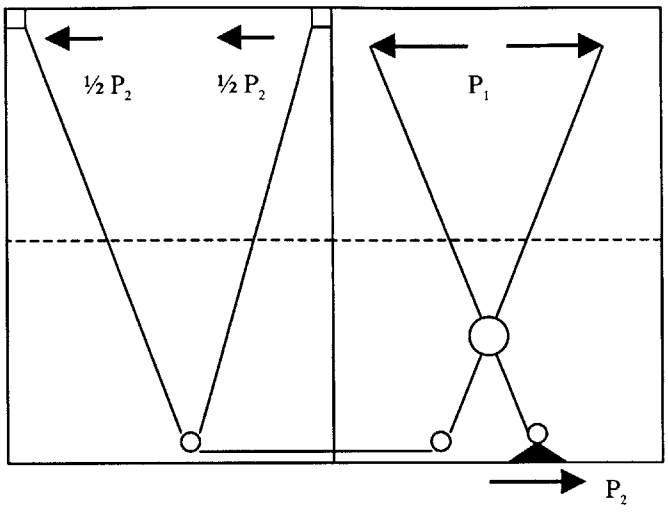

Figure 2.6 – Multi-Story Actuating Assembly

2.3 Maintenance Issues

Because this system will involve many moving parts, routine maintenance will be required to insure proper functioning of the unit. Of specific interest will be the proper lubrication of the pivot joints around which the levers will turn. Furthermore, the levers themselves will need to be monitored, since they will undergo several bending cycles during their lifetime. One possibility for monitoring is the attachment of strain gages to the lever arms to establish a response history of the lever arms. Because these units will be, for the most part, inaccessible once installed, it would make sense to have some kind of intelligent monitoring system as part of the leveraging unit itself. This way the system will "know" when it needs to be serviced, and the proper maintenance can be carried out.

2.4 Production of Actuator Units

Whether the leveraging units become a mass-produced item, with certain sizes available to designers, or else designed on a job to job basis will depend largely on the quantity of their use,

and the variation in loads they must supply. From a design standpoint, it may make more sense for structural engineers to have access to standard prefabricated units with available specifications, to help speed up the design process. Furthermore, designing the structural assembly which will house the actuating components will be a time-consuming task, and will make the units more expensive if it needs to be carried out for every job.

Of course, it would not be reasonable to exclude the possibility of large custom designed modules for "once in a lifetime" jobs that may develop. The limiting size of the actuating units will depend on the strength of the leveraging arms and how much force magnification can be provided, which will be a function of the available space within the structure. Convention suggests that as the loads increase the size of the structural elements housing the pliers and components of the force actuators will have to increase, but this may not necessarily mean more available space for actuator components.

2.5 Materials

2.5.1 High-Strength Steel

The leveraging systems presently being discussed will be required to create forces large enough to control axial deformations in steel and concrete. Therefore, to design the leveraging arms and joints out of conventional steel will not make a lot of sense, since those materials will undergo deformations along with the structural elements, which will limit the effectiveness of the leveraging system. Any material that is used will need to be very resistant to bending, so that the lever effect that takes place within the unit remains as efficient as possible. A sufficient choice of material would be a high-strength steel which possesses a rigidity greater than that of the structural steel in place, so that induced deformations take place in the structure, and not in the leveraging components themselves.

2.5.2 Composite Materials

An alternative to high-strength steel would be a composite material that offers the same high-strength properties, but also weighs significantly less, diminishing the effects of the leveraging

system on the overall weight of the structure. Typically this type of material costs much more than steel, but much of the increased unit cost can be gained back because of the substantially lower weight of the composite materials. Furthermore, once the loading conditions for the lever elements are known, the composite sections can be engineered more precisely, increasing their overall efficiency.

2.6 Section Geometry of Lever Arms

In addition to making the material as strong as possible, the efficiency of the unit will be increased as the inertia of the leveraging arms is increased to resist deflections due to bending. The leveraging arms could be conceived as resembling mini wide-flange shapes, which will provide stiffness in the primary bending direction and additional stiffness in the weak axis direction, enhancing the stability of the lever arms.

2.7 Robustness

In the case of extreme events, maintaining power to the actuating elements is critical to the operation of the control system. It is recommended that the power system used to control the actuating elements be given special consideration and possibly be entirely separate from the power supply for the remainder of the structure. But it should also be able to draw from a dedicated generator, which should be kept at the highest level of operation standards, in preparation for a major seismic event. Rigorous testing of the system components under harsh conditions is the only way to make any relevant claims as to the robustness of the system. Even then, there are certainly no guarantees of performance once the system is in place, which suggests that active control technology may not yet be mature enough to handle life-critical situations.

2.8 Optimizing Displacement and Force Output

As the amount of force magnification increases within a unit, the amount that the same unit can displace decreases proportionately. For example, if at the input end of a leveraging unit, the ends of the lever arms can be moved 10 cm and the force magnification is 10:1, then the amount that the lever arms will be able to move at the output end is 1 centimeter. As the lever arm ratio is increased, the amount the output lever arms move will become smaller and smaller. At some point, it will no longer be practical to magnify the output force by increasing the lever arm ratio. Conversely, if larger output displacements are desired, the amount that the lever arms move at the input end will need to become accordingly larger. Obviously, the size of the unit will restrict how large the displacements can be at the input end, but a compromise will need to be reached between the amount of output force that is generated and how much the lever ends can move. How this trade-off is settled will depend on the size of the forces required for control, the sizes of the available actuators and the expected movement of the structure.

2.9 Optimal Layout of Actuators

Where the actuators are placed in the building will be a function of the cost of the actuators, what level of force can be provided, and what constraints exist to limit installation. In theory, one would like to have actuators along every diagonal and along every column line, to provide complete localized control. In reality however, cost constraints will usually prevent one from achieving this type of dispersed control. Therefore, the best solution would be to place the actuators in the locations where they will have the largest effect.

For example, in the case of bending of a tall, slender structure due to wind loads, the largest axial forces will occur at the outside faces of the structure at the base. This would be the best place to install force actuators, since they can offset the largest amount of bending moment that way. Similarly, if one wanted to control shear deformation in a structure caused by seismic motion, the most useful place to install the actuators would be where the shear deformation is a maximum.

3 Electromagnetic Force System

Electromagnets are capable of generating large forces, large enough to be used for lifting and levitating heavy objects. The idea to use electromagnets to create forces in beams and moments in columns borrows from the technology behind many types of high-speed "maglev" (magnetic levitation) trains used throughout the world. During operation, these trains are levitated through magnetic attraction or repulsion between individually controlled electromagnets fitted to the vehicle and on the guideway. Through an electronic control system, a roughly constant separation distance between the guideway and the bottom of the train is maintained at all times.

3.1 Theory

Electromagnets employ currents to create magnetic fields. Consider a wire with some current moving through it and an identical wire with the same current moving through it placed parallel to the first wire at some distance away from it. The two wires will generate either an attractive or repulsive force, depending on which way the currents are moving. If the currents are moving in the same direction, they will attract; if they are moving in opposite directions, they will repel.
The same idea can be extended to a loop of wire. If now two identical loops of wire are placed one on top of the other, and identical currents are sent through each wire in opposite directions, then a repulsive force will be generated between the two loops. If the force between the two loops is equal to or greater than the weight of the top loop, then the repulsive force between the loops will levitate the top loop.
Obviously this is an unstable arrangement and the top loop will likely fall to the ground since it is not supported laterally. But this demonstrates the theory of magnetic levitation and shows how magnetic forces can be used in structural control schemes.
If multiple loops of wire (known as a solenoid) are used instead of a single loop of wire, much larger magnetic fields can be generated; this will increase the force. Assuming that lateral movements can be constrained, it will be quite easy for one solenoid to repel the other one in a single direction. If the current in either solenoid can be varied, then the magnetic field and force between the solenoids can be controlled as well, and the system is now active.

3.2 Magnetic Levitation (Maglev) System

3.2.1 Electromagnetic Suspension System

This type of system uses the forces of magnetic attraction between electromagnets on the bottom of the vehicle and iron or aluminum plates on the vehicle guideway. Each electromagnet on the vehicle is typically a solenoid with an iron core, which is then used to interact with the metal plates on the guideway. In this case the attractive force between the two elements must be controlled, by varying the current supplied to the electromagnet. Determination of the current is done through monitoring the separation gap between the elements, usually maintained between 10 and 15 mm [1].

3.2.2 Levitation Capacity of Electromagnetic Maglev Vehicles

The table below lists the capacities of the electromagnets used on several different types of magnetic levitation vehicles [1, 2]. In presenting this information it must be remembered that each system has a different definition of what a "magnet" is, i.e. how many solenoids are included in each unit. (For the remainder of this chapter, the terms "coil", "magnet", "electromagnet", and "solenoid" will be used interchangeably.) The capacities shown below are per coil, to provide a means of comparison among the various systems. The gaps indicate the effective gap between the vehicle and the guide rails.

MAGLEV System	Capacity (kN)	Gap (mm)
Birmingham	9.8	15
HSST	8.3	9
Transrapid	18.7	8
U. Tokyo / Fuji (Model A)	5.3	10
U. Tokyo / Fuji (Model B)	7.9	10

Table 3.1 – Capacities and Clearances for Electromagnetic Systems

Although these forces are not on the order to control large civil engineering structures, they do show that sizeable forces can be realized through magnetic technology. One can envision using these magnets to control "light" civil structures, such as transmission towers. Or, these magnets could be used in multiple numbers to generate larger forces, as is done with maglev vehicles. Furthermore, these magnets could be used as the driving actuators for the pliers-like actuators presented in the previous chapter. Nevertheless, one must not disregard magnetic technology because of the seemingly small forces it produces. Rather, one must recognize the potential in further developing this technology to generate larger forces, and the applications that currently exist.

3.2.3 Electrodynamic Suspension System

During this type of suspension, repulsive forces are created through induction occurring between on-board magnets (induction coils) and ground conductors during operation of the vehicle. Only the ground conductors have current supplied to them. The ground coils are placed along the sides of the track in a vertical "figure-8" shape so that the magnetic fields in each loop are of opposite polarity. Each induction coil is aligned on the side of the vehicle, vertically off-center from the ground coil, so that as it is moved past the ground coil, it experiences a net magnetic field which induces current in it. The induced magnetic field in the vehicle magnet is always such that the magnet is attracted to the top loop of the "figure-8" ground coil and repulsed by the bottom loop, creating a net levitation force [3].

The Canadian Maglev System uses a different type of electrodynamic induction system, which employs current-carrying electromagnets on the vehicle and a conducting sheet or surface laid out on the track. If an electromagnet moves over the conducting surface at some distance $d / 2$, the conducting sheet will make it appear as if a second electromagnet exists at some distance d from the electromagnet on the vehicle, and will generate a repulsive force. In some cases rows of ground coils are used in place of the conducting surface, but the principle is essentially the same. When the vehicle electromagnets are moved over the ground coils, current is induced in the ground coils and a repulsive force is generated [4].

3.2.4 Levitation Capacity of Electrodynamic Maglev Vehicles

Force capacities and effective gap lengths for four prototype electrodynamic maglev systems are shown in Table 3.2. Capacities are per coil [1, 4, 5, 6].

MAGLEV System	Capacity (kN)	Gap (mm)
MLU001	12.3	100
MLU002	13.9	110
MLU002N	15.5	Not available
Canadian Maglev	30	220

Table 3.2 – Capacities and Clearances for Electrodynamic Systems

As was the case with the electromagnetic systems, the electrodynamic coils do not appear to have force levels large enough to control civil engineering structures. However, they do show a noticeable increase over the values exhibited by the electromagnetic systems, thereby possessing even more potential. The greater problem becomes then how to install this type of magnetic system within a building or other similar structure, since the coils need to be moving to generate magnetic forces. Section 3.3.2 will attempt to deal with this problem.

3.3 Components of Electromagnetic System

3.3.1 Solenoids

As stated, the magnets themselves are actually solenoids, a series of wire loops designed to amplify the magnetic effects of current flowing through the wire. As the number of loops in the solenoid increases, the magnetomotive force, an indicator of the magnetic field strength of the solenoid, increases accordingly:

$$\text{magnetomotive force (m.m.f.)} = \text{(current)} \times \text{(number of turns)} \tag{3.1}$$

Typically, magnetomotive force is reported in amperes or ampere•turns. Solenoids used in prototype maglev operations have typically had magnetomotive forces of several hundred kilo amperes [5].

Even with such an arrangement, however, it is difficult to generate appreciably large forces because of the resistance of the conducting wire. An attempt to use a simple solenoid to create forces large enough to be used in civil structures or even in maglev operations would require enormously large input voltages, which would be expensive, unsafe, and possibly unrealizable. This problem has been avoided, however, through the use of superconducting materials, which are capable of conducting electricity while offering very low (near zero) resistance. This is achieved by operating the superconducting wires at temperatures near absolute zero. (Typical operating temperatures in maglev superconducting magnets are around 4.5-5 K [7].) Under these conditions, it is possible to achieve large magnetomotive force by using "conventional" voltages, which will lead to magnetic forces that are large enough to be effective.

It is anticipated that the actuating electromagnets will make use of superconducting technology. The best arrangement of the superconducting magnets will be to use them in pairs, so that they can either repel each other, or else attract each other. Each magnet will be tied to the surrounding structural elements, so that the forces generated between the two magnets can be transferred to the structure.

3.3.2 Rotating Disc

Another possibility of creating the individual actuators will involve using only one magnet combined with a rotating disc made of a conducting material. It was mentioned previously that electrodynamic maglev operations do not use two current-carrying electromagnets to achieve levitation, but use one current-carrying electromagnet in conjunction with a conducting sheet, which creates a levitation force when the elements move past each other at a sufficient velocity. The proposed arrangement would situate a single current-carrying electromagnet over a disc made of a conducting material. When the system is not in use, the electromagnet will rest some small distance above the disc, so not contact is made when the unit shuts down. But when the system goes into use, power will be supplied to the electromagnet and the disc will rotate

underneath it, which will create the same effect as the electromagnet moving over a conducting surface.

As the speed of the disc increases, the levitation force will also increase. Maglev trains usually run at operating speeds of around 300 to 500 km/hr, which for a 0.5-m diameter disc would translate into a rotational speed of 3200 to 5300 rpm. This could result in substantial power savings because current will only need to be supplied to one electromagnet in each unit. Of course, the idea of putting a motor within a structural element will not be easily perfected, but could be a very economically attractive choice.

3.3.3 Casing

The casing to house the magnetic components should be such that it allows the components of the system to be packaged as a single unit. Ideally, the units would arrive to the jobsite prepackaged and ready to install. The casing structure should add minimal weight to the unit, suggesting composites as a reasonable choice of material from which to build the casing. The weight of the unit must be kept as small as possible so that installation of a unit requires a minimum number of workers.

3.4 Superconducting Coils

3.4.1 Temperature Control

One of the main problems with using superconducting elements is the required operating temperature of superconductors is around 4.5 K, near the boiling point of helium. Because of this, superconductors require extensive cooling to remain operational, usually through piping in a fluid like liquid helium to keep the coils cold [7]. Doing this will consume large amounts of energy, and will also lessen the robustness of the system because a large power source will need to be maintained at all times to keep the system operational. Supplying a cooling system therefore is a costly, but necessary part of the system.

3.4.2 Quenching

Superconductors are also very prone to quenching (loss of superconducting properties due to excessive heating) because of their low heat capacity, which requires very little input heat to trigger a quench. The source for this heat is often mechanical disturbances within the coil matrix [7]. Because the coils will be subject to significant motion during an earthquake, the problem of quenching becomes very serious, since one cannot afford to have the coils quench as soon as an earthquake starts. The best method of limiting these disturbances is to restrain wire movement within the coil matrix.

3.5 Problems with Magnetic Fields

3.5.1 Interaction with Structural Steel

Steel is of course a conducting material, and could pose a problem to the use of magnetic actuators, because the steel has the potential to disrupt the magnetic flux between the elements of the electromagnetic unit. To alleviate this problem, the structural steel will need to be "separated" from the magnets, through some kind of shielding that prevents magnetic fields from flowing through the structural steel. Covering every piece of steel in the structure with shielding could be prohibitively expensive, so it may prove more prudent to isolate the magnetic components from the structural steel by shielding the exterior of the actuator. In either case, careful attention must be paid to the efficiency of the system and how it varies with the type of shielding provided. This situation could eventually lead to an optimization problem between the loss in efficiency and the increase in cost from shielding.

3.5.2 Interaction with Human Working Space

This problem is very similar to the one encountered in maglev systems, where the concern is over large magnets situated very close to passengers. It is also an extension of the shielding problem that needs to be addressed for the structural steel, and may be solved through the same means. Magnetic fields decrease in magnitude very significantly as they move away from their

source (proportional to $1/r^2$) and most likely will pose no threat to office workers who reside in close proximity to the magnetic units in a building. If it appears that undesirable magnetic fields could be produced in the working area then shielding will be required.

3.6 Element Configuration

3.6.1 Size of Components

Obviously, the smaller the physical size of the actuators, the more attractive they become, since they can be located in a larger variety of places within structural elements. Most of the maglev systems that have been built to date have used very large coils, usually 1.5-2 m long by 0.5-1 m in height, with a thickness of about 0.25 m [3, 5, 6]. However, these magnets are usually made up of more than one coil and could be broken down into smaller elements if necessary. When looking at the design variables of the electromagnets, it becomes apparent that the size of the loops in the superconducting solenoids should be made as small as possible, so that the magnet can fit within a beam or column. This will tend to decrease the available magnetic field because the length of wire in each loop will be smaller. However, this loss can be made up in a few ways. One is to simply increase the number of loops, which will increase the magnetomotive force of the coil. Another is to increase the power supplied to the electromagnet, although this solution should be considered a last resort since power usage should be kept to a minimum.

If the single magnet / rotating disc arrangement is considered, the problem provides a little more flexibility in terms of what parameters can be adjusted, but it also presents more constraints on size. In addition to the superconducting coils needing to be as small as possible, the rotating disc and motor will also need to be made sufficiently small to fit inside the structural components. One way of adapting to the problem is, as in the previous solution, to increase the number of loops in the superconducting coil. Another is to increase the speed of the rotating disc, although this has its drawbacks because it will require additional power input, plus beyond a certain speed of the disc there will be no additional levitating force generated.

3.6.2 Placement of Elements

Two different systems incorporating this technology are proposed. The first is to attach electromagnets to a column to create either compressive or tensile axial forces. The other is to use sets of magnets located along the top and bottom flanges of a beam to generate edge axial forces that will translate into bending moments in the beam.

The idea of installing electromagnets on a column is fairly straightforward. Considering the column to be a standard wide-flange shape, a total of two electromagnets will be placed on the column, in pairs near the middle of each "channel" created by the flanges and web. The exact location and size of these electromagnets will depend on the amount of power necessary to control the electromagnets and how that power requirement varies with the size of the electromagnets. In either case, the electromagnets should be placed symmetrically about the beam to insure that no eccentric loads are created when the electromagnets are activated, or even so that no eccentricities are developed under the dead weight of the electromagnets. In addition to the magnet arrangements proposed in previous sections, a single magnet arrangement, as shown in Figure 3.1, could also be used.

Each solenoid will have a metal rod inserted in its core. As a current passes through the solenoid, the metal bar will move. By restraining the motion of the solenoid and the bar, the magnetic force can be transmitted to the beam or column.

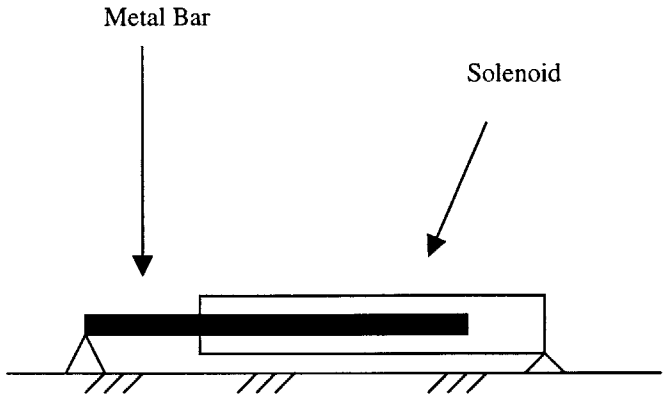

Figure 3.1 – Schematic Representation of Magnet

For the beam elements, the arrangement is very similar except, as mentioned, electromagnets are located along the inside of the top and bottom flanges of the beam, assuming that the beam is a wide-flange shape. The forces are applied in the same manner as in the column, with each pair of electromagnets generating either a compressive or tensile force. But unlike in the column arrangement, if the electromagnets on the top flange generate a compressive force, the electromagnets on the bottom flange will create a tensile force, so as to create an overall bending moment in the beam. On the opposite side of the beam, the electromagnets will be used to generate the same forces, so that no eccentricity is induced in the beam and the beam bends about its major axis. It should be noted that this arrangement could also be used to generate weak-axis moments, and could also be used to create twisting in the beam to combat torsional effects.

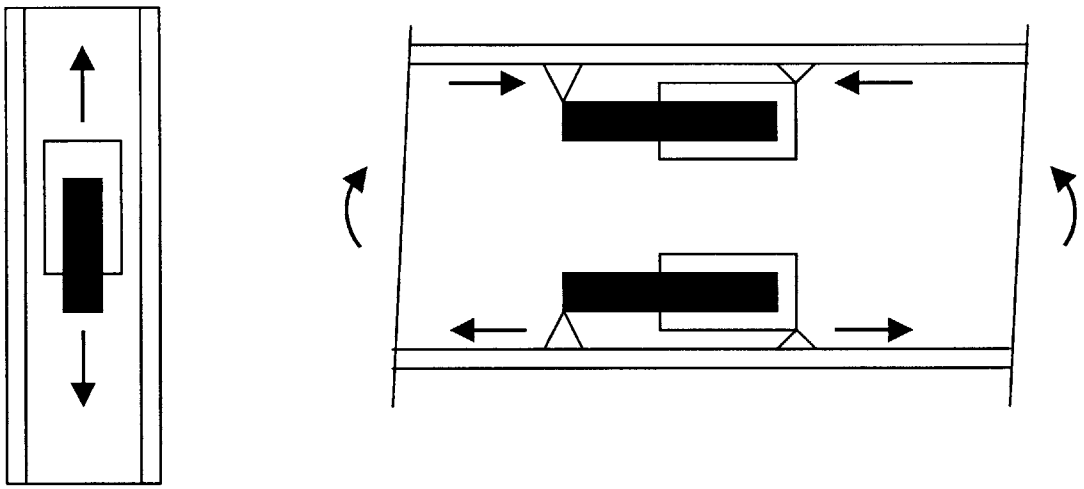

(a) (b)

Figure 3.2 – Electromagnets in (a) Column and (b) Beam

3.7 Power Requirements

Minimizing power input to the system will require that the system be kept as cold as possible to ensure superconducting conditions. As the temperature increases, resistance of the coils will build up, requiring additional power to maintain operation of the system. The larger the sole-

noids are, and the more loops they have, the better, since they will generate more magnetomotive force and larger fields for the same input voltage. Nonetheless, the system is going to require substantial forces to be of any use, so it will need larger currents in order to generate those forces. A more complete analysis of the power requirements would involve examining the requirements of superconductors under various conditions.

3.8 Maintenance

The electromagnetic force actuator system is considerably complex and could suffer breakdowns in several components. As with other actuator systems, one will need to consider the frequency with which components will need replacement and decide on what access should be made available to those components. In this respect, maglev systems can be studied to determine what kind of maintenance was required of them during their operational lifetime, since the electromagnets in this situation will undergo a similar course of operation and will be comprised of similar components.

3.9 Cost of Electromagnetic System

The largest barrier to entry of implementing an electromagnetic actuator system most likely will be the substantial cost associated with the cooling subsystem required for the superconducting coils. However, recent research in maglev technology has experimented with using permanent magnets in place of electromagnets, which would eliminate the need for cooling. Use of permanent magnets had been considered unfeasible in the past because permanent magnets could not produce forces large enough to offset their enormous weight. But by using a configuration known as the Halbach array, the magnets can be placed in such a way that concentrates the power of the magnets in one direction, increasing the force capacity [8]. Use of this technology in actuator systems would eliminate the need for superconductors and drive down the cost of the system.

3.10 Customized Units Versus Standardized Units

Initially, these units are going to be manufactured on an individual, customized basis, since there will be no previous uses of this technology from which to adapt. As the system develops, it may be beneficial to compromise between customizing and standardizing by having units standardized by size but with interchangeable components. For example, the solenoids that are used in the assembly can be interchangeable so that different magnetomotive forces can be selected based on the system requirements. Similarly, for the rotating disc arrangement, the disc diameter could be a standardized parameter, but the system could be supplied with different motors to supply the necessary speeds, depending on how much speed is needed and how precise the control has to be. In addition, as mentioned previously, different conducting materials could be available for the rotating disc to satisfy system requirements.

4 Pulley Actuating System

4.1 Theory of Tension Magnification

Pulleys have been long been used to aid in lifting heavy objects. One pulley by itself can be used to reverse the direction of motion of a cable so that lifting becomes a pulling-down motion, one that is usually easier to implement than pulling up, since it can use gravity to its advantage. If one considers the pulley and weight arrangement shown below in Figure 4.1, the tension in the cable is equal to the weight of the object, T = W.

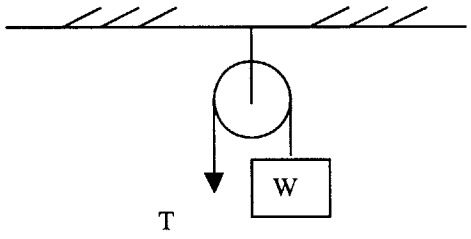

Figure 4.1 – Simple Pulley

But if a second pulley is added to the system, as shown below, the same weight can be lifted and held in equilibrium by a reduced amount of tension in the cable. In this case, T is now equal to W/ 2, so the required tension is cut in half.

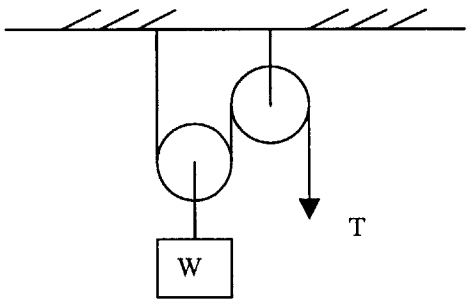

Figure 4.2 – 1-Degree Compound Pulley

In general, if pulleys are added to the system in this manner, the tension required to hold the weight in equilibrium will decrease as the number of pulleys increases, and will be calculated by the following equation:

$$T = \frac{W}{2^X}, \tag{4.1}$$

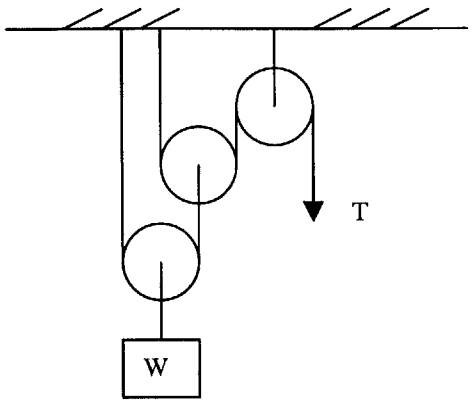

Figure 4.3 – Multi-Degree Compound Pulley

where, x is the total number of pulleys minus 1. So for example, if the system were set up in such a way to include 11 total pulleys, the required tension to maintain equilibrium would be

$$T = \frac{W}{2^{10}} = \frac{W}{1024}, \tag{4.2}$$

which means that it the weight to be sustained is 1 kN, the required tension in the cable to hold the weight in place will be about 1 N. This arrangement rapidly demonstrates its usefulness in civil engineering structures, where small input forces can be increased in such a way as to provide effective control of large structures through force actuation.

This system offers yet additional advantages in its method of force magnification, demonstrated by Figure 4.4 below.

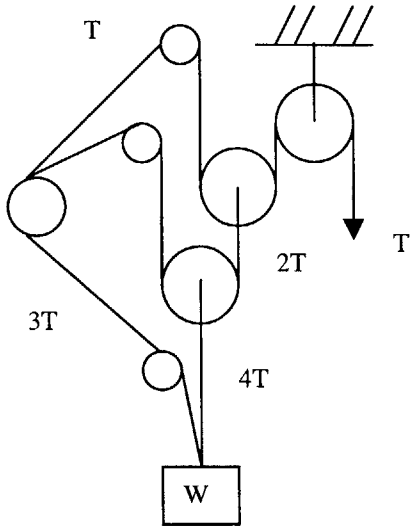

Figure 4.4 – Incorporation of Intermediate Reactions into Control Tension

Each of the intermediate pulleys generates a reaction force that needs to be restrained by some type of anchor. An alternative to anchoring the ends of these cables is to couple them with the output cable, providing additional force on the structure, without additional input.

A suitable application for this concept is to control the bending of tall slender structures. The most efficient use of the forces in the output cables is to use them on the perimeter of the structure, to control the bending of the structure through axial forces. In other words, the cables will be used to create bending moments to counteract the bending induced in the structure through dynamic loading.

Optimization of this system requires examining several factors. One is how many iterations of the input force through pulley action are necessary and at what point do the costs outweigh the benefits. Another is how the output force should be distributed: among several floors or several different columns on one floor, or all at the same column, with additional units for other columns. A third issue is how many of these systems should be incorporated into a structure, and where they should be placed.

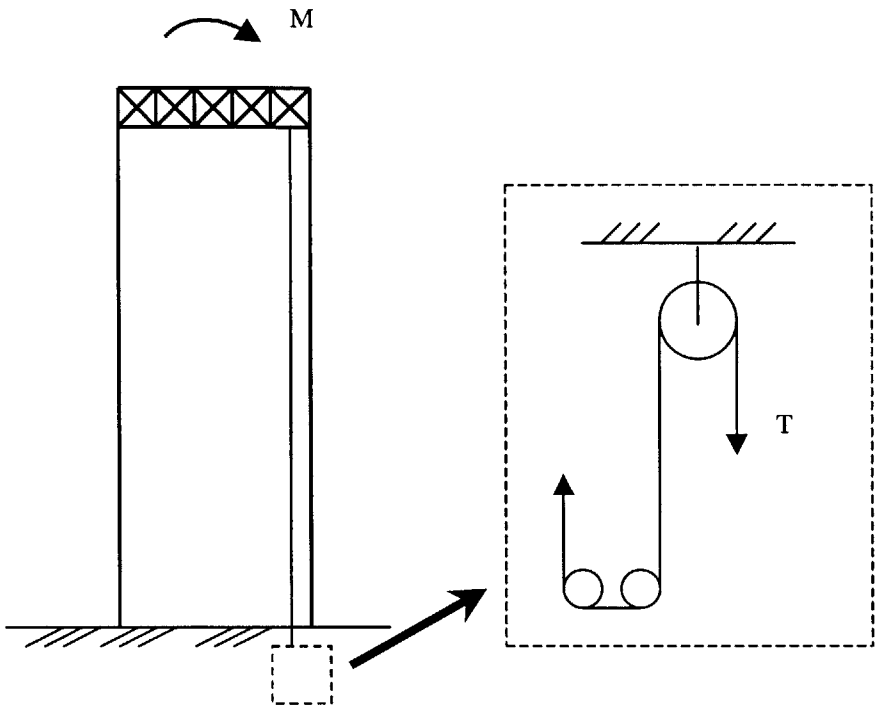

Figure 4.5 – Schematic of Pulley System in Tall Building

4.2 Cable Locations

The path that each cable follows should be as short as possible, which implies a path that goes more or less straight from the anchorage to the tie-in at the truss. Ideally a cable will run from the anchorage and, assuming that the columns are wide-flanged shapes, will then follow close to the webs of the columns up the side of the building, to limit eccentricity. For additional control of the cable path, small guide rings can be welded onto the webs of the perimeter columns so that the cable does not move around excessively when it is not in tension.

Where to house the pulley assemblies that are responsible for the force magnification is another situation altogether. The most obvious option is to put the pulleys in the basement of the structure, where more space is usually available. From there, the cables can continue up the side of the building, virtually unobstructed. An alternative to this is to place the cables in mechanical floors at different levels throughout the building.

4.3 Cable Materials

Ideally, one would want the cables to be much stiffer than the structural elements of the building, to make the system as efficient as possible. The obvious solution to this problem is to choose a material for the cables that has a modulus of elasticity much higher than that of the structural steel in the building. Finding a material that not only meets this stiffness requirement but is also economically reasonable could prove difficult, and it may be necessary to look at other ways on increasing the stiffness of the cables. One such way is to increase the cross sectional areas of the cables, another is to decrease the length of the cables, both of which will make up for the less than desired stiffness of the cable material.

4.4 Access and Maintenance

As opposed to the leveraging and electromagnetic systems, access to the cables should not be a major concern and should not require extensive planning and installation of otherwise unnecessary access entries. Because the pulleys will all be located on a mechanical floor or in the basement of the structure, they can be easily inspected visually and should not have to rely on an expensive monitoring system. Similarly, the motor that is used to provide tension to the system will be easily available for inspection, repair and maintenance, which could prolong its operational lifetime.

The cables will tie into a rigid truss spanning the width of the building. Since the cables will be undergoing several cycles of loading, the connections used to transfer the cable load to the truss will be prone to fatigue and will need to be checked from time to time and occasionally replaced. Replacement of the connections should be fairly easily accomplished- first tension in the cable will be released so that the cable can be easily manipulated. Then, the cable will be clamped near the top so that is does not drop down through the column shaft, and jacked up so that enough slack is available. From there the process of detaching the cable from the connections and attaching it to new connections is fairly simple.

Fatigue in the cables can be measured through the use of strain gages, which will monitor the strain in the cable at different locations for various reference temperatures. Once a cable has

undergone a sufficient number of cycles that it can no longer be considered reliable, it can be removed and a new one put in its place. It should be noted that the need to replace a cable is an extremely unlikely scenario, since bridge cables undergo similar loadings and last for several decades. It should be expected that the cables inside the building would last even longer than this, since they will not be prone to any adverse environmental conditions, and should remain in operation for the entire life of the structure. It is much more likely that a cable failure would be due to faulty material, the chances of which can be minimized through a solid quality control program. Also, as the cables begin to creep and elongate over time, the system can adjust by increasing the tension in the cables.

4.5 Optimization

The several intermediate cables that are used in the force magnification process have the potential to be incorporated into the output of the system through careful configuration. Considering the pulley system in Figure 4.4, it is noted that there is typically one cable to which the "input" tension is applied, and there is one cable with the "output" tension that is usually attached to the object the system is trying to restrain. The intermediate cables, which allow for magnification between the input tension and output tension, are usually anchored and are not really used in any way. However, if instead of anchoring these intermediate cables to a floor or mass, they were tied into the perimeter columns in the same manner as the output cable, additional force could be realized for control purposes.

Due to space limitations, and depending on the diameter of the cables, it may be difficult to attach all of the cables at the same point on the column, although this may not be the most efficient location of all cables. Rather, it may be advantageous to attach the cables at several different floor levels, in order to "spread out" the control forces. The control forces will not be independent of each other, however, although they will vary considerably in magnitude.

Consider a tall slender structure under a lateral load. It should be apparent that the largest perimeter axial loads created by the bending induced in the structure occur at the lower levels of the structure and decrease further up in the structure. In this case, it may be more efficient to apply the "output" cable close to the bottom of the structure and tie-in the intermediate cables so

that the cables with smaller tensions are attached at the higher floors and the cables with greater tensions are attached at the lower floors.

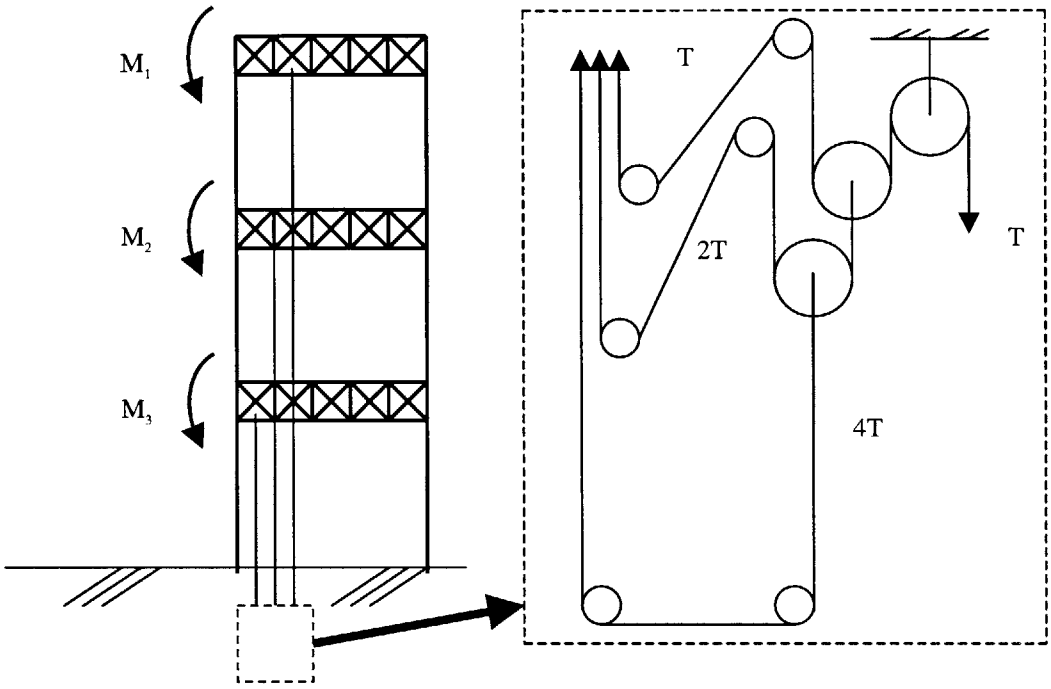

Figure 4.6 – Schematic of Compound Pulley System in Tall Building

5 Active Structural Control

5.1 Process of Active Structural Control

The objective of active structural control is to achieve a desired displacement of a structure through the application of control forces. The control algorithm is comprised of three basic steps: monitoring of the system, determination of the proper control force, and implementation of that force. Determination of the proper force depends on the nature of the loading on the structure, the present state of the structure, and the cost of applying the control force. This "cost" should be thought of in terms of the energy required to produce the force, with the understanding that the force that one needs to apply to achieve a certain displacement may not be possible because of the energy required to produce the force. Structural control then becomes a problem of optimization, determining what kind of motion can be realized at what cost.

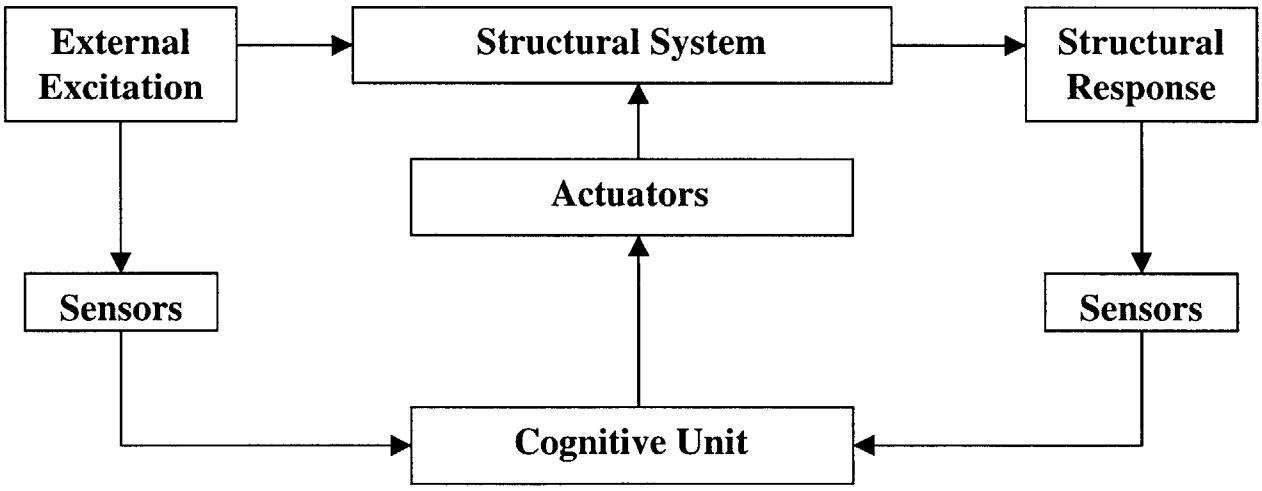

Figure 5.1 – Schematic Representation of Active Structural Control [10]

5.1.1 Monitoring of the Structure

Because the control force to be applied at time t+1 is directly proportional to the motion of the system at time t, it becomes extremely important that the motion of the structure is known as

accurately as possible. Motion sensors are typically used to measure velocity, displacement, or acceleration of the structure at a given time. The performance of the sensors is not only related to their accuracy, but also to their speed, since as the time to determine the state of the system increases, the system will deviate further from that state, rendering the measurements less precise.

5.1.2 Decision Making

The cognition component of the active control system is responsible for deciding what control force to apply and how to apply it. It must first identify the state of the system from the given sensory input, and then from that decide on the appropriate "course of action", in other words, what forces to apply and where. Once this has been done, the instructions can be relayed to the force actuators to apply the control forces.

5.1.3 Implementation

Control of civil engineering structures requires the generation of large forces (typically on the order of meganewtons), and finding practical ways to produce them is not a trivial process. The previous chapters discussed methods of achieving the necessary forces required to control a structure, but putting such a system into place is an expensive and risky process, and will remain that way until more conventional, robust, simpler systems can be implemented and proven to be effective.

5.2 Determination of Optimal Control Force

The focal point of the decision making process is determining what force needs to be applied to the structure in order to achieve its optimal state. One first looks at a simple one degree of freedom system, for which the governing equation of motion is

$$m\ddot{u} + c\dot{u} + ku = -ma_g + F_c, \tag{5.1}$$

where m is the mass of the structure, c is the damping coefficient, k is the stiffness, a_g is the ground acceleration, and F_c is the applied control force. This equation can be rearranged in state-space representation, which will provide a much more convenient format with which to work. In state-space formulation the equation of motion becomes [10]:

$$\dot{\boldsymbol{U}} = \boldsymbol{A}\boldsymbol{U} + \boldsymbol{B}F_c + \boldsymbol{D}F_g . \tag{5.2}$$

Each of the component matrices is defined as follows:

$$\boldsymbol{U} = \begin{bmatrix} u \\ \dot{u} \end{bmatrix}, \tag{5.3}$$

$$\boldsymbol{A} = \begin{bmatrix} 0 & 1 \\ \dfrac{-k}{m} & \dfrac{-c}{m} \end{bmatrix}, \tag{5.4}$$

$$\boldsymbol{B} = \begin{bmatrix} 0 \\ \dfrac{1}{m} \end{bmatrix}, \tag{5.5}$$

and

$$\boldsymbol{D} = \begin{bmatrix} 0 \\ \dfrac{1}{m} \end{bmatrix}. \tag{5.6}$$

F_c is the control force, as previously defined, and F_g is the force due to ground motion, equal to $-ma_g$. In order to manipulate a time history input, it is necessary to convert this relation to a discrete time-step equation. The result is [9]:

$$\boldsymbol{U}(i+1) = \overline{\boldsymbol{A}}\boldsymbol{U}(i) + \overline{\boldsymbol{B}}F_c(i) + \overline{\boldsymbol{D}}F_g(i). \tag{5.7}$$

In this case, the state of the system is known at time i, and can be found at time i+1, based on the applied ground motion and control force. The coefficient matrices are defined as [9]:

$$\overline{\boldsymbol{A}} = e^{\boldsymbol{A}\Delta t}, \tag{5.8}$$

$$\overline{\boldsymbol{B}} = \left[\int_0^{\Delta t} e^{\boldsymbol{A}t}\, dt \right] \boldsymbol{B}, \tag{5.9}$$

and

$$\overline{\boldsymbol{D}} = \left[\int_0^{\Delta t} e^{\boldsymbol{A}t}\, dt \right] \boldsymbol{D}, \tag{5.10}$$

where Δt is the time interval between iterations. It is prudent to make Δt as small as realistically possible, since as Δt is reduced the system will approach the continuous case. In other words, the state of the system will be known virtually all the time. Conversely, as Δt gets larger, the equations will begin to deteriorate, since the state of the system will be more uncertain between successive iterations of the control equation.

Determination of the value of the optimal control force is a complicated process, and only the basics of this determination will be presented here. In order to give some measure of the energy requirements needed to apply the optimal control force, a cost function, J, is defined for a single degree of freedom system as [9]:

$$J = \sum_{k=1}^{\infty} \left[\boldsymbol{U}(i)^T \boldsymbol{Q} \boldsymbol{U}(i) + F_c(i)^T \boldsymbol{R} F_c(i) \right]. \tag{5.11}$$

This will provide some bound of the value of the control force that can actually be applied to the system. For the single degree of freedom case **R** = r. It will later be shown that the amount of control force that can be applied to a system decreases as r increases. To maintain the efficiency of the system, the objective is to minimize the cost function J. This leads to the following result for the optimal control force [9]:

$$F_c(i) = -\left(\boldsymbol{R} + \overline{\boldsymbol{B}}^T \boldsymbol{X} \overline{\boldsymbol{B}}\right)^{-1} \overline{\boldsymbol{B}}^T \boldsymbol{X} \overline{\boldsymbol{A}}\, \boldsymbol{U}(i) = \boldsymbol{G}\boldsymbol{U}(i), \tag{5.12}$$

where **X** is the solution to the discrete-time Ricatti Equation

$$\boldsymbol{X} = \boldsymbol{Q} + \overline{\boldsymbol{A}}^T \boldsymbol{X} \overline{\boldsymbol{A}} - \overline{\boldsymbol{A}}^T \boldsymbol{X} \overline{\boldsymbol{B}} \left(\boldsymbol{R} + \overline{\boldsymbol{B}}^T \boldsymbol{X} \overline{\boldsymbol{B}}\right)^{-1} \overline{\boldsymbol{B}}^T \boldsymbol{X} \overline{\boldsymbol{A}}. \tag{5.13}$$

This leads to an expression for $F_c(i)$ of the following form:

$$F_c(i) = \begin{bmatrix} G_{11} & G_{12} \end{bmatrix} \boldsymbol{U}(i), \tag{5.14}$$

where G_{11} and G_{12} are the components of the negative gain matrix **G**. One notes that in the cost equation J, if the cost parameter **Q** is set to

$$\boldsymbol{Q} = \begin{bmatrix} 0 & 0 \\ 0 & 1 \end{bmatrix}, \tag{5.15}$$

the solution for $F_c(i)$ approaches pure velocity feedback [9, 10]. For the continuous case, the solution is that of pure velocity feedback, in other words $G_{11} = 0$. For the discrete case this is nearly true; G_{12} is typically much greater than G_{11}, so $F_c(i)$ is approximated as

$$F_c(i) \cong \begin{bmatrix} 0 & G_{12} \end{bmatrix} \boldsymbol{U}(i) . \tag{5.16}$$

An active control algorithm with no time delay effects and pure velocity feedback will be unconditionally stable for a single degree of freedom system [10].

5.3 Stability of Active Control Algorithm

With the application of a control force to a structural system, there is always the inherent danger of applying a control force incorrectly in such a way as to make the system unstable. This problem can arise from unsuitable monitoring of the system, which will lead to an incorrect representation of the current state of the system. Or it could be caused by inappropriate time lag in the system, whether it is between the monitoring system and cognition unit, or between the cognition unit and the force actuators. In any case great effort must be taken to assure that any attempt to control the structure will not drive it towards a further undesirable state.

5.3.1 Stability of the Physical System

If one first considers a single degree of freedom system with no control force and no external excitation, the state-space equation reduces to

$$\dot{\boldsymbol{U}} = \boldsymbol{A}\boldsymbol{U} , \tag{5.17}$$

where **A** has been previously defined as

$$\boldsymbol{A} = \begin{bmatrix} 0 & 1 \\ \dfrac{-k}{m} & \dfrac{-c}{m} \end{bmatrix} . \tag{5.18}$$

It can be shown that for this case the system is stable if the real component of the eigenvalues of **A**, defined as λ^r, is less than zero [10]. Noting that

$$\lambda^r = -\frac{c}{2m} = -\xi\omega , \tag{5.19}$$

and that both damping and mass obviously have to be positive quantities, one can conclude that the uncontrolled system is always stable.

5.3.2 Stability of the Physical System with Continuous Active Control

It is now considered how the stability of the system changes when a control force F_c is applied to the system. The state-space equation is examined for the continuous case, this time with the addition of the control term:

$$\dot{\boldsymbol{U}} = \boldsymbol{AU} + \boldsymbol{BF}_c . \tag{5.20}$$

In general, the control force is of the form

$$F_c = -\boldsymbol{K}_f \boldsymbol{U} , \tag{5.21}$$

where

$$\boldsymbol{K}_f = \begin{bmatrix} k_d & k_v \end{bmatrix}. \tag{5.22}$$

Substituting this expression into the state-space equation, one obtains

$$\dot{\boldsymbol{U}} = \boldsymbol{AU} - \boldsymbol{BK}_f \boldsymbol{U} = \left[\boldsymbol{A} - \boldsymbol{BK}_f\right]\boldsymbol{U} . \tag{5.23}$$

The components of the eigenvalues of $[\mathbf{A} - \mathbf{BK_f}]$ are then

$$\lambda^r = -\frac{c + k_v}{2m} \tag{5.24}$$

and

$$\lambda^i = \sqrt{\left[\frac{k + k_d}{m}\right] - \left[\frac{c + k_v}{2m}\right]^2} . \tag{5.25}$$

Because stability requires $\lambda^r < 0$ [10], it is seen that the stability of the control algorithm is only affected by k_v. Furthermore, it can be concluded that the system will remain unconditionally stable for $k_v > 0$, which corresponds to negative velocity feedback since $F_c = -\mathbf{K_f}\,\mathbf{U}$. Because displacement feedback cannot offer any control over the stability of the system, the control force algorithm is defined to have pure negative velocity feedback, by setting

$$\boldsymbol{Q} = \begin{bmatrix} 0 & 0 \\ 0 & 1 \end{bmatrix}. \tag{5.26}$$

This leads to the final expression for the control force

$$F_c = -\begin{bmatrix} 0 & k_v \end{bmatrix} U \,, \tag{5.27}$$

where k_v equals G_{12}.

5.3.3 Stability of the Physical System with Discrete Active Control

The discrete time step state-space equation with applied control force is revisited, for the case of no external excitation:

$$\boldsymbol{U}(i+1) = \overline{\boldsymbol{A}}\,\boldsymbol{U}(i) + \overline{\boldsymbol{B}}\,\boldsymbol{F}_c(i). \tag{5.28}$$

Substituting the expression for F_c, specialized for discrete time, one gets

$$\boldsymbol{U}(i+1) = \overline{\boldsymbol{A}}\,\boldsymbol{U}(i) - \overline{\boldsymbol{B}}\,\boldsymbol{K}_f\boldsymbol{U}(i) = \left[\overline{\boldsymbol{A}} - \overline{\boldsymbol{B}}\,\boldsymbol{K}_f\right]\boldsymbol{U}(i). \tag{5.29}$$

Stability requires the modulus of the largest eigenvalue of $\left[\overline{\boldsymbol{A}} - \overline{\boldsymbol{B}}\,\boldsymbol{K}_f\right]$ to be less than 1 [10]. In general however, since the discrete case is an extension of the continuous case, and degrades to the continuous case for very small values of Δt, it should be expected that the discrete case would be stable for pure velocity feedback.

5.3.4 Time Delay Effects on Discrete Active Control Algorithm

Up until this point, it has been assumed that the correct control force determined for the state at time i can be applied at time i. However, one must consider what happens to the system as the time it takes between the ordering of the control force and the implementation of the control force increases. As this time delay grows the state of the system is going to move further and further away from the state it was in when the control force was calculated. Subsequently, the potential for instability increases as the time lag increases.

The discrete time step state-space equation is rewritten to include the effects of time delay:

$$\boldsymbol{U}(i+1) = \overline{\boldsymbol{A}}\,\boldsymbol{U}(i) - \overline{\boldsymbol{B}}\,\boldsymbol{K}_f\boldsymbol{U}(i-v), \tag{5.30}$$

where v is the number of time steps between the determination of the control force and its implementation into the system. Given a general solution of the form $\boldsymbol{U} = \rho^i \boldsymbol{V}$, the eigenvalue problem now becomes

$$\left[\overline{\boldsymbol{A}} - \rho\boldsymbol{I} - \rho^{-v}\boldsymbol{K}_f\right]\boldsymbol{V} = \boldsymbol{0}. \tag{5.31}$$

Stability of the algorithm requires $|\rho| < 1$. [10] presents a solution which determines the value of v for which $\rho = 1$. An outline of the procedure (for a single degree of freedom system) is as follows. The state vector **U**(t) is rewritten as

$$\boldsymbol{U}(t) = \boldsymbol{V}q(t), \tag{5.32}$$

where **V** is the eigenvector of $\overline{\mathbf{A}}$. Substituting this expression into the time delay state-space equation, one obtains

$$q(i+1) = \lambda q(i) - gq(i-v) \tag{5.33}$$

where

$$g = \boldsymbol{W}^T \overline{\boldsymbol{B}} \boldsymbol{K}_f \boldsymbol{V}. \tag{5.34}$$

W is the eigenvector of $\overline{\mathbf{A}}^{\mathrm{T}}$ and both $\overline{\mathbf{B}}$ and $\mathbf{K}_{\mathbf{f}}$ are as defined previously. The general solution of (5.33) is considered to be of the form

$$q(i) = \rho^i \tag{5.35}$$

which leads to the following expression for ρ:

$$\rho = \lambda - g\rho^{-v}. \tag{5.36}$$

To find the value of v for which $|\rho| = 1$, ρ is set equal to $e^{i\theta}$, which leads to

$$e^{i\theta} = \lambda - ge^{-iv\theta}. \tag{5.37}$$

By separating out the real and imaginary components of the above equation and squaring and adding them, one can solve for v. The coefficient K is defined as

$$K \equiv \frac{1}{2g}\left(\left[\lambda^r\right]^2 + \left[\lambda^i\right]^2 + g^2 - 1 \right). \tag{5.38}$$

Subsequently, an expression for $v\theta$ can be found from

$$v\theta = 2\arctan\left[\frac{-\lambda^i \pm \sqrt{\left[\lambda^i\right]^2 - \left(K^2 - \left[\lambda^r\right]^2\right)}}{K + \lambda^r} \right]. \tag{5.39}$$

Similarly, an expression for θ can be written as

$$\theta = \arccos\left(\lambda^r - g\cos(v\theta)\right) \tag{5.40}$$

or

$$\theta = \arcsin\left(\lambda^i + g\sin(v\theta)\right). \tag{5.41}$$

One then determines v by dividing $v\theta$ by θ.

Appendix F contains plots showing how the maximum allowable time delay varies as mass, stiffness, and damping vary. The default values for the exercise were m = 50,000 kg, k = 2,000,000 N/m, and c = 12,500 kg/sec. Only one parameter was varied at a time to show how v responds to each individually. As mass or damping of the system is increased, the maximum allowable time delay increases, as expected, since an increase in mass or damping should slow the response of the system, so that the change in state between some times i and i+1 should not be as drastic. Conversely, as stiffness increases, the allowable time delay decreases sharply, since obviously a stiffer system will have a higher frequency and is going to move more rapidly.

5.4 Examples of Active Control Systems

One practical example of structural control that has been successful is the tuned mass damper (TMD), which is essentially a large mass that sits at the top of a structure to dampen its motion. TMD technology has been mainly used in tall buildings to control the buildings' response to wind excitation, by moving out of phase with the motion of the structure. This technology is limited however in that it is a completely passive solution; the TMD is typically designed to respond to the first mode of response, and while it is quite effective in controlling that motion, it can do little to limit the response of the higher modes. There have been other developments, however, which provide solutions to this problem through active control.

5.4.1 Active Mass Driver

The active mass driver (AMD) is similar to the tuned mass damper in that it is a mass that sits on top of the structure to control motion but it is a fully active system and can be used to generate control forces. The AMD control system is comprised of the following components: (1) sensors on the structure to measure the motion of the building and the mass, (2) a central computer to calculate the necessary control force, (3) actuators situated at the top of the structure to provide the control force, (4) a large auxiliary mass to provide counter force to the actuators through inertia, and (5) supports to bear the mass smoothly and provide restoring force when

necessary [11]. By "pushing off" of the auxiliary mass, the actuators can implement a control force to restore the structure to its original position. Typically the actuators are in the form of large hydraulic pistons that can vary the magnitude of the control force through varying hydraulic pressure.

Active mass driver technology has been implemented in a number of buildings in Japan. The AMD system was installed in the Kyobashi Seiwa Building in 1989. This building is an 11-story structure and has two auxiliary masses at the top level of 4 tf and 1 tf to control vibrations in the transverse and torsional directions, respectively [12].

Because of the large weight of the auxiliary mass, often times it is economical to use existing parts of the structure as the auxiliary mass, rather than add more weight to the structure for that specific purpose. The Sendagaya Intes Building in Tokyo (11 stories) uses its ice storage tanks and air conditioning units as the auxiliary masses for its AMD system [11].

One of the taller structures to use AMD technology is the Hankya Applause Tower in Osaka. This building is 34 stories tall and was completed in 1992. The auxiliary mass for this building is actually a massive heliport at the top of the structure that sits on multistage rubber bearings that allow it to move. The heliport weighs roughly 480 tf, making it the largest auxiliary mass for an AMD system at the time of its completion [11].

Despite its successful implementation in these structures, the AMD system does have some problems. One is the simply immense size of the auxiliary masses. Even though they are typically no more than a few percent of the building weight, this still amounts to an enormous amount of mass at the top of the structure. Installing this mass usually requires significant bracing and support at the upper levels of the structure, and can take up valuable rental space, which could have an impact on the overall profitability of the structure. Furthermore, the hydraulics associated with the force actuators are expensive, take up large amounts of space, and require large amounts of power to operate. In the event of a power outage (a very real possibility during a seismic event) the AMD system would be rendered useless unless it could be powered by a backup supply that would be very costly to implement.

5.4.2 Active-Passive Composite Tuned Mass Damper

A hybrid alternative to the AMD system is the active-passive DUOX system, which offers the same controllability of the AMD system but with smaller required control forces. The system has two auxiliary masses that work in tandem- a large passive TMD, and a smaller active mass. When the building vibrates, the TMD moves a quarter cycle behind the building response, so as to pull the building back towards the original position. The AMD, which sits on top of the TMD, pushes the active mass in the direction opposite the motion of the TMD, so as to magnify the motion of the TMD. When the building is returning to its original position, the AMD works to slow down the TMD [13].

This system has been installed in the Ando Nishikicho Building in Japan, a 14-story building completed in 1993. The weight of the AMD component is 2 tf, and the weight of the TMD component is 20 tf, which make the total system about 10 % of the total building weight [12].

5.4.3 Hybrid Pendulum Damper

This system works along very similar principles to that of a TMD, with the exception that the hybrid pendulum damper can be "tuned" to dampen out different dominant modal frequencies of the structure. The auxiliary mass sits in a V-shaped groove at the top of the structure and rocks back and forth in a pendulum-like motion to dampen out the building motion. The control comes by changing the base angle of the V-shaped groove, which serves to change the "effective length" of the "pendulum" and hence the fundamental frequency of the damper [14]. With this system in place, one now has a tuned mass damper that can be adjusted for different dominant frequencies, as opposed to the tradition TMD systems that could only respond to a single dominant frequency and dominant mode. The Shinjuku Park Tower (completed 1994) in Japan features the hybrid pendulum damper system. There are three separate units installed on this building, each weighing 110 tf [12].

Each of these systems provides a means of active structural control, but not without their price. Each system requires the installation of very large masses at the tops of the buildings and large amounts of energy to control them. The hybrid systems show a movement away from fully

active control, to take advantage of the benefits of passive control. Doing so can reduce the energy requirements of the system significantly, which translates into cost savings over the life of the system.

In order to make active control systems more attractive to engineers and owners, the systems must become more economical and more reliable. The key to doing this is reducing power requirements and the size of the components of the system. Doing these two things will reduce the costs of maintaining the system, as well as the costs of installation.

5.5 Principles of Adaptive Structural Control

As its name implies, adaptive structural control refers to systems that can actually change their physical properties in order to behave in a desired manner. In other words, the system *adapts* to the loading it undergoes, with the intent being to minimize the structure's response. In a classical mass-spring-damper system, control of the system can be achieved by changing the stiffness or the damping of the system, or else both. These changes can typically be made with minimal energy input into the system, and are very effective at achieving the desired response. One can envision a control scheme where stiffness and damping are varied to bring the system to approximately the desired level of motion, at which point force actuators can be engaged to "fine tune" the response. Thus the control scheme takes on a third variable, in the form of actuator force, and the problem becomes one of determining the desired motion of the structure, and finding what combination of stiffness, damping and actuator force is the best way to achieve it. Some type of quantification of the relative cost of implementing each type of change will be necessary to properly distribute the control force among the different options. Obviously, the system would want to invoke the "cheaper" options first, before having to revert to the more expensive ones.

5.5.1 Variable Stiffness System

An active variable stiffness (AVS) system was installed at the Kajima Technical Research Institute Building No. 21 (Experiment Control Building) in Chofu, Tokyo, to demonstrate the

effectiveness of variable stiffness. The building is a three story steel frame weighing 400 tf and has at each level an inverted V-shaped brace which can be locked or unlocked via a variable stiffness device (VSD). The VSD is essentially a hydraulically driven clamp that can lock the brace to the structure to increase the structure's stiffness, or else remain open, so the brace has no effect on the stiffness of the structure, providing two distinct states of stiffness [15].

The system operates on a feed-forward control algorithm that updates the state of stiffness every four milliseconds. When the building is hit with an earthquake, an earthquake accelerometer on the first floor detects the motion and passes the information on to a motion analyzer that determines the dominant period of the seismic motion. The computer then selects which of the three stiffness states (shown below) that would provide the minimal response [16].

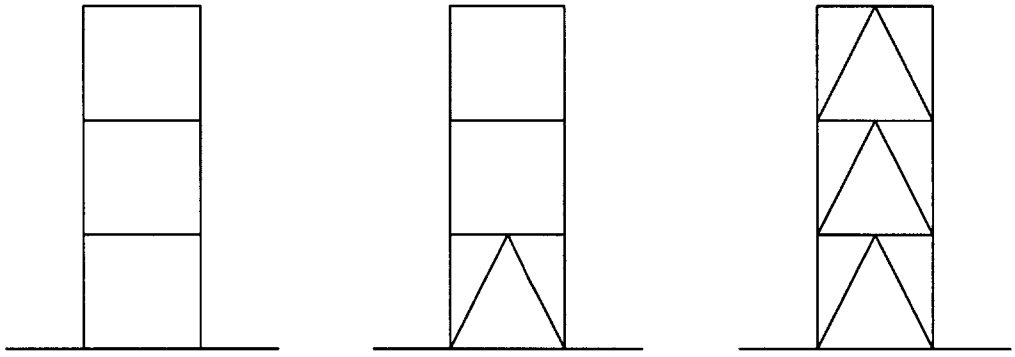

Figure 5.2 – Stiffness Types for AVD

The power required to run each VSD is 20 watts. In addition to the main power supply, the system is equipped with a backup generator that can provide power to the system for an additional 30 minutes.

5.5.2 Variable Damping System

A model structure similar to the Kajima Experiment Control Facility was built and had installed in it an active variable damping (AVD) system to control seismic response. The system is a

three-story steel frame built on a large shaking table and features inverted V-shaped braces and variable hydraulic dampers at each level- two at the first and second levels, along the sides, and one at the top level in the center [11].

The system is able to control the damping force in each damper by regulating a control valve within the damper that limits the flow of oil through the damper. The control algorithm is such that the variable damping force approaches the optimal control force. Like the variable stiffness system, the AVD system can be run on very little power (30 watts). But it is limited in its applicability in that in order to apply the control force, it is necessary that the structure is moving in the same direction as which the control force is to be applied. In other words [11]:

$$F_{damper} = \begin{cases} F_{damper} & if\ F_{damper} \times v \geq 0 \\ 0 & if\ F_{damper} \times v < 0 \end{cases}. \tag{5.42}$$

For the single degree of freedom system with pure velocity feedback, the structure will always be moving in the correct direction to apply the control force.

5.5.3 Electrorheological (ER) Fluids

In addition to using purely mechanical means to create variable damping, there appears to be some promise in the use of electrorheological (ER) fluids. These fluids have small particles suspended in them and undergo significant changes in material properties when an electric field is applied. Under the presence of an electric field, the suspended particles change their random configuration and form a chain-like pattern along the direction of the field lines, which increases the viscosity, and hence damping, of the fluid. When very high fields are applied, the fluid can take on the consistency of a gel-like solid. In addition, the quick (10^{-4} seconds) reaction time of these fluids makes them an excellent option for use in variable dampers to control seismic motion. It has been proposed to use ER fluids as part of a hybrid active / passive damper, in which the passive component of damping would be supplied by a more traditional viscous fluid, like oil, and the ER fluid would be used for active control [17]. ER fluids typically possess some zero field viscosity, though this is usually very small in comparison to the electric field-induced viscosity. It would be possible however to enhance the zero field component of the viscosity towards the same order of magnitude as the field component, so that the ER fluid could

be used alone as an active / passive damper [17]. In this case the zero field viscosity would provide the passive control, supplemented by the field-induced variable viscosity as the active component. One drawback is that ER fluids usually do not possess very reliable properties, an effect that must be taken into consideration.

5.5.4 Magnetorheological (MR) Fluids

MR fluids behave very similarly to ER fluids, except that MR fluids exhibit variable viscosity effects under an applied magnetic field, not an electric field. When a field is run across the MR fluid, suspended magnetizeable particles in the fluid align themselves along the field direction, changing the viscous liquid to a semi-solid with controllable yield strength, referred to as a Bingham solid. Manufacturers of MR fluids have claimed that they are up to 50 times stronger than ER fluids, and operate just as fast, in terms of reaction time [18].

A full-scale variable damper using a magnetorheological fluid was tested at the University of Notre Dame. This damper could generate damping forces up to 200,000 N, demonstrating its potential applicability to civil engineering structures. It required very little power to operate, only about 40 watts, which could easily be supplied by a battery if necessary [19, 20].

6 Control Algorithms Applied to a Single Degree of Freedom System

In order to prove the effectiveness of the adaptive control algorithm, a series of simulations were carried out on a single degree of freedom system. The objectives of this exercise were to (1) develop a method of controlling structural motion of a system through adaptive measures and (2) compare these results with the non-adaptive case, and determine if adaptive control could produce results comparable to that of non-adaptive (active) control.

6.1 System Parameters

While the definition of the physical system was not extremely critical, it was necessary to create a system that was a realistic representation of a physical structure, and would also give "good" results. In other words, the system should behave in such a way that it is easy to recognize changes in the response as conditions change. The "uncontrolled" or default system parameters are presented below in Table 6.1.

Quantity	Symbol	Value
Mass	m	50,000 kg
Stiffness	k	2,000,000 N/m
Damping Coefficient	c	12,500 kg/sec
Percentage Damping	ζ	2.0 %
Natural Frequency	ω	6.3 rad/sec
Natural Period	T	1.0 sec

Table 6.1 – Values of System Parameters for Control Simulation

6.2 Active Control Algorithm

6.2.1 Sinusoidal Ground Motion

The first task was to check the validity of the control algorithm as presented in Chapter 5. Initially the system was subjected to a sinusoidal ground motion, and the controlled response was compared with the uncontrolled response. Appendix A contains program var_damp.m, a MATLAB program used to carry out the simulation. The ground motion was represented as

$$a_g(i) = a_g|_{\max} \sin(\Omega t), \tag{6.1}$$

where Ω is the period of the ground motion, $a_g|_{max}$ is the maximum ground acceleration, and $a_g(i)$ is the ground acceleration at time i. For the simulation, Ω was set equal to 2π rad/sec, so that the system would be in a near-resonant state, to better illustrate the benefits of control; the value of $a_g|_{max}$ was set equal to 9.81 m/sec^2.

The discrete time control algorithm was chosen over the continuous one, since it was felt that discrete control would be more indicative of a real system. The time step Δt was set at 0.02 sec, which was sufficiently small enough to keep the algorithm stable, and produced results that appear to be very close to the continuous case.

Producing results for both the controlled and uncontrolled cases proved to be a relatively easy task, since all that was required to reduce the controlled case to the uncontrolled case was omission of the control force term from the discrete time step state-space equation. In other words, for the controlled case, the time step equation was

$$\boldsymbol{U}(i+1) = \overline{\boldsymbol{A}}\boldsymbol{U}(i) + \overline{\boldsymbol{B}}F_c(i) + \overline{\boldsymbol{D}}F_g(i), \tag{6.2}$$

while for the uncontrolled case, the equation reduced to

$$\boldsymbol{U}(i+1) = \overline{\boldsymbol{A}}\boldsymbol{U}(i) + \overline{\boldsymbol{D}}F_g(i). \tag{6.3}$$

Time history responses are contained in Appendix A. They generally concur with what one would expect. The cost parameter r was set at different values to show how the system behaved for various levels of control.

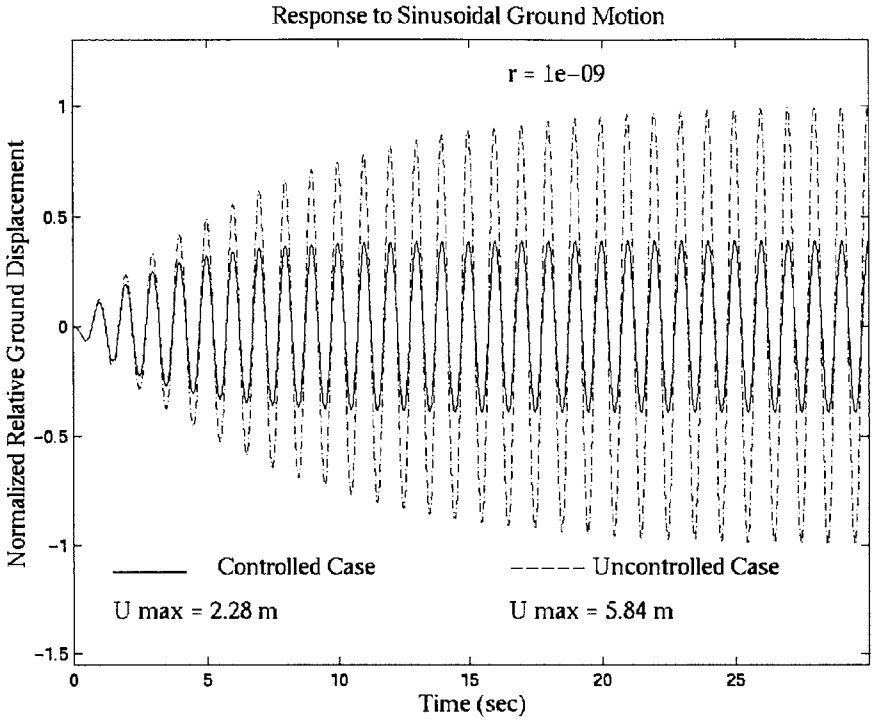

Figure 6.1 – Response to Sinusoidal Ground Motion, r = 1 x 10^{-9}

Because of the scale of the system, a "large" value of r corresponded to 10^{-7}, for which there was virtually no difference between the controlled and uncontrolled cases. As r was decreased however, the applicable control force could be increased, and the controlled response became gradually smaller. The results are summarized below in Table 6.2. Listed are $u_u|_{max}$, the maximum relative displacement for the uncontrolled case; $u_c|_{max}$, the maximum relative displacement for the controlled case; and $F_c|_{max}$, the maximum value of the control force that is applied. Clearly one can see the benefits of applying the control force to the system.

	Values of Cost Parameter, r			
	10^{-7}	**10^{-8}**	**10^{-9}**	**10^{-10}**
$u_u|_{max}$	5.84 m	5.84 m	5.84 m	5.84 m
$u_c|_{max}$	5.68 m	4.68 m	2.28 m	0.79 m
$F_c|_{max}$	1.40 x 10^4 N	1.02 x 10^5 N	3.05 x 10^5 N	4.27 x 10^5 N

Table 6.2 – Changes in Response and Control Force with Changing r

6.2.2 Earthquake Time Histories

Once it was confirmed that the algorithm was working correctly for a sinusoidal input, the next step was to examine how the algorithm responded to an earthquake time history. A second MATLAB program, titled var_damp_2a.m, was written for this case. The operations were exactly the same as for the sinusoidal input, except that the acceleration values were supplied by a time history. Six different time histories were used in all to test the algorithm. They are summarized below in Table 6.3.

Name	Max. Acceleration (m/sec^2)	Duration (sec)
El Centro (Component S00E)	3.417	53.76
Helena, MT Carroll Coll. (Comp. S00W)	1.435	50.92
Olympia Western, WA (Comp. N04W)	1.616	89.08
Parkfield, CA (Component N05W)	3.478	43.94
SF Golden Gate (Component N10E)	0.818	40.00
Taft Lincoln School Tunnel (Comp. N21E)	1.527	54.38

Table 6.3 – Earthquake Time Histories Used in Control Simulations

Each of the time histories is a series of accelerations taken at intervals of 0.02 seconds. (This is why a time step of 0.02 seconds was used in the sinusoidal case.) The analysis that was run was very similar to what was done for the sinusoidal case. The value of r was varied over the same range of values, first for the El Centro time history, to observe the effects of the control force on the response. As expected, the control force was able to limit the response of the system considerably from the uncontrolled case. A summary is presented in the table below; Appendix B contains plots of the controlled and uncontrolled responses, as well as the variation of the control force.

	Values of Cost Parameter, r			
	10^{-7}	10^{-8}	10^{-9}	10^{-10}
$u_u\|_{max}$	0.17 m	0.17 m	0.17 m	0.17 m
$u_c\|_{max}$	0.17 m	0.16 m	0.12 m	0.07 m
$F_c\|_{max}$	464 N	3.96×10^3 N	1.91×10^4 N	4.80×10^4 N

Table 6.4 - Summary of Response to El Centro Time History

In order to test the algorithm's applicability, the simulation was run for the remaining time histories, with r set equal to 10^{-10}, which provided a level of control that corresponded to very high damping. The responses and control force variations can also be viewed in Appendix B; maximum force and relative displacement values are shown in the table below.

Name	$u_u\|_{max}$	$u_c\|_{max}$	$F_c\|_{max}$
Helena, MT Carroll Coll. (Comp. S00W)	0.008 m	0.007 m	6.85×10^3 N
Olympia Western, WA (Comp. N04W)	0.07 m	0.03 m	2.23×10^4 N
Parkfield, CA (Comp. N05W)	0.05 m	0.02 m	2.34×10^4 N
SF Golden Gate (Comp. N10E)	0.007 m	0.005 m	3.34×10^3 N
Taft Lincoln School Tunnel (Comp. N21E)	0.05 m	0.03 m	1.82×10^4 N

Table 6.5 – Response of System to Various Time Histories

It should be noted that even though in some of the cases the uncontrolled response is so small that the control force does not seem to be of much use, this is not a suitable reason to disregard the control scheme. Just because this particular system did not have a very large response to some of these time histories does not mean that a different system will have the same success. The point is to demonstrate how the control force reduces the response *in relation to* the uncontrolled case, which is significant for every time history.

6.2.3 Time Delay Effects

Assuming that the control force required at time i can be applied at time i, the system should remain stable unconditionally, since the modulus of the largest eigenvalue of $[\overline{A} - \overline{B}K_f]$ is less than 1. But once time delay is introduced into the system, so that $F_c(i)$ is applied at some time i+v, the system experiences a very real chance of becoming unstable. Logic dictates that as v increases (as the time delay grows), the system will eventually reach a point where the control force will be so out of phase with the state of the system that the controlled response will become unstable and could actually be larger than the uncontrolled response. A solution for finding the critical value of v, the number of time step iterations between calculation and application of the control force, was presented in the previous chapter. This solution was used to find the critical value of v for various values of r. In addition to using this approach it was decided to run the simulation for various values of v, at a specified value of r, to determine what value of v made the system become unstable. For purposes of this analysis, the system was considered to be unstable when the maximum displacement for the controlled response was at least an order of magnitude higher than the maximum displacement for the uncontrolled response. MATLAB program var_damp_2b.m was created to model time delay effects in the system. The value of the control force at time i was stored at the end of an array of size v, and was moved up one step in the array every time step. At every time step the value at the top of the control force array was applied to the system.

Because the stability of the system is based on the homogeneous solution to the equation of motion, it was anticipated that the system should become unstable for the same value of v for any time history applied. Appendix C shows the controlled and uncontrolled responses for the El Centro time history for v = 1, v = 10, v = 11, v = 12, and v = 13 (t_d = 0.02 sec, t_d = 0.20 sec, t_d = 0.22 sec, t_d = 0.24 sec, and t_d = 0.26 sec). Once v is equal to 11, the maximum relative displacement of the controlled response is the same as for the uncontrolled case. At v = 12, the controlled response is noticeably larger than the uncontrolled response, although it is still stable. Finally, at v = 13 the control algorithm breaks down, and the controlled response balloons to a maximum relative displacement of 13.21 m. Appendix C also contains responses for the other five time histories at v = 12 and v = 13, to show that in fact the point of instability is

independent of the loading. For all of the time histories shown, instability is considered to occur at v = 13. A summary of how the maximum allowable time delay varies with r is shown in Table 6.6 below.

For $r = 10^{-7}$ and $r = 10^{-8}$, it appeared that the effect of the control force on the system was so small that time delay did not seem to affect the stability of the algorithm at all. For each of these cases, simulations were run up to a maximum of v = 200 and the system remained completely stable. The results are also compared with the values of v calculated from the method presented in Chapter 5. Slight discrepancies occur between the two methods. However, the somewhat arbitrary definition of instability in the simulation trial method results, and the scaling of the eigenvectors **W** and **V** in the numerical method can account for most of this discrepancy. For the results shown, both **W** and **V** were scaled so that the norm of each vector equaled 1.

	Values of Cost Parameter, r				
	10^{-7}	10^{-8}	10^{-9}	10^{-10}	10^{-11}
v_{trial}	N/A	N/A	20	13	9
$u_u\|_{max}$	N/A	N/A	0.17 m	0.17 m	0.17 m
$u_c\|_{max}$	N/A	N/A	1.5 m	13.2 m	64.9 m
$v_{predicted}$	23.0-42.6i	23.3-25.3i	23.7-10.4i	14.7	11.0

Table 6.6 – Response of System to Time Delay Effects for Varying r

6.3 Adaptive Control Algorithm

6.3.1 Adaptive Control Versus Active Control

The simulations run for the adaptive case do not actually use pure adaptive control, but rather use a combination of non-adaptive and adaptive control to affect the motion of the system. The reason for this was to demonstrate how an adaptive system could choose among different ways to control its motion, depending on which way was the most effective. In these simulations, one of the choices available to the system was actuator force, which is why the system cannot be considered truly adaptive. Even though this algorithm is not purely adaptive, it will be referred

to as adaptive for the rest of the chapter. Similarly, non-adaptive control will refer to the type of active control in which control is obtained solely through the use of actuator forces.

The differences between the non-adaptive and adaptive control simulations can best be explained by looking at the progression of the time step iteration of each algorithm. For both non-adaptive and adaptive control, the time step state-space equation for discrete time is

$$\boldsymbol{U}(i+1) = \overline{\boldsymbol{A}}\boldsymbol{U}(i) + \overline{\boldsymbol{B}}F_c(i) + \overline{\boldsymbol{D}}F_g(i). \tag{6.4}$$

For non-adaptive control $\overline{\mathbf{A}}$, $\overline{\mathbf{B}}$ and $\overline{\mathbf{D}}$ are constant throughout the time step process. The elements of these coefficient matrices are based on mass, stiffness, damping and the time step interval, all of which are unchanging throughout the simulation. Similarly, the expression for the control force,

$$F_c = -\begin{bmatrix} 0 & k_v \end{bmatrix}\boldsymbol{U}, \tag{6.5}$$

is "constant" in the sense that k_v does not change over the course of the simulation. This is important due to the fact that solving for k_v involves the solution to the discrete time Ricatti equation, which is somewhat computationally intensive, even for an efficient program such as MATLAB. For the non-adaptive algorithm the Ricatti equation only needs to be solved one time at the beginning of the simulation. All of the computations that are carried out in the time step iteration loop are algebraic ones, so they can be done fairly quickly.

The time step process becomes much more complex for the adaptive algorithm, however. For every time i, the program must compute the optimal control force, and then decide what values of stiffness, damping and actuator force will equate to applying the optimal control force, for the current state of the system. This means that $\overline{\mathbf{A}}$ and $\overline{\mathbf{B}}$ need to be recomputed at every time step, as does k_v; this increases the run time of the algorithm significantly over the non-adaptive case.

6.3.2 Modifications to the Adaptive Control Algorithm

Running the adaptive control simulation at first proved to be a futile task, since the run time was extraordinarily long, for the reasons mentioned in the previous section. The majority of this problem was caused by computing $\overline{\mathbf{A}}$ and $\overline{\mathbf{B}}$ at every time step; therefore it was decided to substitute approximate expressions for $\overline{\mathbf{A}}$ and $\overline{\mathbf{B}}$, to speed up the simulation.

The expressions for $\overline{\mathbf{A}}$ and $\overline{\mathbf{B}}$ can both be expanded as summations. $\overline{\mathbf{A}}$ is written as [10]:

$$\overline{A} = e^{A\Delta t} = I + \frac{[A\Delta t]^1}{1!} + \frac{[A\Delta t]^2}{2!} + \frac{[A\Delta t]^3}{3!} + \cdots + \frac{[A\Delta t]^n}{n!}, \tag{6.6}$$

where

$$A = \begin{bmatrix} 0 & 1 \\ \frac{-k}{m} & \frac{-c}{m} \end{bmatrix} \tag{6.7}$$

and

$$I = \begin{bmatrix} 1 & 0 \\ 0 & 1 \end{bmatrix}. \tag{6.8}$$

However, because Δt is much less than 1, only the first few terms of this expansion will have any significant effect on the value of $\overline{\mathbf{A}}$. Therefore, $\overline{\mathbf{A}}$ can be rewritten as

$$\overline{A} \cong I + [A\Delta t] + \frac{1}{2}[A\Delta t]^2 . \tag{6.9}$$

Substituting in the appropriate values, $\overline{\mathbf{A}}$ finally becomes

$$\overline{A} \cong \begin{bmatrix} 1 - \frac{k}{2m}\Delta t^2 & \Delta t - \frac{c}{2m}\Delta t^2 \\ -\frac{k}{m}\Delta t - \frac{ck}{2m^2}\Delta t^2 & 1 - \frac{c}{m}\Delta t - \frac{k}{2m}\Delta t^2 + \frac{c^2}{2m^2}\Delta t^2 \end{bmatrix}. \tag{6.10}$$

A similar process can be done to $\overline{\mathbf{B}}$. The complete expression for $\overline{\mathbf{B}}$ is

$$\overline{B} = \int_0^{\Delta t} e^{At} dt\, B = \int_0^{\Delta t} \left(I + \frac{[A\Delta t]^1}{1!} + \frac{[A\Delta t]^2}{2!} + \frac{[A\Delta t]^3}{3!} + \cdots + \frac{[A\Delta t]^n}{n!} \right) dt\, B, \tag{6.11}$$

recalling that

$$\mathbf{B} = \begin{bmatrix} 0 \\ \frac{1}{m} \end{bmatrix}. \tag{6.12}$$

Carrying out the integration, the expression for $\overline{\mathbf{B}}$ can be approximated as

$$\overline{\boldsymbol{B}} \cong \left(\boldsymbol{I}\Delta t + \frac{1}{2}\boldsymbol{A}\Delta t^2 + \frac{1}{3}[\boldsymbol{A}]^2\Delta t^3 \right) \boldsymbol{B}. \tag{6.13}$$

Plugging in the appropriate terms, $\overline{\mathbf{B}}$ is written as

$$\overline{\boldsymbol{B}} \cong \begin{bmatrix} \dfrac{\Delta t^2}{2m} - \dfrac{c\Delta t^3}{6m^2} \\ \dfrac{\Delta t}{m} - \dfrac{c\Delta t^2}{2m^2} - \dfrac{k\Delta t^3}{6m^2} + \dfrac{c^2\Delta t^3}{6m^3} \end{bmatrix}. \tag{6.14}$$

However, since Δt^3 is such an extremely small quantity, it makes sense to eliminate all of the Δt^3 terms. This leads to the final expression for $\overline{\mathbf{B}}$:

$$\overline{\boldsymbol{B}} \cong \begin{bmatrix} \dfrac{\Delta t^2}{2m} \\ \dfrac{\Delta t}{m} - \dfrac{c\Delta t^2}{2m^2} \end{bmatrix}. \tag{6.15}$$

With these expressions in place in the time step algorithm, the simulation was able to run smoothly in an acceptable amount of time.

6.3.3 Calculation of Adaptive Stiffness

In developing the adaptive control algorithm, one of the most crucial aspects was determining how to modify the stiffness and damping to achieve the same state as would be achieved through application of a control force. The discrete time step equation for non-adaptive control,

$$\boldsymbol{U}(i+1) = \overline{\boldsymbol{A}}\boldsymbol{U}(i) + \overline{\boldsymbol{B}}\boldsymbol{F}_c(i) + \overline{\boldsymbol{D}}\boldsymbol{F}_g(i), \tag{6.16}$$

was expanded to include the recently developed approximations for $\overline{\mathbf{A}}$ and $\overline{\mathbf{B}}$, yielding

$$\begin{bmatrix} u(i+1) \\ \dot{u}(i+1) \end{bmatrix} = \begin{bmatrix} 1-\frac{k}{2m}\Delta t^2 & \Delta t-\frac{c}{2m}\Delta t^2 \\ -\frac{k}{m}\Delta t-\frac{ck}{2m^2}\Delta t^2 & 1-\frac{c}{m}\Delta t-\frac{k}{2m}\Delta t^2+\frac{c^2}{2m^2}\Delta t^2 \end{bmatrix} \begin{bmatrix} u(i) \\ \dot{u}(i) \end{bmatrix} + \cdots$$

$$\cdots + \begin{bmatrix} \frac{\Delta t^2}{2m} \\ \frac{\Delta t}{m}-\frac{c\Delta t^2}{2m^2} \end{bmatrix} F_c(i) + \begin{bmatrix} \frac{\Delta t^2}{2m} \\ \frac{\Delta t}{m}-\frac{c\Delta t^2}{2m^2} \end{bmatrix} F_g(i). \quad (6.17)$$

Separating the equations, one gets

$$u(i+1) = \left(1-\frac{k}{2m}\Delta t^2\right)u(i) + \left(\Delta t-\frac{c}{2m}\Delta t^2\right)\dot{u}(i) + \frac{\Delta t^2}{2m}F_c(i) + \frac{\Delta t^2}{2m}F_g(i) \quad (6.18)$$

and

$$\dot{u}(i+1) = -\left(\frac{k}{m}\Delta t+\frac{ck}{2m^2}\Delta t^2\right)u(i) + \left(1-\frac{c}{m}\Delta t-\frac{k}{2m}\Delta t^2+\frac{c^2}{2m^2}\Delta t^2\right)\dot{u}(i) + \cdots$$

$$\cdots + \left(\frac{\Delta t}{m}-\frac{c\Delta t^2}{2m^2}\right)F_c(i) + \left(\frac{\Delta t}{m}-\frac{c\Delta t^2}{2m^2}\right)F_g(i). \quad (6.19)$$

The expressions for the adaptive case are very similar, except that the control force terms drop out and k becomes a time dependant variable. (For this derivation, it is assumed that the control in the adaptive case is implemented only through changes in stiffness.) It becomes necessary to introduce some modifications to the nomenclature, to avoid improper combining of terms. In the state equations for the adaptive case, k is replaced with $k_{tot}(i)$, which refers to the total stiffness of the adaptive system. In the state equations for the non-adaptive case, k is the "normal" system stiffness, which remains unchanged. This distinction will become readily apparent when the result is presented.

Writing the state equations for the adaptive case, one obtains

$$u(i+1) = \left(1 - \frac{k_{tot}(i)}{2m}\Delta t^2\right)u(i) + \left(\Delta t - \frac{c}{2m}\Delta t^2\right)\dot{u}(i) + \frac{\Delta t^2}{2m}F_g(i) \tag{6.20}$$

and

$$\dot{u}(i+1) = -\left(\frac{k_{tot}(i)}{m}\Delta t + \frac{c\,k_{tot}(i)}{2m^2}\Delta t^2\right)u(i) + \left(1 - \frac{c}{m}\Delta t - \frac{k_{tot}(i)}{2m}\Delta t^2 + \frac{c^2}{2m^2}\Delta t^2\right)\dot{u}(i) + \cdots$$

$$\cdots + \left(\frac{\Delta t}{m} - \frac{c\Delta t^2}{2m^2}\right)F_g(i). \tag{6.21}$$

One should expect the state equations for both the non-adaptive and adaptive cases to yield the same result for $\boldsymbol{U}(i+1)$, in other words,

$$\boldsymbol{U}(i+1)\,|_{non-adaptive} = \boldsymbol{U}(i+1)\,|_{adaptive}, \tag{6.22}$$

so the state equations for each case are set equal. Because the only unknown is k_{tot}, both the displacement and velocity equations should yield the same result for k_{tot}. The displacement equation is worked with in this case, since it is easier to manipulate k_{tot} this way. Thus the equation

$$\left(1 - \frac{k_{tot}(i)}{2m}\Delta t^2\right)u(i) + \left(\Delta t - \frac{c}{2m}\Delta t^2\right)\dot{u}(i) + \frac{\Delta t^2}{2m}F_g(i) = \cdots$$

$$\cdots \left(1 - \frac{k}{2m}\Delta t^2\right)u(i) + \left(\Delta t - \frac{c}{2m}\Delta t^2\right)\dot{u}(i) + \frac{\Delta t^2}{2m}F_g(i) + \frac{\Delta t^2}{2m}F_c(i) \tag{6.23}$$

can be reduced to

$$k_{tot}(i) = -\frac{F_c(i)}{u(i)} + k. \tag{6.24}$$

This means that the variable stiffness, or the "control" stiffness, is equal to $-F_c(i) / u(i)$. This is the stiffness that should be added to or subtracted from the system at time i to achieve a desired state at time i+1 that would otherwise be achieved by applying a control force, F_c, to the unchanged system. It must be noted however that this result could lead to negative stiffness quantities; therefore the expression for $k_{tot}(i)$ must be adjusted slightly:

$$k_{tot}(i) = -\frac{F_c(i)}{u(i)} + k \quad > 0. \tag{6.25}$$

It is stipulated that $k_{tot}(i)$ must be greater than zero since negative stiffness cannot be achieved physically. In theory $k_{tot}(i)$ could equal zero exactly, but this result leads to instability in the simulation, so the '>' sign is maintained. Furthermore, if u(i) is zero, then the variable stiffness must be set to zero. It is also noted that if one were to repeat this entire analysis on the velocity equations, the exact same result for $k_{tot}(i)$ would be achieved, as expected.

6.3.4 Calculation of Adaptive Damping

The above analysis that was used to determine the appropriate expression for the variable stiffness can also be used to find the necessary variable damping for adaptive control. The state equations for the adaptive case are modified to include the term $c_{tot}(i)$, the total damping of the system. Since stiffness is not being varied in this analysis, $k_{tot}(i)$ reverts back to k. The expressions take the form

$$u(i+1) = \left(1 - \frac{k}{2m}\Delta t^2\right)u(i) + \left(\Delta t - \frac{c_{tot}(i)}{2m}\Delta t^2\right)\dot{u}(i) + \frac{\Delta t^2}{2m}F_g(i) \tag{6.26}$$

and

$$\dot{u}(i+1) = -\left(\frac{k}{m}\Delta t + \frac{c_{tot}(i)k}{2m^2}\Delta t^2\right)u(i) + \left(1 - \frac{c_{tot}(i)}{m}\Delta t - \frac{k}{2m}\Delta t^2 + \frac{c_{tot}(i)^2}{2m^2}\Delta t^2\right)\dot{u}(i) + \cdots$$
$$\cdots + \left(\frac{\Delta t}{m} - \frac{c_{tot}(i)\Delta t^2}{2m^2}\right)F_g(i). \tag{6.27}$$

Again, these expressions are set equal to the state equations for the non-adaptive case. The displacement equation provides a simpler means of obtaining $c_{tot}(i)$. One begins with

$$\left(1 - \frac{k}{2m}\Delta t^2\right)u(i) + \left(\Delta t - \frac{c_{tot}(i)}{2m}\Delta t^2\right)\dot{u}(i) + \frac{\Delta t^2}{2m}F_g(i) = \cdots$$

$$\cdots \left(1-\frac{k}{2m}\Delta t^2\right)u(i)+\left(\Delta t-\frac{c}{2m}\Delta t^2\right)\dot{u}(i)+\frac{\Delta t^2}{2m}F_g(i)+\frac{\Delta t^2}{2m}F_c(i) \qquad (6.28)$$

which leads to

$$c_{tot}(i)=-\frac{F_c(i)}{\dot{u}(i)}+c\,. \qquad (6.29)$$

One obtains the same result for $c_{tot}(i)$ if the velocity equations are used instead of the displacement equations. For pure negative velocity proportional feedback, the sign of $F_c(i)$ will always be opposite that of $\dot{u}(i)$, so $c_{tot}(i)$ will always be a positive quantity.

6.3.5 Distribution of Control Force

In order for the system to makes choices among variable stiffness, variable damping, and actuator forces to control motion, some sort of cost structure needed to be set in place to give the cognitive unit some basis on which to make its decisions. There are several ways in which to do this and much discussion could be generated around what would be the optimal method. However that is besides the point of this exercise. For the simulations, it was decided that stiffness would be the "cheapest" way of controlling the structure, followed by damping, and then actuator forces. In actuality this may not necessarily be true, but it serves to illustrate how the control force can be distributed among different methods of implementation.

What this means is that the algorithm determines what control force it needs, and then tries to get as much of that force as possible from stiffness. A limit is placed on the allowable variable stiffness however, so if the variable stiffness cannot provide all of the control force, then the control unit will next look to damping to provide the remainder. Similarly, the variable damping has some limit that it cannot exceed, so if the system still requires additional control force, it must be provided by force actuators, which have been assumed to have limitless capacity for the simulations. One can summarize these rules as follows:

(1) $$F_c(i)=-\begin{bmatrix}0 & k_v(i)\end{bmatrix}U(i)\,, \qquad (6.30)$$

(2)
$$k_c(i)=\begin{cases} -\dfrac{F_c(i)}{u(i)}, & -k < k_c(i) \le k \qquad u(i)\neq 0 \\ \\ 0 & u(i)=0 \end{cases}, \tag{6.31}$$

(3)
$$F_c(i)\,|_{remaining} \;=\; F_c(i) \;+\; k_c(i)\,u(i), \tag{6.32}$$

(4)
$$c_c(i)=\begin{cases} -\dfrac{F_c(i)}{\dot{u}(i)}, & c_c(i) \le c \qquad \dot{u}(i)\neq 0 \\ \\ 0 & \dot{u}(i)=0 \end{cases}, \tag{6.33}$$

(5)
$$F_c(i)\,|_{actuator} \;=\; F_c(i)\,|_{remaining} \;+\; c_c(i)\;\dot{u}(i)\,. \tag{6.34}$$

It then follows that

$$\boldsymbol{U}(i+1) = \overline{\boldsymbol{A}}(i)\boldsymbol{U}(i) + \overline{\boldsymbol{B}}(i)F_c(i)\,|_{\,actuator} + \overline{\boldsymbol{D}}(i)F_g(i), \tag{6.35}$$

where

$$\overline{\boldsymbol{A}}(i) \;\cong\; \begin{bmatrix} 1-\dfrac{k_{tot}(i)}{2m}\Delta t^2 & \Delta t-\dfrac{c_{tot}(i)}{2m}\Delta t^2 \\ \\ -\dfrac{k_{tot}(i)}{m}\Delta t-\dfrac{c_{tot}(i)\,k_{tot}(i)}{2m^2}\Delta t^2 & 1-\dfrac{c_{tot}(i)}{m}\Delta t-\dfrac{k_{tot}(i)}{2m}\Delta t^2+\dfrac{c_{tot}(i)^2}{2m^2}\Delta t^2 \end{bmatrix}, \tag{6.36}$$

$$\overline{\boldsymbol{B}}(i) \;\cong\; \begin{bmatrix} \dfrac{\Delta t^2}{2m} \\ \\ \dfrac{\Delta t}{m}-\dfrac{c_{tot}(i)\Delta t^2}{2m^2} \end{bmatrix}, \tag{6.37}$$

$$\overline{\boldsymbol{D}}(i) \cong \begin{bmatrix} \dfrac{\Delta t^2}{2m} \\ \dfrac{\Delta t}{m} - \dfrac{c_{tot}(i)\Delta t^2}{2m^2} \end{bmatrix}, \tag{6.38}$$

$$c_{tot}(i) = c + c_c(i), \tag{6.39}$$

and

$$k_{tot}(i) = k + k_c(i). \tag{6.40}$$

For the purpose of clarification, it is worth explaining why, in the equations for $F_c(i)|_{remaining}$ and $F_c(i)|_{actuator}$, there is a plus sign instead of a minus sign, when $F_c(i)|_{remaining}$ is supposed to be the difference between $F_c(i)$ and the force provided by stiffness, and $F_c(i)|_{actuator}$ is the difference between $F_c(i)|_{remaining}$ and the force provided by damping. Consider the following scenario, where a single degree of freedom system has negative velocity and positive displacement at time i. For velocity proportional feedback, $F_c(i)$ will be a positive quantity, since $F_c(i) = -k_v \dot{u}(i)$. If $u(i)$ is positive, then $k_c(i)$ will be a negative quantity. (It is assumed that $k_c(i)$ is within the appropriate limits.) This means that $k_c(i)u(i)$ will be a negative quantity. In order then to find the difference between $F_c(i)$ and $k_c(i)u(i)$, it is necessary to add the terms together, since one is positive and one is negative.

Continuing this scenario, $F_c(i)|_{remaining}$ must be positive (assuming it is not zero), since $k_c(i)u(i)$ cannot exceed $F_c(i)$, because of the definition of $k_c(i)$. It was already stated that $c_c(i)$ will always be a positive quantity for velocity proportional feedback, so combining that with negative $\dot{u}(i)$, the resultant term must be negative. Again, this is opposite the sign of $F_c(i)|_{remaining}$, so a plus sign is used in computing the difference rather than a negative sign. If $F_c(i)|_{actuator}$ is not zero, it must be a positive quantity. Table 6.7 indicates whether the relevant terms will be positive or negative for various combinations of $u(i)$ and $\dot{u}(i)$.

	$\dot{u}(i) > 0$		$\dot{u}(i) < 0$	
	$u(i) > 0$	$u(i) < 0$	$u(i) > 0$	$u(i) < 0$
$F_c(i)$	-	-	+	+
$k_c(i)$	+	-	-	+
$k_c(i)u(i)$	+	+	-	-
$F_c(i)\|_{remaining}$	-	-	+	+
$c(i)\dot{u}(i)$	+	+	-	-
$F_c(i)\|_{actuator}$	-	-	+	+

Table 6.7 – Magnitudes of Force Terms for Adaptive Control

To further examine the logic of adaptivity, one looks at these qualitative results in terms of a free body diagram.

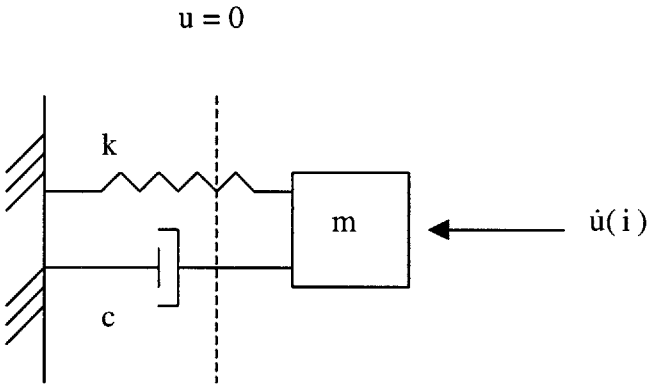

(a)

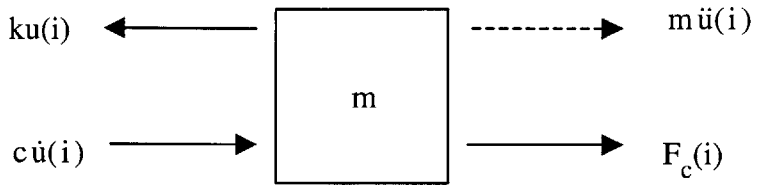

(b)

Figure 6.2 – (a) Single Degree of Freedom System and (b) Free Body Diagram

The system is first considered for the non-adaptive case, with the forces acting in the directions as shown in Figure 6.1. If these forces are replaced with the ones from the adaptive case, the result should be the same. One begins by replacing $F_c(i)$ with the actuator force $F_c(i)|_{actuator}$. Next, the force due to variable stiffness is added. This can be thought as a force of (positive) magnitude $-k_c(i)u(i)$ with positive sense to the right. Similarly, the force due to variable damping is added as $-c_c(i)\dot{u}(i)$ with its positive sense also to the right. This gives the following free body diagram:

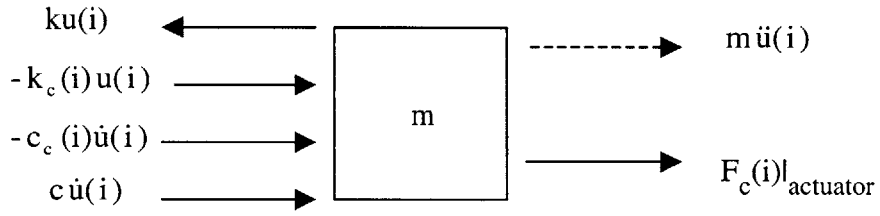

Figure 6.3 – Free Body Diagram for Adaptively Controlled SDOF System

All the magnitudes shown are positive values. It is noted that this is exactly equal to the active control case when the magnitude of $F_c(i)$ is such that

$$F_c(i) = -k_c(i)u(i) - c_c(i)\dot{u}(i) + F_c(i)\,|_{actuator} \tag{6.41}$$

for the sign convention show in Figure 6.2.

6.3.6 Results for Adaptive Case

The adaptive control simulation was performed for the El Centro time history, for various values of the cost parameter r. The values of r were the same as those used for the fully active simulation run earlier, so that a comparison could be made between the two algorithms. A summary of the maximum displacements and control forces for the non-adaptive case was presented in Table 6.4 (Section 6.2.2); it is reprinted below for convenience.

	Non-Adaptive Control – Values of Cost Parameter, r			
	10^{-7}	10^{-8}	10^{-9}	10^{-10}
$\|u_u\|_{max}$	0.17 m	0.17 m	0.17 m	0.17 m
$\|u_c\|_{max}$	0.17 m	0.16 m	0.12 m	0.07 m
$\|F_c\|_{max}$	464 N	3.96×10^3 N	1.91×10^4 N	4.80×10^4 N

Table 6.8 - Summary of Response to El Centro Time History (Non-Adaptive Control)

For the adaptive case, the amount of control that could be achieved was exactly the same as for the non-adaptive case. Below are presented the results for maximum relative displacement values, as well as maximum control forces and variable stiffness and damping. (See Appendix D for more detailed results.) As expected, the required control forces are less than those for the non-adaptive case, due to the addition of variable stiffness and damping. Because methods of adaptive control typically require much less energy to implement than non-adaptive ones, it is clear that using adaptive control can provide a much more efficient solution to motion problems without sacrificing any amount of control.

	Adaptive Control – Values of Cost Parameter, r			
	10^{-7}	10^{-8}	10^{-9}	10^{-10}
$\|u_u\|_{max}$	0.17 m	0.17 m	0.17 m	0.17 m
$\|u_c\|_{max}$	0.17 m	0.16 m	0.12 m	0.07 m
$\|k_c\|_{max}$	2×10^6 N/m	2×10^6 N/m	2×10^6 N/m	2×10^6 N/m
$\|c_c\|_{max}$	287 kg/s	3.23×10^3 kg/s	1.25×10^4 kg/s	1.25×10^4 kg/s
$\|F_c\|_{max}$	7.1×10^{-15} N	1.4×10^{-14} N	4.71×10^3 N	3.05×10^4 N

Table 6.9 - Summary of Response to El Centro Time History (Adaptive Control)

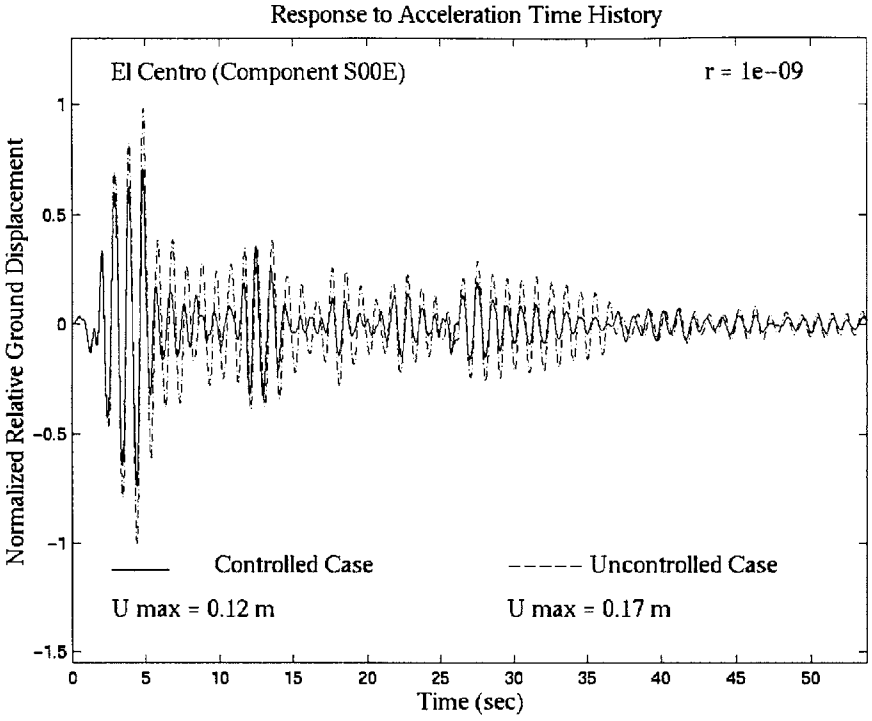

Figure 6.4 – Response to El Centro Time History, r = 1 x 10^{-9} (Adaptive Control)

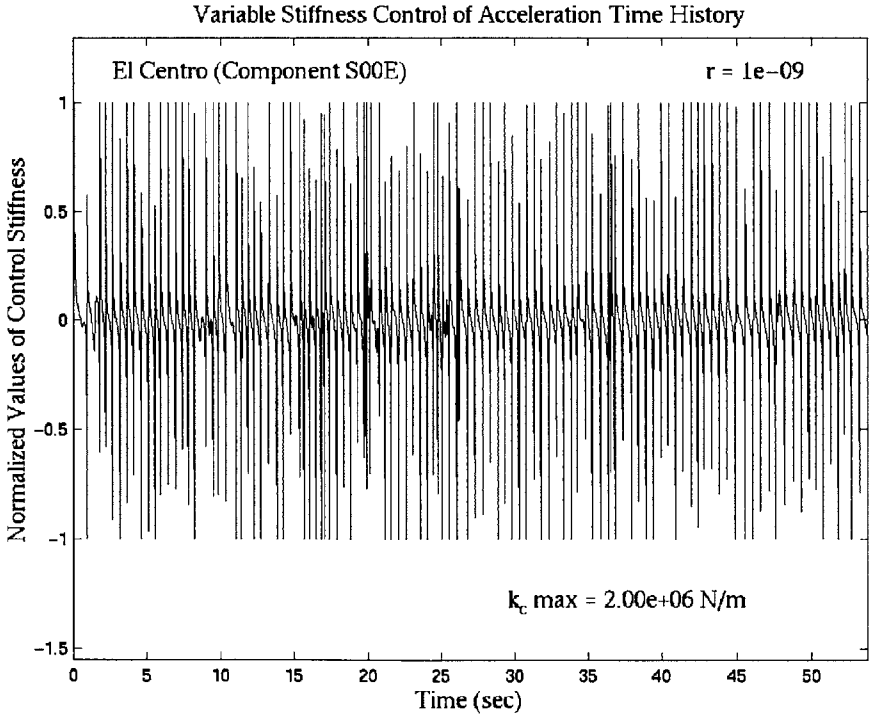

Figure 6.5 – Time History of Variable Stiffness for El Centro Excitation, r = 1 x 10^{-9}

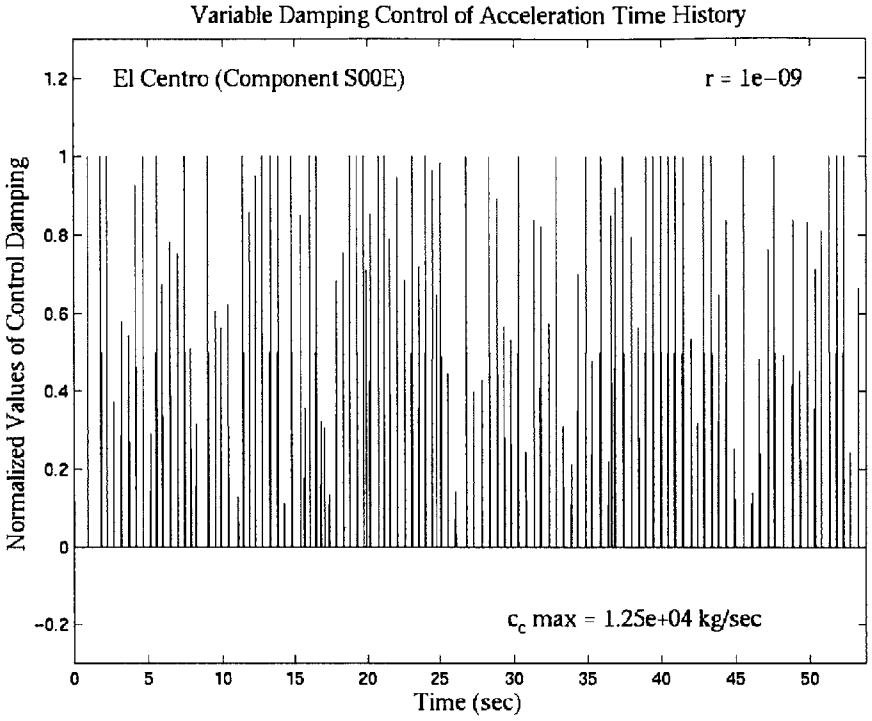

Figure 6.6 – Time History of Variable Damping for El Centro Excitation, r = 1 x10^{-9}

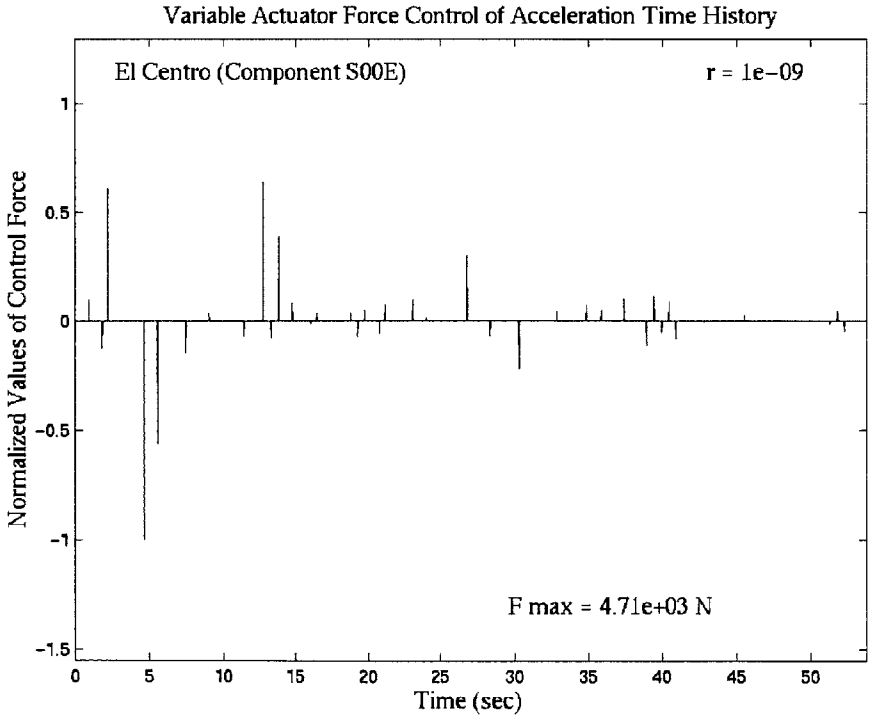

Figure 6.7 – Time History of Control Force for El Centro Excitation, r = 1 x10^{-9}

6.3.7 Stability of the Adaptive Control Algorithm

In reality the adaptive control algorithm is the same as the classic non-adaptive (active) control algorithm, with the exception that the stiffness and damping of the system change at each iteration. In terms of measuring the stability of the system however, the requirement is still that the modulus of the largest eigenvalue of $\left[\overline{A}(i) - \overline{B}(i)K_f(i)\right]$ must be less than 1. For each simulation run above, a plot of the modulus of the eigenvalues at each time step was made, to insure that the algorithm remained stable. These plots can be viewed in Appendix D.

At r = 10^{-7}, the modulus values are close to 0.9975, save for a single spike up to about 0.9997. All values, however, are clearly less than 1. As r is decreased, one can see that the modulus values slowly begin to increase, but at no time are they greater than 1.

6.3.8 Time Delay Effects on the Adaptive Control Algorithm

As was done with the active case, the simulations were manipulated to show how time delay between the determination and application of the control actions would affect the stability of the system. Again, the system was considered to be unstable once the maximum relative displacement of the controlled response was an order of magnitude greater than that of the uncontrolled response. The results are presented in Table 6.9 below. Additional results are in Appendix E.

	Values of Cost Parameter, r				
	10^{-7}	**10^{-8}**	**10^{-9}**	**10^{-10}**	**10^{-11}**
v_{trial}	N/A	N/A	20	13	10
$u_u\|_{max}$	N/A	N/A	0.17 m	0.17 m	0.17 m
$u_c\|_{max}$	N/A	N/A	1.3 m	1.6 m	5.5 x 10^8 m
$v_{predicted}$	23.0-42.6i	23.3-25.3i	23.7-10.4i	14.7	11.0

Table 6.10 - Response of System to Time Delay Effects for Varying r (Adaptive Control)

As in the non-adaptive case, time delay did not appear to impact the system for r = 10^{-7} and r = 10^{-8}. In general, the values of v found from the trial methods corresponded closely with those

for the non-adaptive case. (See Table 6.6.) The values of $v_{predicted}$ shown are based on the "normal" system parameters of m = 50,000 kg, c = 12,500 kg/sec and k = 2,000,000 N/m, but in reality these values should change with every iteration, since the stiffness and damping are constantly changing. But because the adaptive system loses control at roughly the same time delay values as the non-adaptive system, it appears that on average the adaptive system behaves in the same manner as the non-adaptive system.

7 Summary and Conclusions

7.1 Discussion

As the expectations of structural performance under extreme loads become higher, non-adaptive and adaptive control systems will play a major role in achieving the desired performance results. In their present state, most non-adaptive control systems have the problem of being too expensive and too cumbersome to implement to provide a practical solution. As a result, they have been used in very limited applications.

With adaptive control however, the solutions become much more feasible. By using low energy devices that can alter a structure's stiffness or damping, or produce low level actuator forces, one can provide a level of control that is equal to that of non-adaptive control. Furthermore, the components for adaptive control systems are usually much smaller than those used in non-adaptive systems. And because adaptive systems are much less susceptible to the power problems and questions about robustness that plague active systems, the engineering community should be more willing to incorporate adaptive control systems into practice.

7.2 Further Development

Establishment of adaptive control systems as an integral part of structural systems is a very realistic goal for the near future. The demand for control exists but acceptance of the solution will require risk-taking and proving of the technology. Devices such as active variable stiffness systems and active variable damping systems have been shown to work at the experimental level, but what is needed is more experiments at larger scales, to bring the technology into the mainstream, and show that adaptive control makes sense. Slowly adaptive control systems will become incorporated into full-scale civil engineering structures, to provide the benefits of which they are capable.

Appendix A

Active Control for Sinusoidal Ground Motion

```
%     Michael Cusack

%       var_damp.m

%       input:                sinusoidal ground motion
%       control algorithm:    classical

syms i; syms m; syms c; syms delta_t; syms r; syms t; syms k;

k = 2000000;              % (N/m)        stiffness of structure
m = 50000;                % (kg)         mass of structure
c = 12500;                % (kg/s)       damping coefficient
delta_t = 0.02;           % (sec)        time-step duration
r = 0;                    %              weighting/cost parameter
omega = 6.28;             % (rad/sec)    forcing frequency
a_ground_max = 9.81;      % (m/sec^2)    maximum ground acceleration

w_n = (k/m)^(1/2);        % natural frequency of structure
zeta = c/(2*w_n*m);       % damping fraction of structure
rho = omega/w_n;          % ratio of forcing to natural frequency

A = [0, 1; -k/m, -c/m];   % Coefficient matrices for state-space
B = [0; 1/m];             %  representation of system
D = [0; 1/m];             %

Q = [0, 0; 0, 1];         % weighting/cost parameter
R = r;                    % weighting/cost parameter

Abar = expm(A*delta_t);                      % A integrated over time step
Bbar = eval(int(expm(A*t),t,0,delta_t)*B); % B integrated over time step
Dbar = eval(int(expm(A*t),t,0,delta_t)*D); % D integrated over time step

num_trials = 1500;                          % number of iterations
x=(0:num_trials)';                          % time step values
U_controlled = zeros(num_trials+1,1);       % controlled response values
U_uncontrolled = zeros(num_trials+1,1);     % uncontroled response values
F_control = zeros(num_trials+1,1);          % control force values
C_viscous = zeros(num_trials+1,1);     % viscous damping parameter values

H2 = ( rho^4 / ( (1-rho^2)^2 + 4*zeta^2*rho^2 ) )^(1/2);
                                            % dyn response factor
u_ground_max = -a_ground_max/omega^2;       % maximum ground displacement
u_rel_max = H2*u_ground_max;                % maximum relative
displacement
delta = - atan(2*zeta*rho / (1 - rho^2)); % phase shift of response

U_i_c = [0; 0];      % initial conditions for controlled case
U_i_u = [0; 0];      % initial conditions for uncontrolled case

[X,L,G,RR] = dare(Abar,Bbar,Q,R);   % Ricatti Equation with solution [X]

for i = 0 : 1 : num_trials

      time = i*delta_t;
      a_ground_i = a_ground_max*sin(omega*time);
      F_ground_i = -m*a_ground_i;
```

```
        % Uncontrolled case:

        U_i1_u = Abar*U_i_u + Dbar*F_ground_i;
        U_i_u = U_i1_u;

        F_control_i1 = -[0, G(2)]*U_i_c;    %  control force at time i+1

        U_i1_c = Abar*U_i_c + Bbar*F_control_i1 + Dbar*F_ground_i;
        U_i_c = U_i1_c;

        x(i+1) = time;
        U_controlled(i+1) = U_i1_c(1);
        U_uncontrolled(i+1) = U_i1_u(1);
        F_control(i+1) = F_control_i1;

end

j = size(U_uncontrolled);
j = j(1);
U_max_u = 0;
U_max_c = 0;

for i = 1 : 1 : j
        if(abs(U_uncontrolled(i)) > U_max_u & U_uncontrolled(i) ~= Inf)
          U_max_u = abs(U_uncontrolled(i));
        end
        if(abs(U_controlled(i)) > U_max_c & U_controlled(i) ~= Inf)
          U_max_c = abs(U_controlled(i));
        end
end

for i = 1 : 1 : j
        U_controlled(i) = U_controlled(i) / U_max_u;
        U_uncontrolled(i) = U_uncontrolled(i) / U_max_u;
end

F_max = 0;

for i = 1 : 1 : j
        if(abs(F_control(i)) > F_max & F_control(i) ~= Inf)
        F_max = abs(F_control(i));
      end
end

for i = 1 : 1 : j
        F_control(i) = F_control(i) / F_max;
end

figure

whitebg('white');

plot(x, U_controlled, 'black',x, U_uncontrolled, '-.black');
xlabel('\fontname{times} Time (sec)','FontSize',14);
ylabel('\fontname{times}Normalized Relative Ground
Displacement','FontSize',14);
text(0.55*x(num_trials+1),1.15,'\fontname{times}r = 0.0','FontSize',14);
text(0.05*x(num_trials+1),-1.06,'_____','FontSize',14);
text(0.18*x(num_trials+1),-1.1,'\fontname{times}Controlled
Case','FontSize',14);
text(0.05*x(num_trials+1),-1.3,'\fontname{times}U max = 0.05
m','FontSize',14);
text(0.55*x(num_trials+1),-1.1,'\fontname{times}----- Uncontrolled
Case','FontSize',14);
```

```
text(0.55*x(num_trials+1),-1.3,'\fontname{times}U max = 5.84
m','FontSize',14);
title('\fontname{times}Response to Sinusoidal Ground
Motion','FontSize',14);
axis([0 x(num_trials) -1.55 1.3]);

figure

plot(x,F_control,'black');
xlabel('\fontname{times}Time (sec)','FontSize',14);
ylabel('\fontname{times}Normalized Control Force','FontSize',14);
text(0.35*x(num_trials+1),1.45,'\fontname{times}Sinusoidal Ground
Motion','FontSize',14);
text(0.35*x(num_trials+1),1.15,'\fontname{times}r = 0.0','FontSize',14);
text(0.35*x(num_trials+1),1.3,'\fontname{times}F max = 5.22e+05
N','FontSize',14);
title('\fontname{times}Values of Control Force','FontSize',14);
axis([0 x(num_trials) -1.6 1.6]);
```

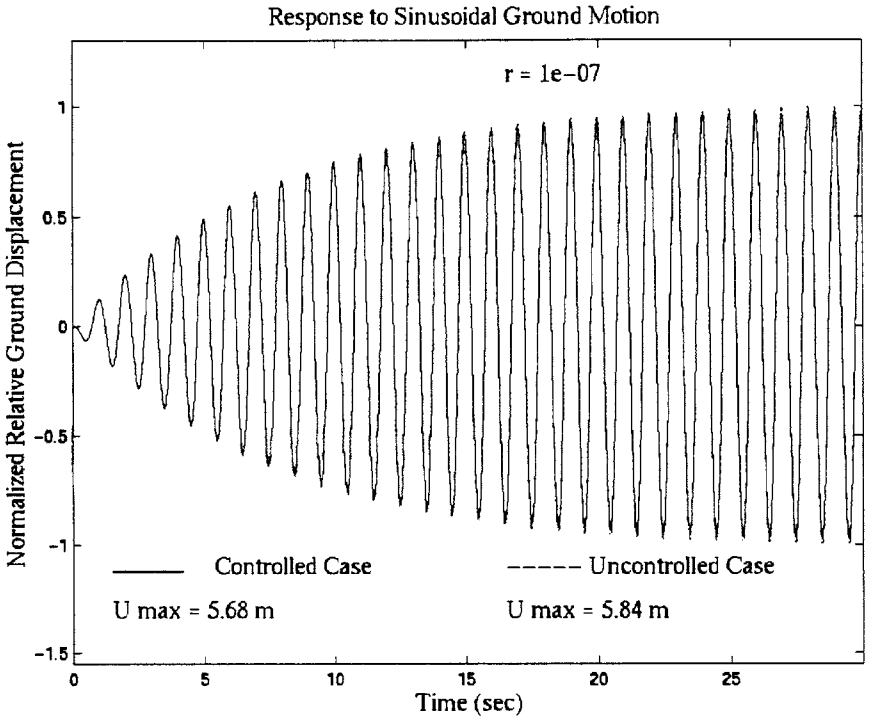

Figure A1 – Response to Sinusoidal Ground Motion, r = 1 x 10^{-7}

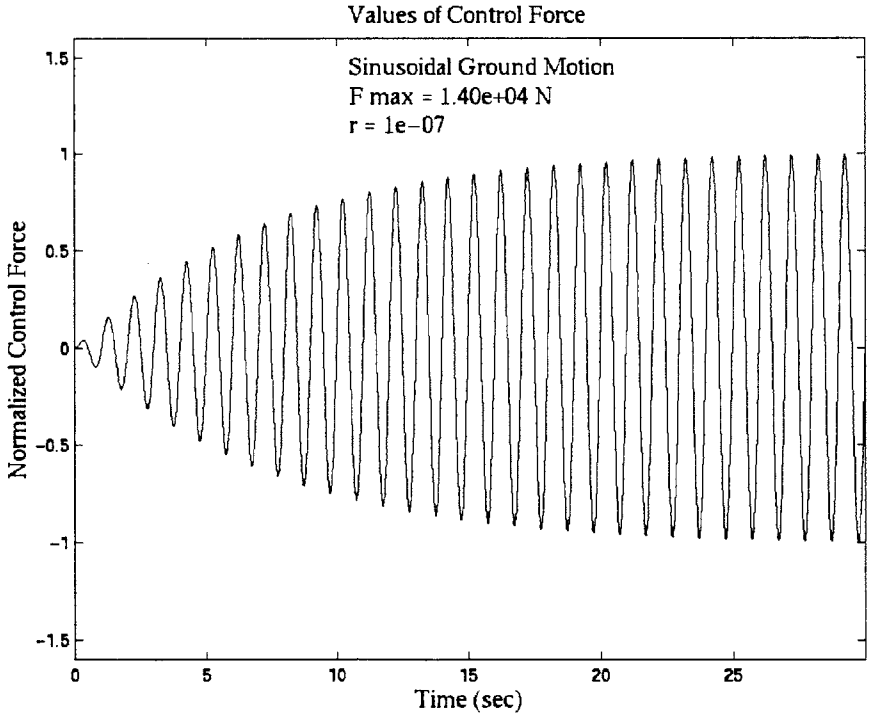

Figure A2 – Time History of Control Force for Sinusoidal Ground Motion, r = 1 x 10^{-7}

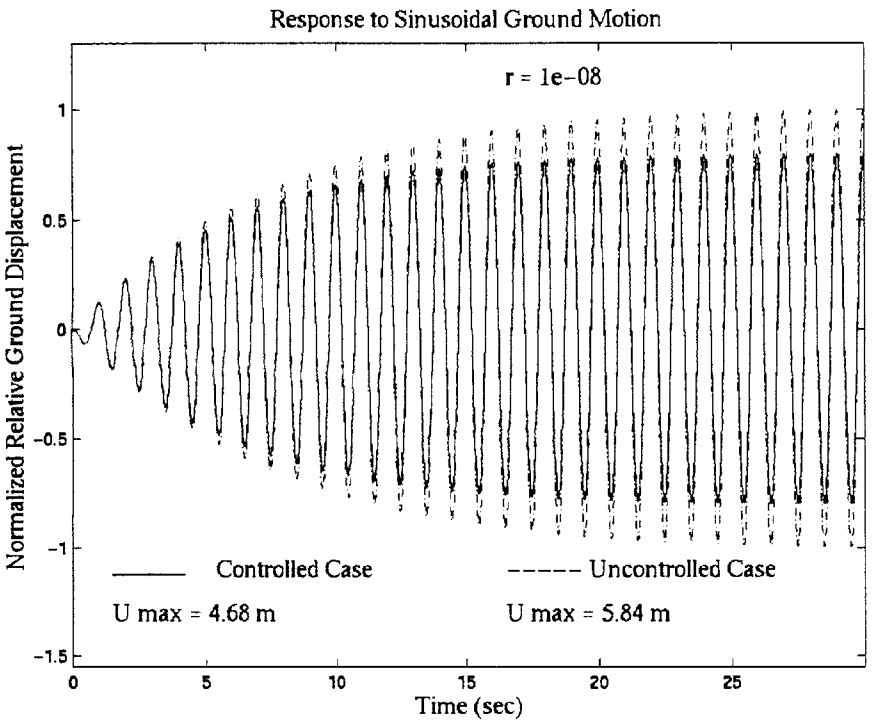

Figure A3 – Response to Sinusoidal Ground Motion, r = 1 x 10^{-8}

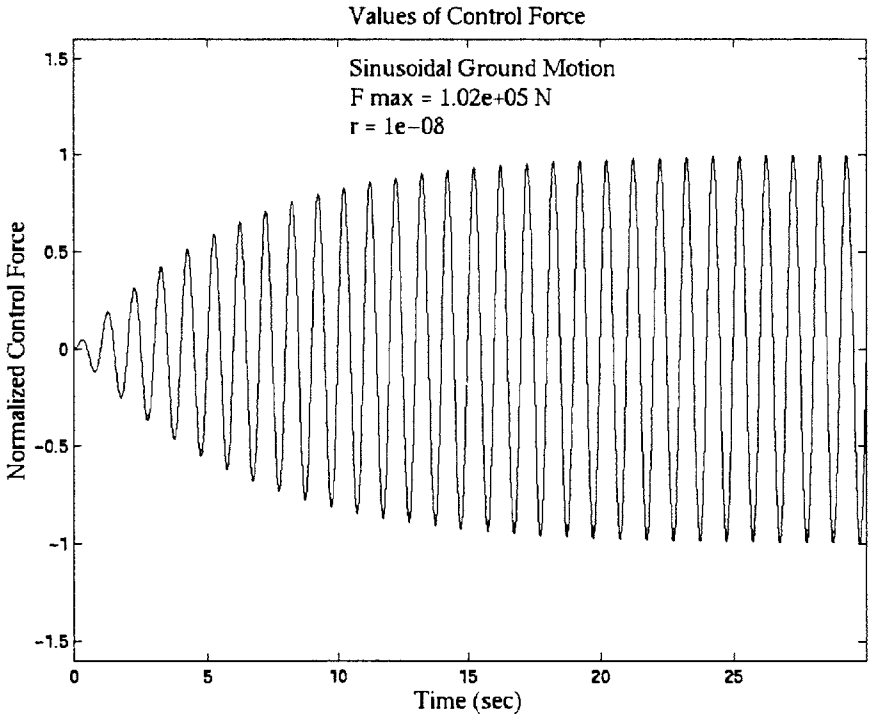

Figure A4 – Time History of Control Force for Sinusoidal Ground Motion, r = 1 x 10^{-8}

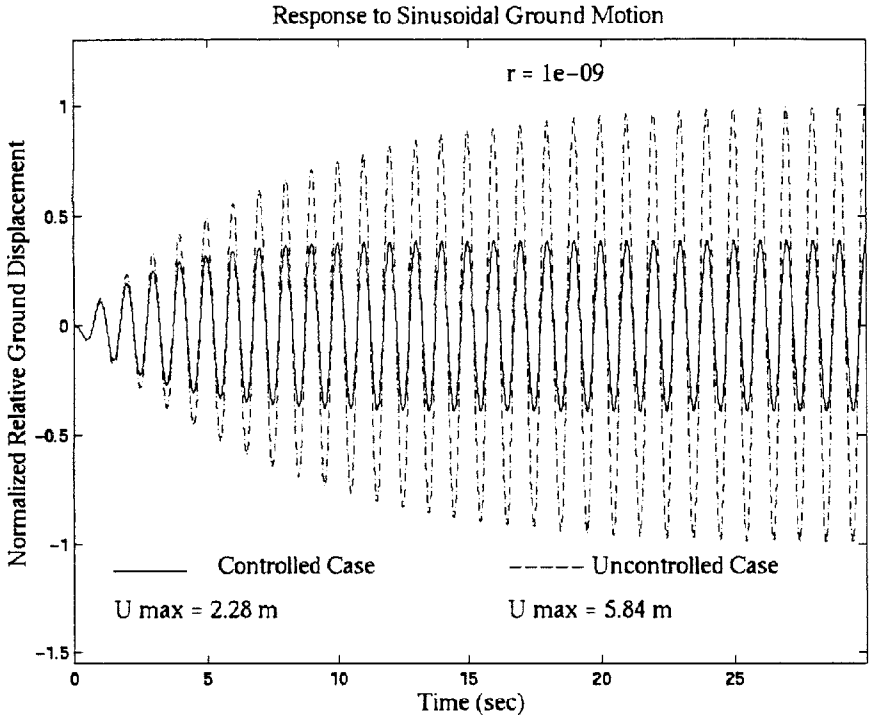

Figure A5 – Response to Sinusoidal Ground Motion, r = 1 x 10^{-9}

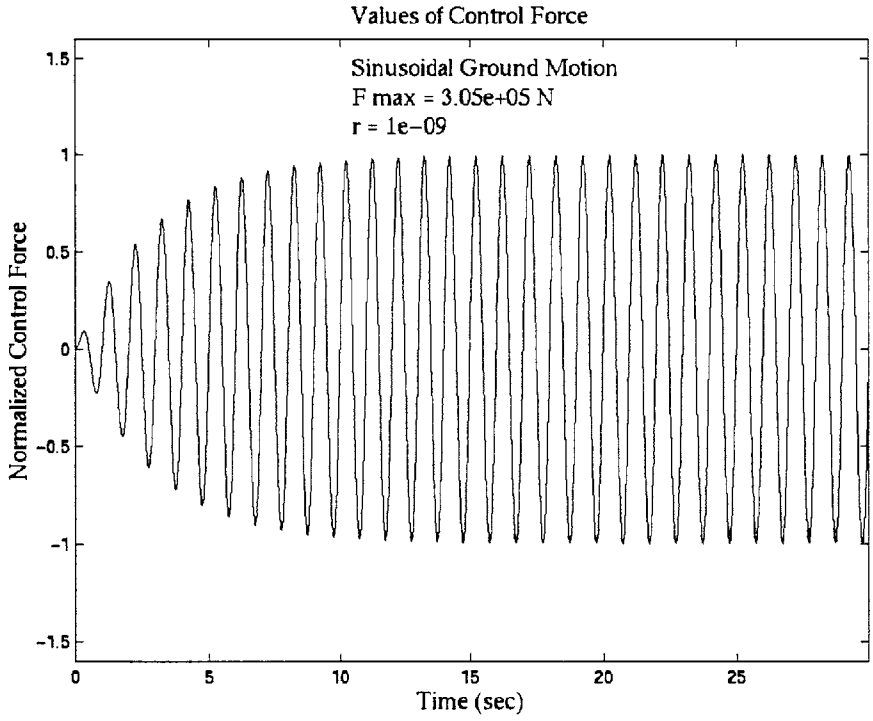

Figure A6 – Time History of Control Force for Sinusoidal Ground Motion, r = 1 x 10^{-9}

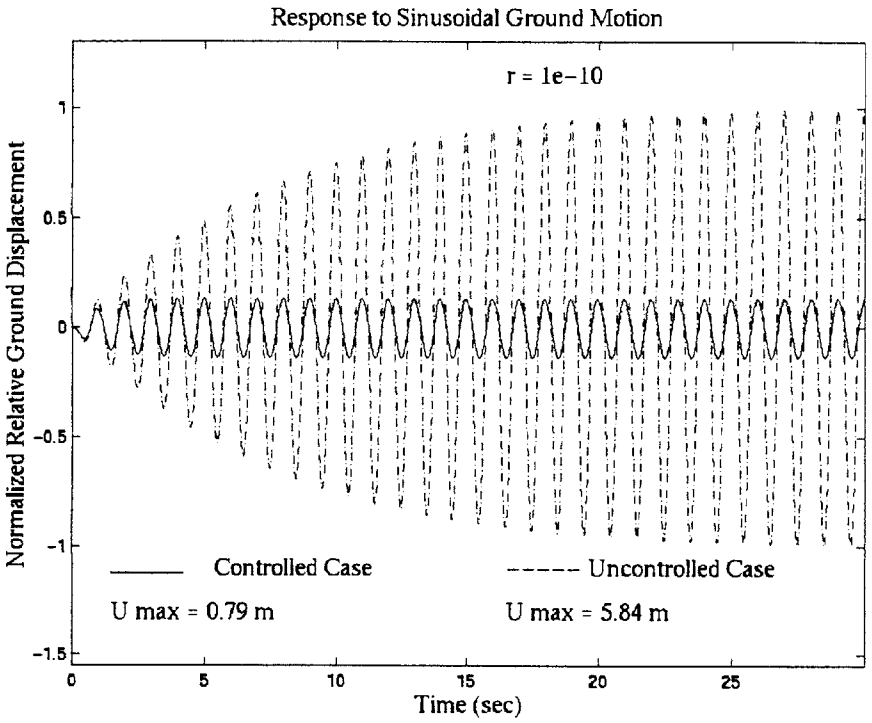

Figure A7 – Response to Sinusoidal Ground Motion, r = 1 x 10^{-10}

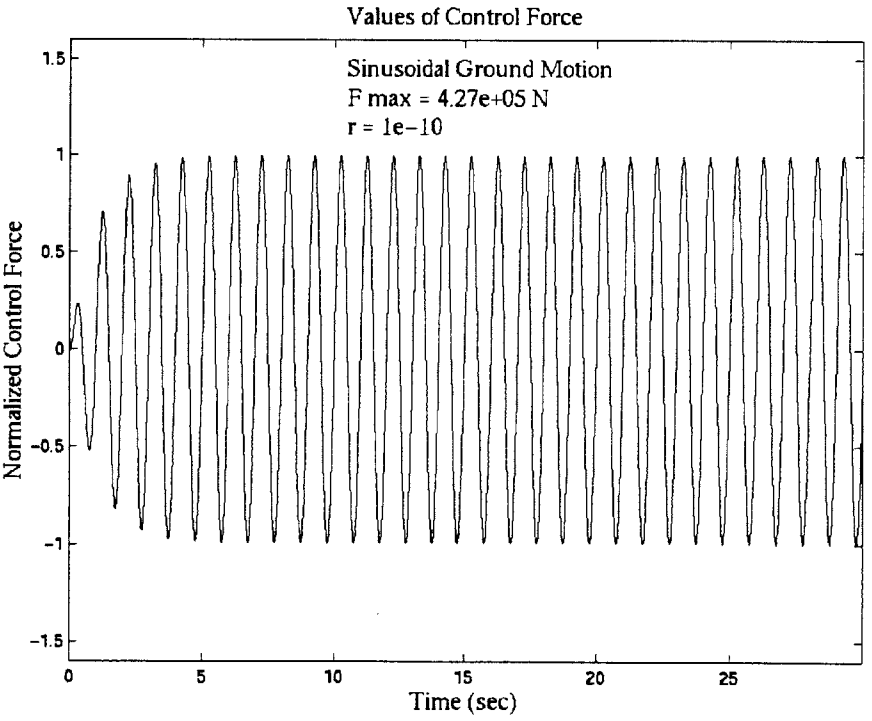

Figure A8 – Time History of Control Force for Sinusoidal Ground Motion, r = 1 x 10^{-10}

Appendix B

Active Control for Earthquake Time Histories

```
%     Michael Cusack

%       var_damp_2a.m

%       input:                earthquake accleration time history
%       control alogrithm:    classical

%       Response Approximation Methods

%       controlled:    discrete time state equation
%       uncontrolled:  discrete time state equation (w/o control force)

syms i; syms m; syms c; syms delta_t; syms r; syms t; syms k;

k = 2000000;              % (N/m)          stiffness of structure
m = 50000;                % (kg)           mass of structure
c = 12500;                % (kg/s)         damping coefficient
delta_t = 0.02;           % (sec)          time-step duration
r = 1e-10;                %                weighting/cost parameter

w_n = (k/m)^(1/2);        % natural frequency of structure
zeta = c/(2*w_n*m);       % damping fraction of structure

A = [0, 1; -k/m, -c/m]; %  These matrices are used in writing the
B = [0; 1/m];           %  state equation for the structure:
D = [0; 1/m];           %  U_i1 = A*U_i + B*F_control_i1 + D*F_ground_i

Q = [0, 0; 0, 1];         % weighting/cost parameter
R = r;                    % weighting/cost parameter

Abar = expm(A*delta_t);                      % A integrated over time step
Bbar = eval(int(expm(A*t),t,0,delta_t)*B); % B integrated over time step
Dbar = eval(int(expm(A*t),t,0,delta_t)*D); % D integrated over time step

[X,L,G,RR] = dare(Abar,Bbar,Q,R);  %  Ricatti Equation with solution [X]

filename = 'Taft_Lincoln_School_Tunnel_Comp_N21E';
quake_title = '\fontname{times}Taft Lincoln School Tunnel (Comp. N21E)';
fid = fopen(filename);                       % time history of acceleration
accel_data = fscanf(fid,'%g %g',[2 inf]); % values
accel_data = accel_data';                    %
fclose(fid);                                 %

num_trials = size(accel_data);
num_trials = num_trials(1) - 2;

x=(0:num_trials)';                           % time step values
U_controlled = zeros(num_trials+1,1);        % controlled response values
U_uncontrolled = zeros(num_trials+1,1);      % uncontroled response values
F_control = zeros(num_trials+1,1);           % control force values

U_i_c = [0; 0];      % initial conditions for controlled case
U_i_u = [0; 0];      % initial conditions for uncontrolled case

for i = 0 : 1 : num_trials

      time = i*delta_t;
```

```
      a_ground_i = accel_data(i+1, 2);
      F_ground_i = -m*a_ground_i;
      F_ground_i1 = -m*accel_data(i+2, 2);

      % Uncontrolled case:

      U_i1_u = Abar*U_i_u + Dbar*F_ground_i;
      U_i_u = U_i1_u;

      % Controlled Case

      F_control_i1 = -[0, G(2)]*U_i_c;    %  control force at time i+1

      U_i1_c = Abar*U_i_c + Bbar*F_control_i1 + Dbar*F_ground_i;
      U_i_c = U_i1_c;

      x(i+1) = time;
      U_controlled(i+1) = U_i1_c(1);
      U_uncontrolled(i+1) = U_i1_u(1);
      F_control(i+1) = F_control_i1;
end

j = size(U_uncontrolled);
j = j(1) - 1;
U_max_u = 0;
U_max_c = 0;
for i = 1 : 1 : j
        if(abs(U_uncontrolled(i)) > U_max_u & U_uncontrolled(i) ~= Inf)
        U_max_u = abs(U_uncontrolled(i));
      end
        if(abs(U_controlled(i)) > U_max_c & U_controlled(i) ~= Inf)
        U_max_c = abs(U_controlled(i));
      end
end

for i = 1 : 1 : j
        U_controlled(i) = U_controlled(i) / U_max_u;
        U_uncontrolled(i) = U_uncontrolled(i) / U_max_u;
end

F_max = 0;

for i = 1 : 1 : j
        if(abs(F_control(i)) > F_max & F_control(i) ~= Inf)
        F_max = abs(F_control(i));
      end
end

for i = 1 : 1 : j
        F_control(i) = F_control(i) / F_max;
end

figure

whitebg('white');

plot(x, U_controlled, 'black',x, U_uncontrolled, '-.black');
xlabel('\fontname{times} Time (sec)','FontSize',14);
ylabel('\fontname{times}Normalized Relative Ground
Displacement','FontSize',14);
text(0.05*x(num_trials+1),1.15,quake_title,'FontSize',14);
text(0.8*x(num_trials+1),1.15,'\fontname{times}r = 1e-
10','FontSize',14);
text(0.05*x(num_trials+1),-1.06,'_____','FontSize',14);
```

```
text(0.18*x(num_trials+1),-1.1,'\fontname{times}Controlled
Case','FontSize',14);
text(0.05*x(num_trials+1),-1.3,'\fontname{times}U max = 0.05
m','FontSize',14);
text(0.55*x(num_trials+1),-1.1,'\fontname{times}----- Uncontrolled
Case','FontSize',14);
text(0.55*x(num_trials+1),-1.3,'\fontname{times}U max = 0.03
m','FontSize',14);
title('\fontname{times}Response to Acceleration Time
History','FontSize',14);
axis([0 x(num_trials+1) -1.55 1.3]);

figure

plot(x,F_control,'black');
xlabel('\fontname{times}Time (sec)','FontSize',14);
ylabel('\fontname{times}Normalized Control Force','FontSize',14);
text(0.05*x(num_trials+1),1.23,quake_title,'FontSize',14);
text(0.7*x(num_trials+1),1.09,'\fontname{times}r = 1e-
10','FontSize',14);
text(0.05*x(num_trials+1),1.09,'\fontname{times}F max = 1.82e+04
N','FontSize',14);
title('\fontname{times}Values of Control Force','FontSize',14);
axis([0 x(num_trials+1) -1.2 1.4]);
```

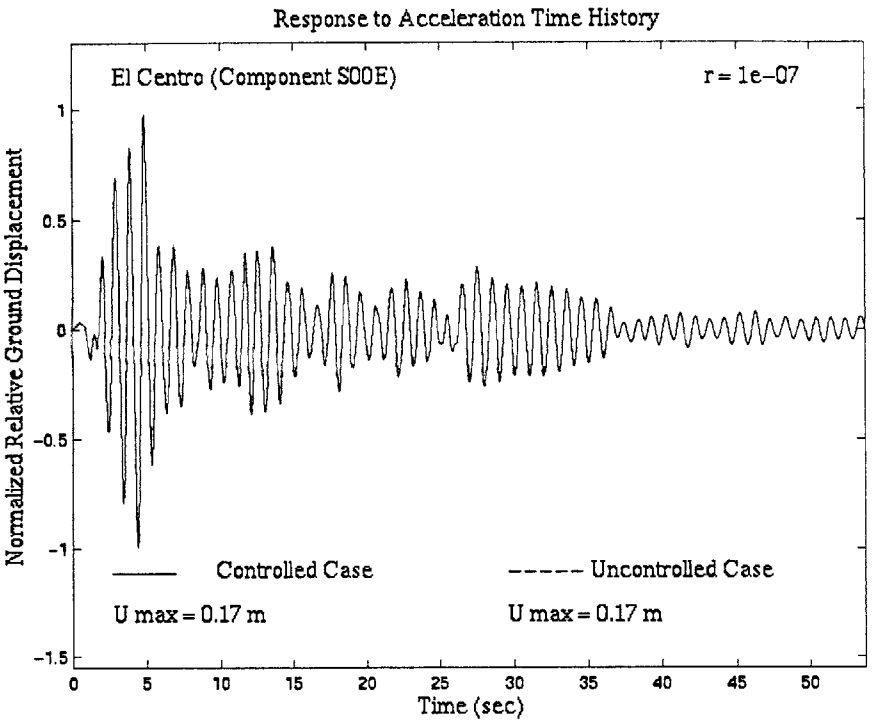

Figure B1 – Response to El Centro Time History, r = 1 x 10^{-7}

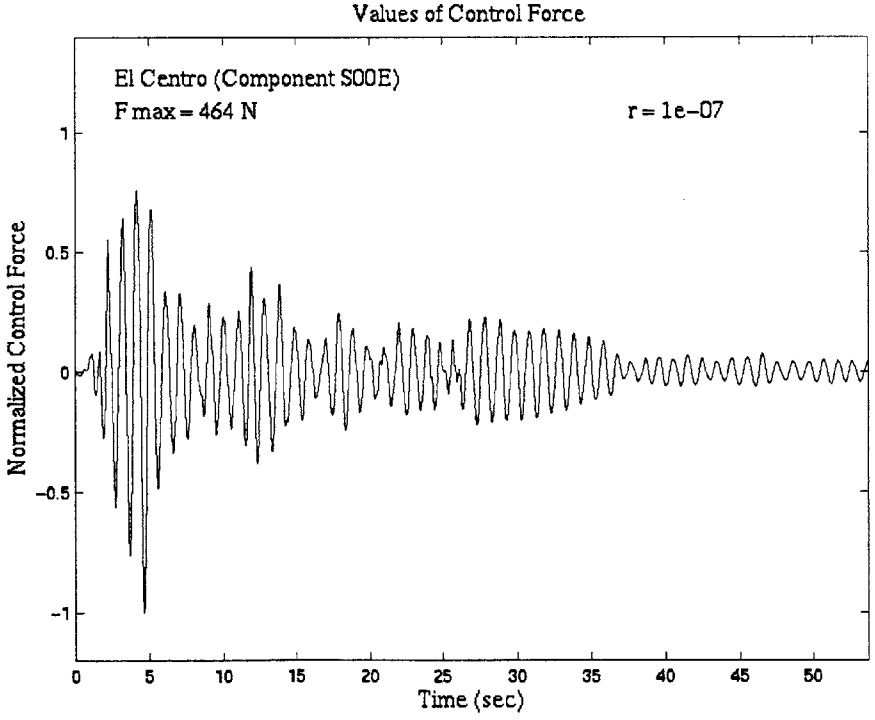

Figure B2 – Time History of Control Force for El Centro Excitation, r = 1 x 10^{-7}

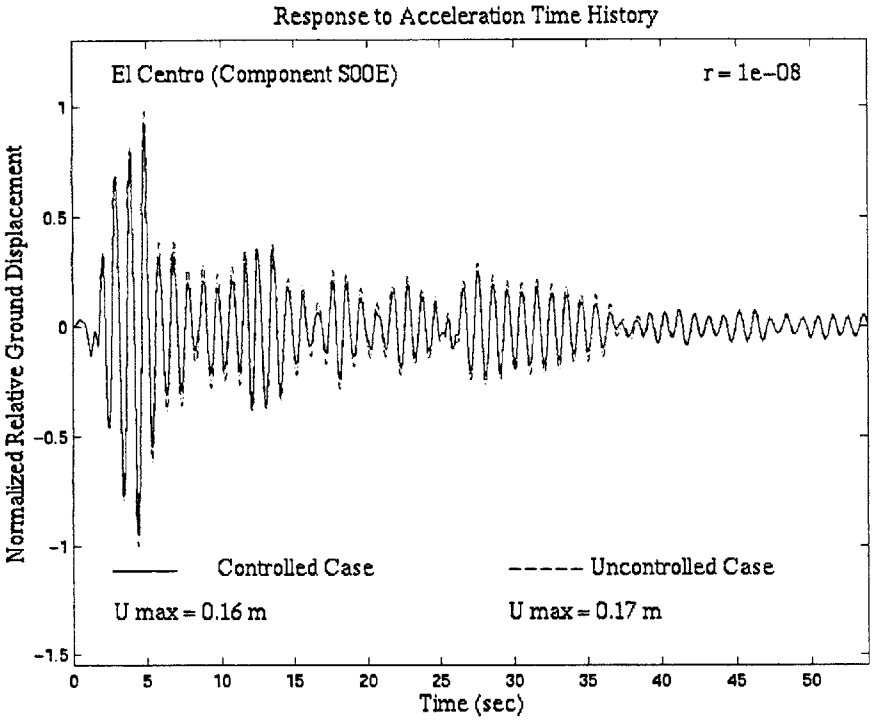

Figure B3 – Response to El Centro Time History, r = 1 x 10^{-8}

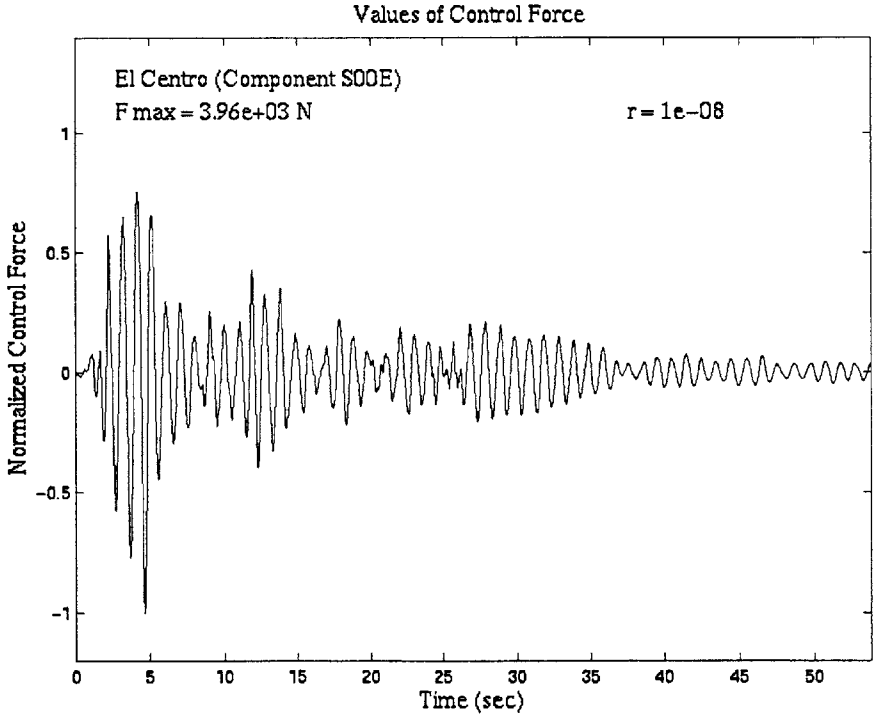

Figure B4 – Time History of Control Force for El Centro Excitation, r = 1 x 10^{-8}

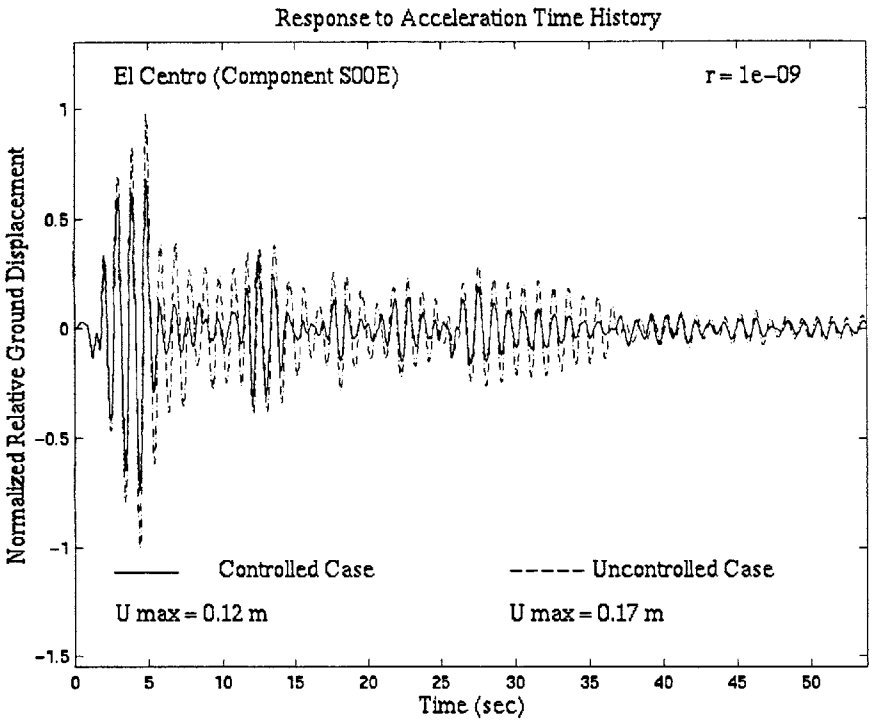

Figure B5 – Response to El Centro Time History, r = 1 x 10^{-9}

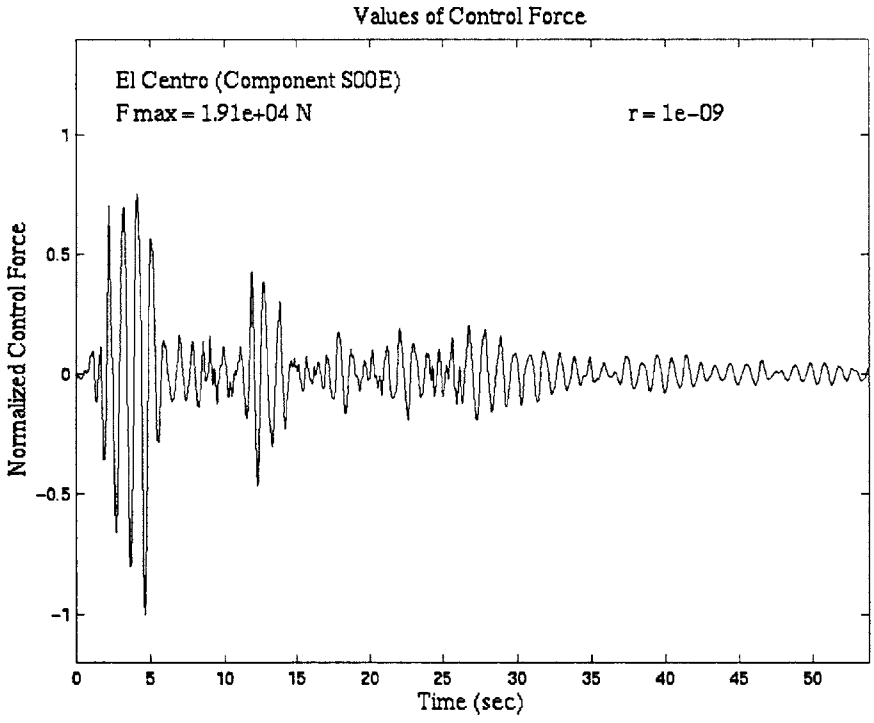

Figure B6 – Time History of Control Force for El Centro Excitation, r = 1 x 10^{-9}

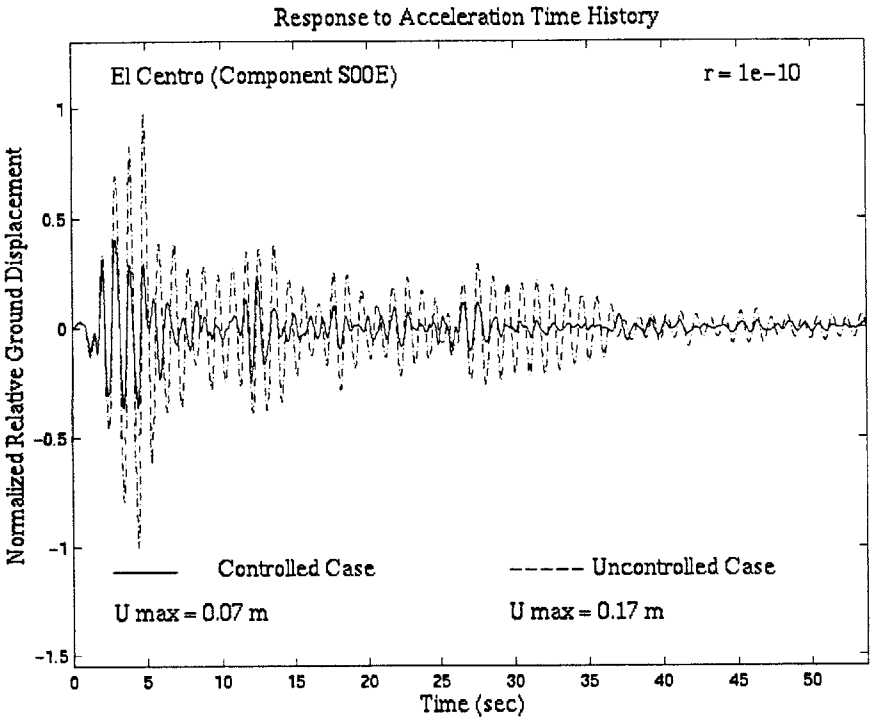

Figure B7 – Response to El Centro Time History, r = 1 x 10^{-10}

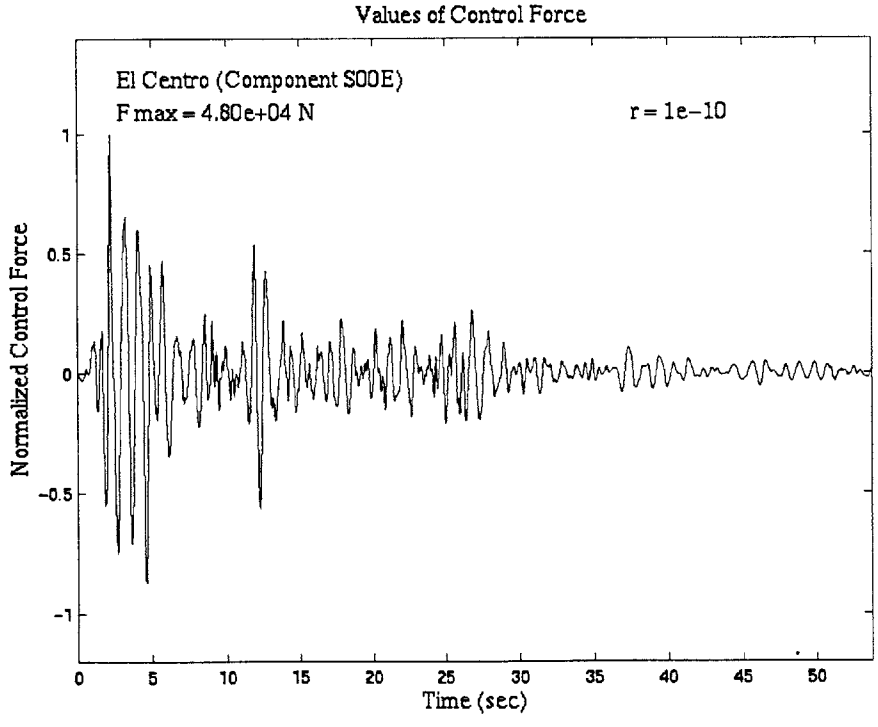

Figure B8 – Time History of Control Force for El Centro Excitation, r = 1 x 10^{-10}

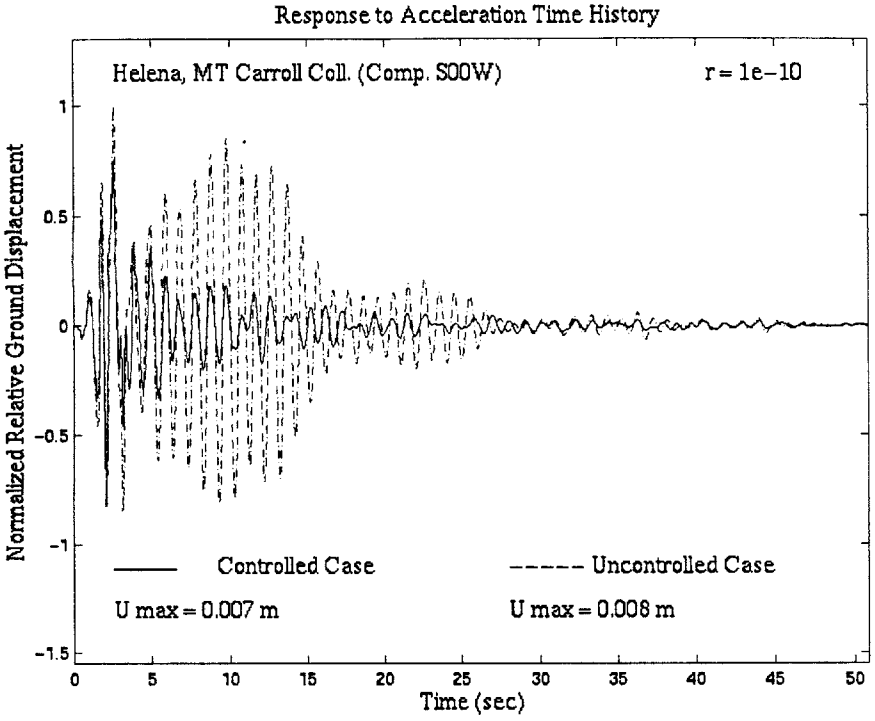

Figure B9 – Response to Helena, MT Carroll College Time History

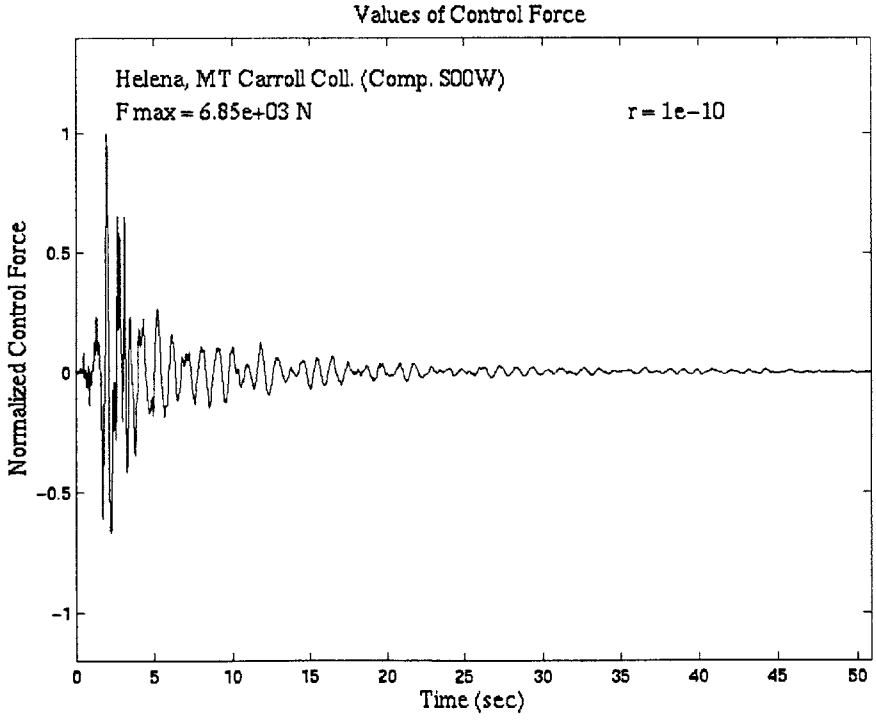

Figure B10 – Time History of Control Force for Helena, MT Carroll College Excitation

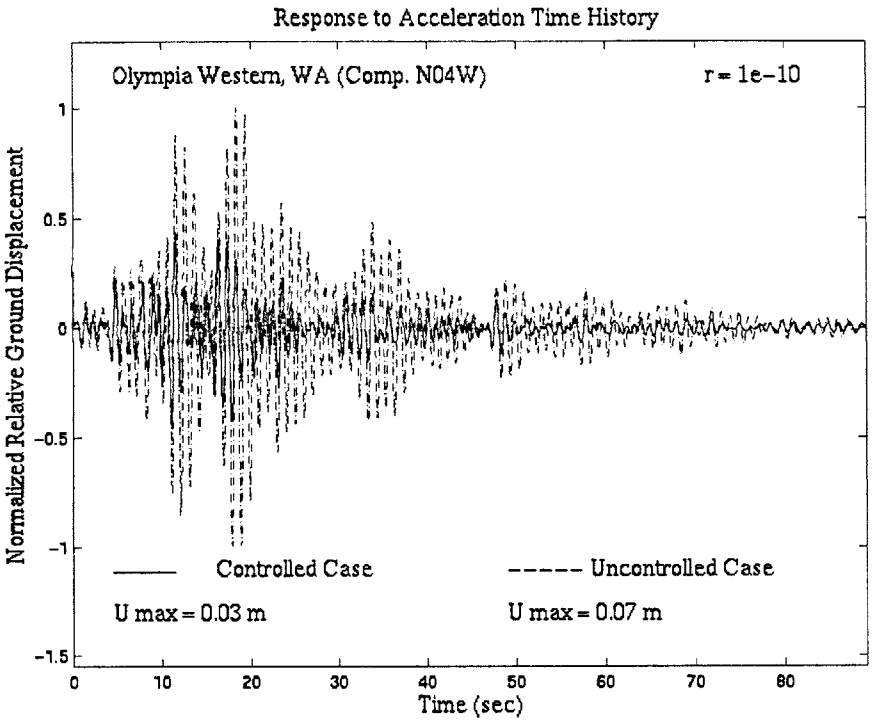

Figure B11 – Response to Olympia Western, WA Time History

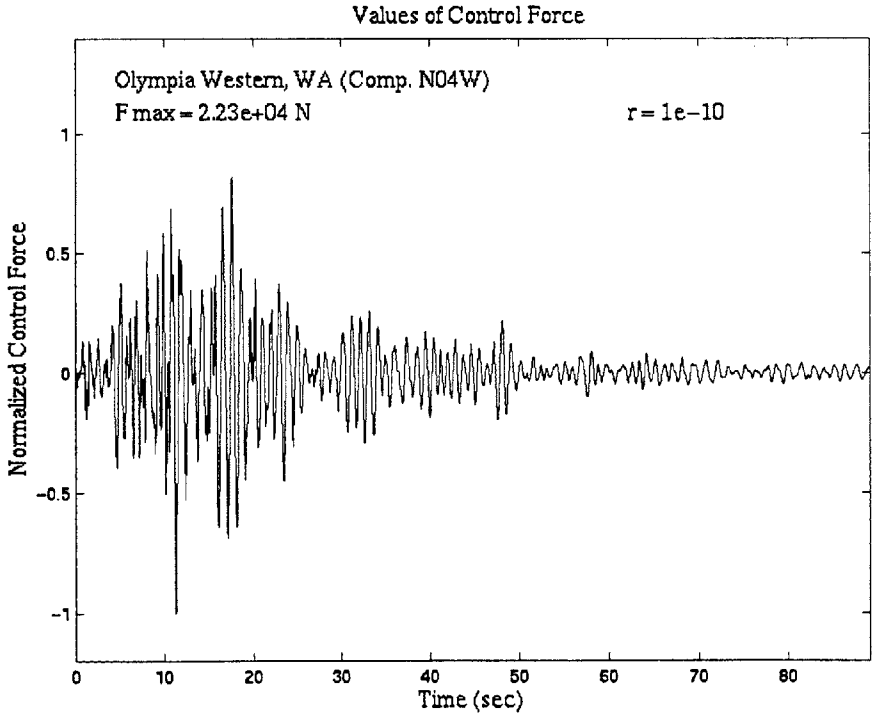

Figure B12 – Time History of Control Force for Olympia Western, WA Excitation

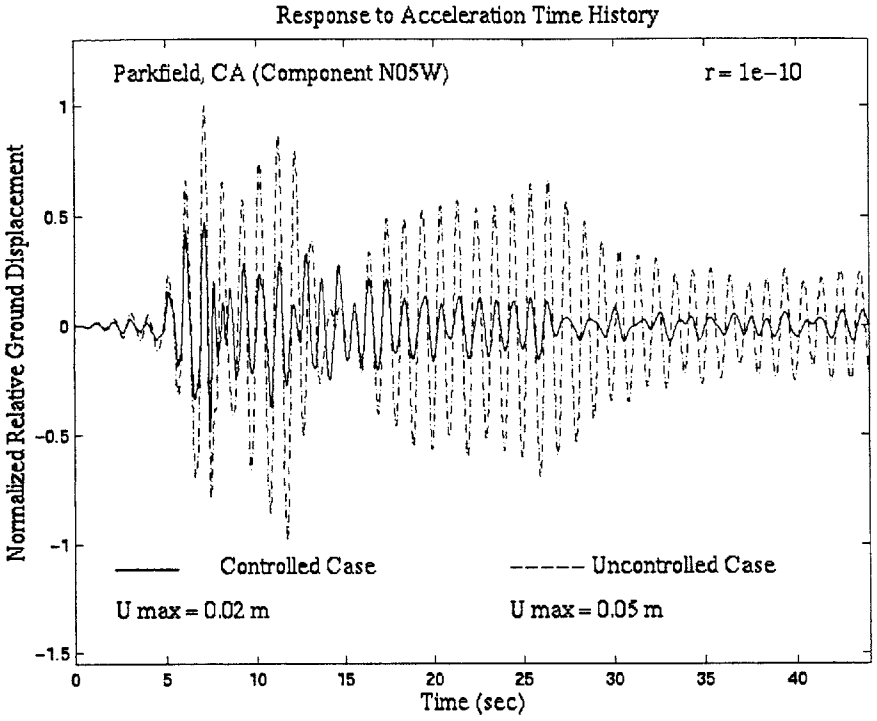

Figure B13 – Response to Parkfield, CA Time History

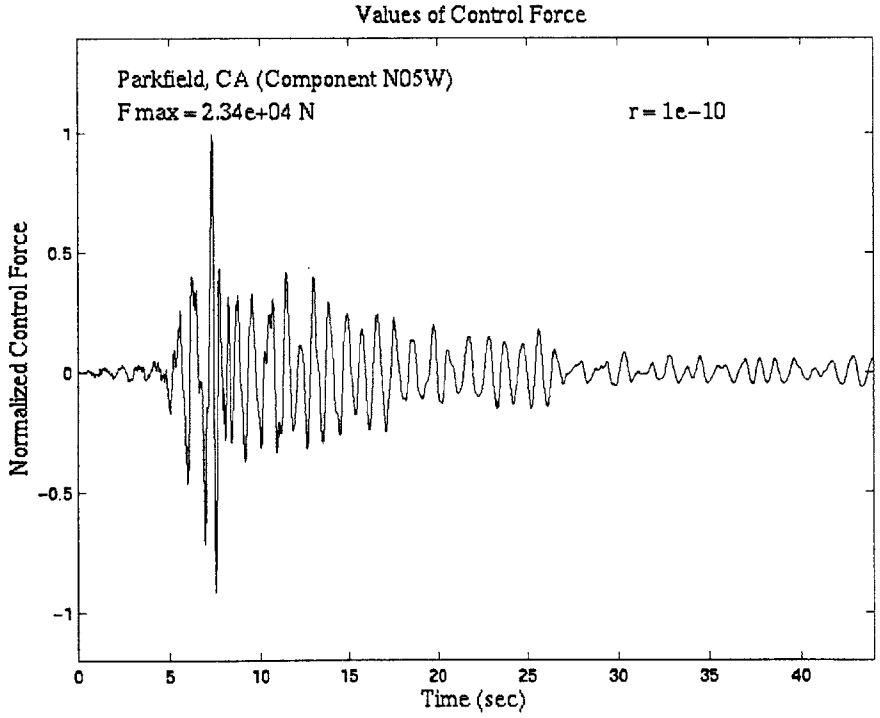

Figure B14 – Time History of Control Force for Parkfield, CA Excitation

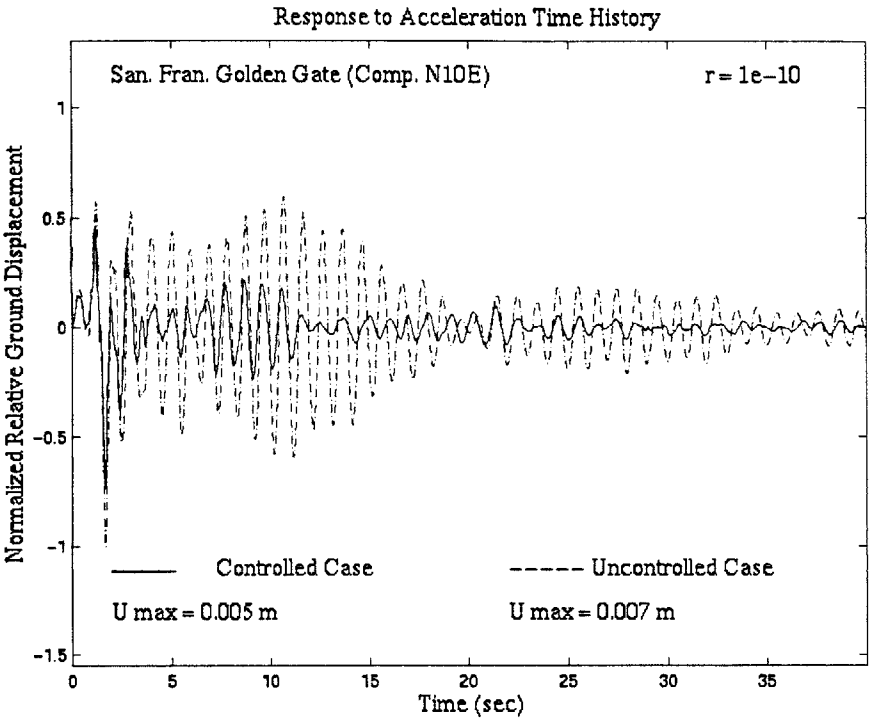

Figure B15 – Response to San Francisco Golden Gate Time History

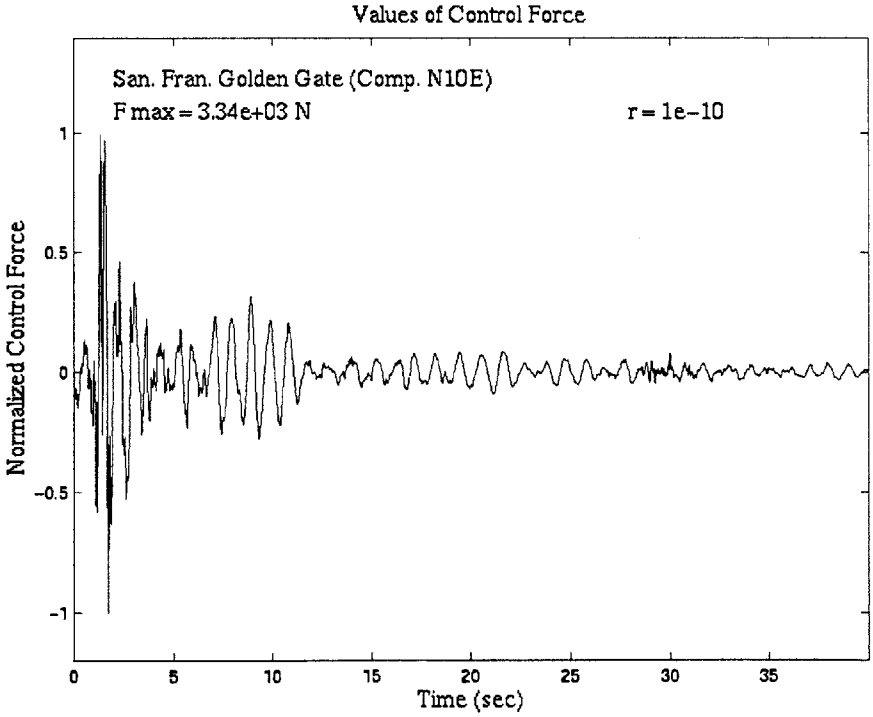

Figure B16 – Time History of Control Force for San Francisco Golden Gate Excitation

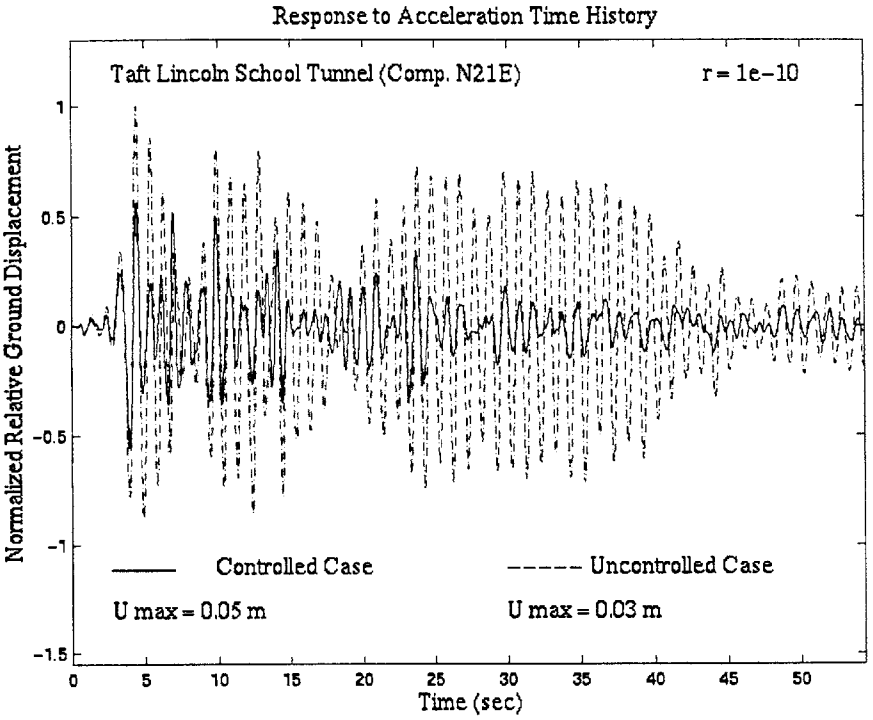

Figure B17 – Response to Taft Lincoln School Tunnel Time History, r = 1 x 10^{-10}

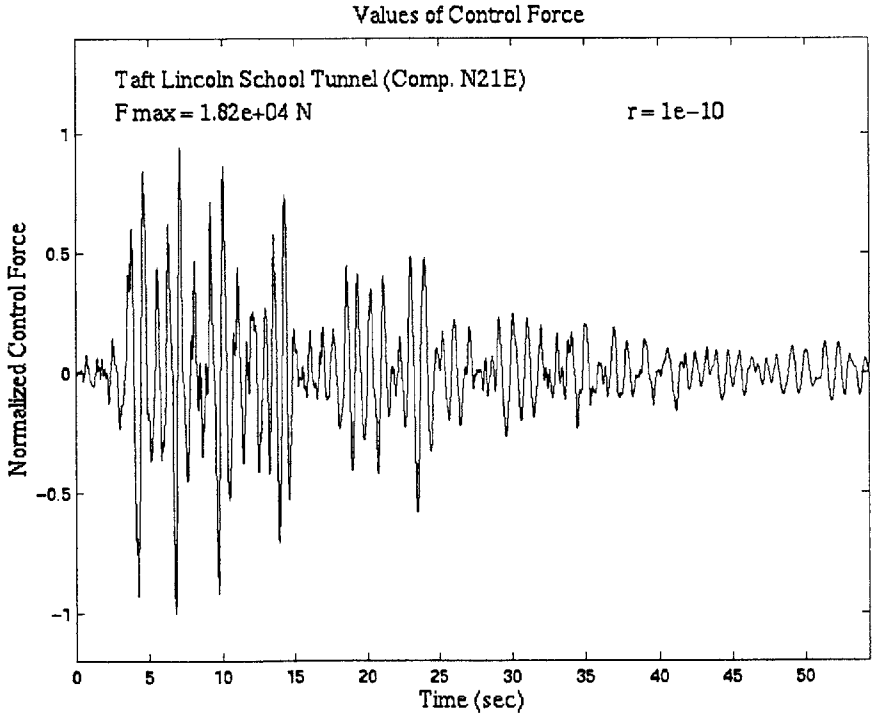

Figure B18 – Time History of Control Force for Taft Lincoln School Tunnel Excitation

Appendix C

Active Control with Time Delay

```
%     Michael Cusack

%       var_damp_2b.m

%       input:                earthquake accleration time history
%       control alogrithm:    classical

%       Response Approximation Methods

%       controlled:     discrete time state equation
%       uncontrolled:   discrete time state equation (w/o control force)

% *********************  TIME DELAY EFFECTS  ***************************

syms i; syms m; syms c; syms delta_t; syms r; syms t; syms k;

k = 2000000;                    % (N/m)          stiffness of structure
m = 50000;                      % (kg)           mass of structure
c = 12500;                      % (kg/s)         damping coefficient
delta_t = 0.02;                 % (sec)          time-step duration
r = 0;                          %                weighting/cost parameter

w_n = (k/m)^(1/2);              % natural frequency of structure
zeta = c/(2*w_n*m);             % damping fraction of structure
c_viscous_max = 2.0e7;          % max. allowable damping coefficient

A = [0, 1; -k/m, -c/m];         %  These matrices are used in writing the
B = [0; 1/m];                   %  state equation for the structure:
D = [0; 1/m];                   %  U_i1 = A*U_i + B*F_control_i1 +
D*F_ground_i

Q = [0, 0; 0, 1];               % weighting/cost parameter
R = r;                          % weighting/cost parameter

Abar = expm(A*delta_t);                      % A integrated over time step
Bbar = eval(int(expm(A*t),t,0,delta_t)*B); % B integrated over time step
Dbar = eval(int(expm(A*t),t,0,delta_t)*D); % D integrated over time step

[X,L,G,RR] = dare(Abar,Bbar,Q,R);  %  Ricatti Equation with solution [X]

filename = 'El_Centro_Comp_S00E';
quake_title = '\fontname{times}El Centro (Component S00E)';
fid = fopen(filename);                       % time history of acceleration
accel_data = fscanf(fid,'%g %g',[2 inf]); % values
accel_data = accel_data';                    %
fclose(fid);                                 %

num_trials = size(accel_data);
num_trials = num_trials(1) - 2;

x=(0:num_trials)';                           % time step values
U_controlled = zeros(num_trials+1,1);        % controlled response values
U_uncontrolled = zeros(num_trials+1,1);      % uncontroled response values
F_control = zeros(num_trials+1,1);           % control force values

U_i_c = [0; 0];      % initial conditions for controlled case
U_i_u = [0; 0];      % initial conditions for uncontrolled case
```

```
num_delays = 3;
time_delay = num_delays*delta_t;
F_control_i1 = zeros(num_delays,1);

for i = 0 : 1 : num_trials

      time = i*delta_t;
      a_ground_i = accel_data(i+1, 2);
      F_ground_i = -m*a_ground_i;
      F_ground_i1 = -m*accel_data(i+2, 2);

      % Uncontrolled case:

      U_i1_u = Abar*U_i_u + Dbar*F_ground_i;
      U_i_u = U_i1_u;

      % Controlled Case:

      F_control_i1(num_delays) = -[0, G(2)]*U_i_c;
                                          %  control force at time i+1

      U_i1_c = Abar*U_i_c + Bbar*F_control_i1(1) + Dbar*F_ground_i;
      U_i_c = U_i1_c;

      for j = 1 : 1 : num_delays-1
        F_control_i1(j) = F_control_i1(j+1);
      end

      x(i+1) = time;
      U_controlled(i+1) = U_i1_c(1);
      U_uncontrolled(i+1) = U_i1_u(1);
      F_control(i+1) = F_control_i1(1);
end

j = size(U_uncontrolled);
j = j(1) - 1;
U_max_u = 0;
U_max_c = 0;
for i = 1 : 1 : j
        if(abs(U_uncontrolled(i)) > U_max_u & U_uncontrolled(i) ~= Inf)
        U_max_u = abs(U_uncontrolled(i));
      end
        if(abs(U_controlled(i)) > U_max_c & U_controlled(i) ~= Inf)
        U_max_c = abs(U_controlled(i));
      end
end

for i = 1 : 1 : j
        U_controlled(i) = U_controlled(i) / U_max_u;
        U_uncontrolled(i) = U_uncontrolled(i) / U_max_u;
end

F_max = 0;

for i = 1 : 1 : j
        if(abs(F_control(i)) > F_max & F_control(i) ~= Inf)
        F_max = abs(F_control(i));
      end
end

for i = 1 : 1 : j
        F_control(i) = F_control(i) / F_max;
end
```

```
figure

whitebg('white');

plot(x, U_controlled, 'black',x, U_uncontrolled, '-.black');
xlabel('\fontname{times} Time (sec)','FontSize',14);
ylabel('\fontname{times}Normalized Relative Ground
Displacement','FontSize',14);
text(0.05*x(num_trials+1),1.15,quake_title,'FontSize',14);
text(0.75*x(num_trials+1),1.15,'\fontname{times}delay = 0.26
s','FontSize',14);
text(0.05*x(num_trials+1),-1.06,'_____','FontSize',14);
text(0.18*x(num_trials+1),-1.1,'\fontname{times}Controlled
Case','FontSize',14);
text(0.05*x(num_trials+1),-1.3,'\fontname{times}U max = 16.26
m','FontSize',14);
text(0.55*x(num_trials+1),-1.1,'\fontname{times}----- Uncontrolled
Case','FontSize',14);
text(0.55*x(num_trials+1),-1.3,'\fontname{times}U max  = 0.072
m','FontSize',14);
title('\fontname{times}Response to Acceleration Time
History','FontSize',14);
axis([0 x(num_trials+1) -1.55 1.3]);

figure

plot(x,F_control,'black');
xlabel('\fontname{times}Time (sec)','FontSize',14);
ylabel('\fontname{times}Normalized Control Force','FontSize',14);
text(0.05*x(num_trials+1),1.23,quake_title,'FontSize',14);
text(0.7*x(num_trials+1),1.09,'\fontname{times}delay = 0.26
s','FontSize',14);
text(0.05*x(num_trials+1),1.09,'\fontname{times}F max = 8.07e+06
N','FontSize',14');
title('\fontname{times}Values of Control Force','FontSize',14);
axis([0 x(num_trials+1) -1.2 1.4]);
```

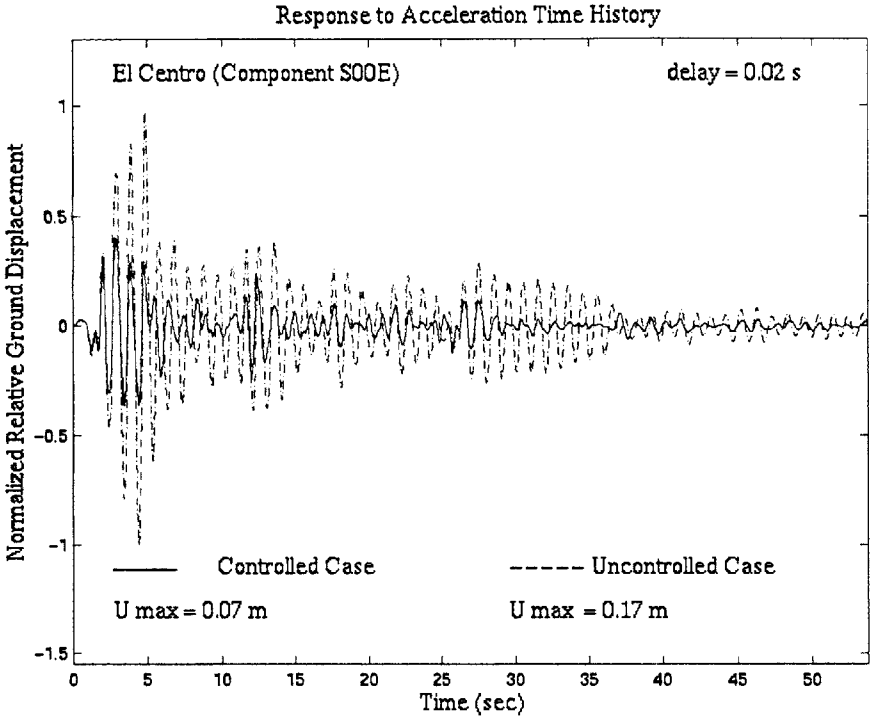

Figure C1 – Response to El Centro Time History, $t_d = 0.02$ sec

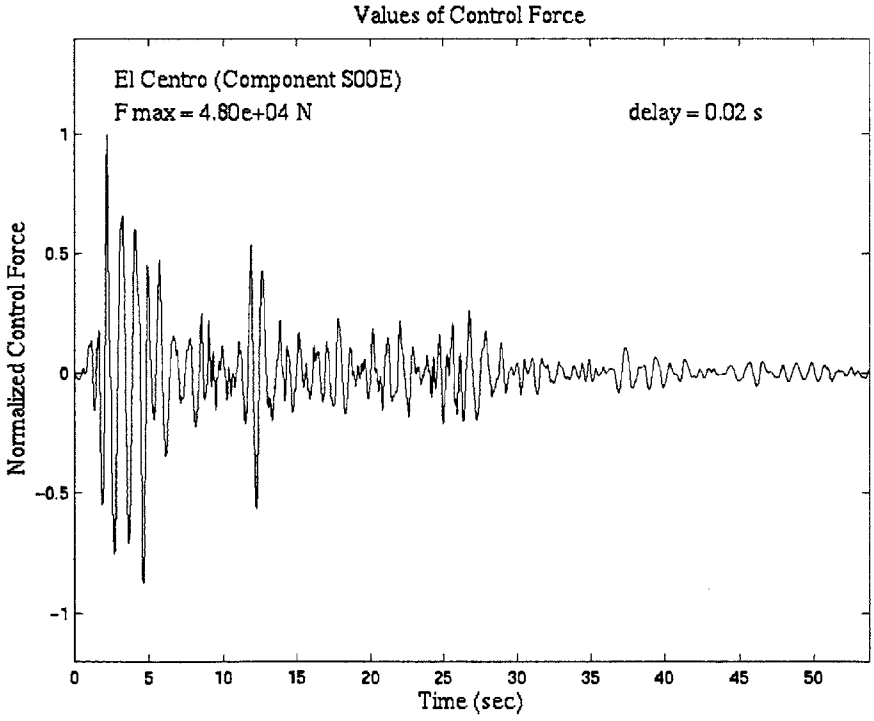

Figure C2 – Time History of Control Force for El Centro Excitation, $t_d = 0.02$ sec

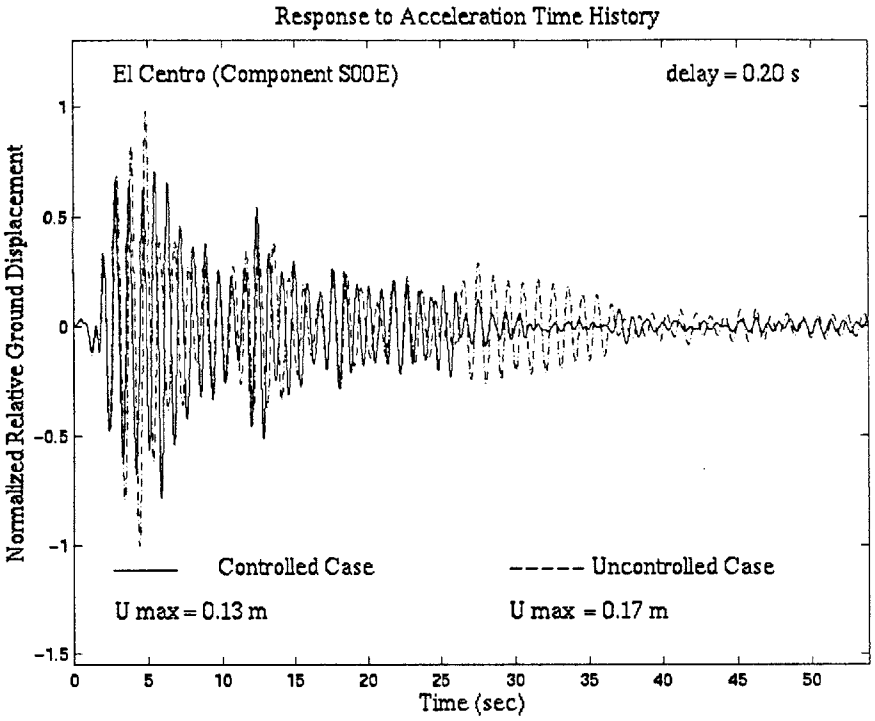

Figure C3 – Response to El Centro Time History, $t_d = 0.20$ sec

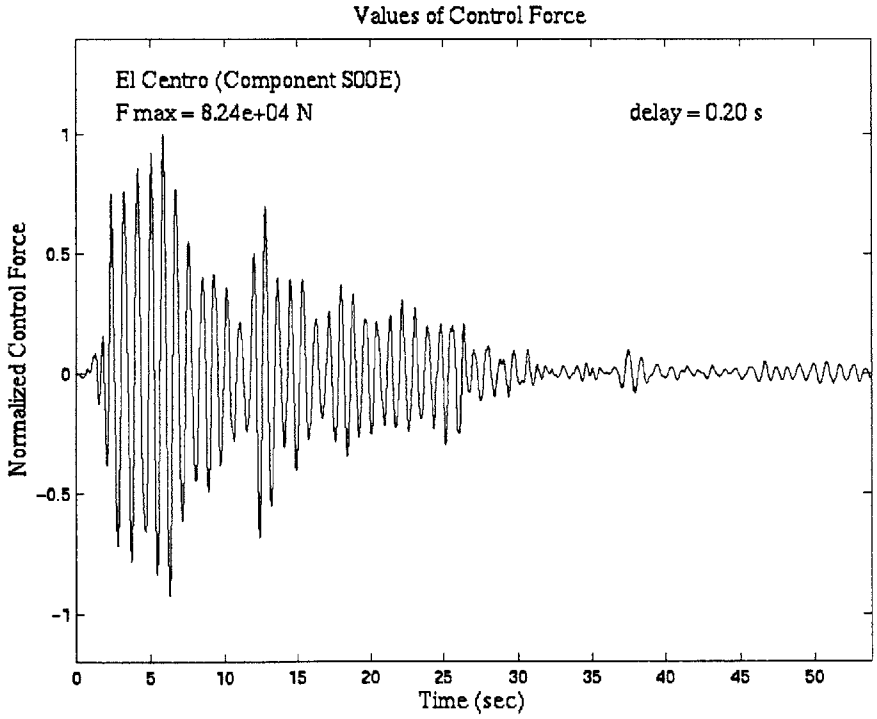

Figure C4 – Time History of Control Force for El Centro Excitation, $t_d = 0.20$ sec

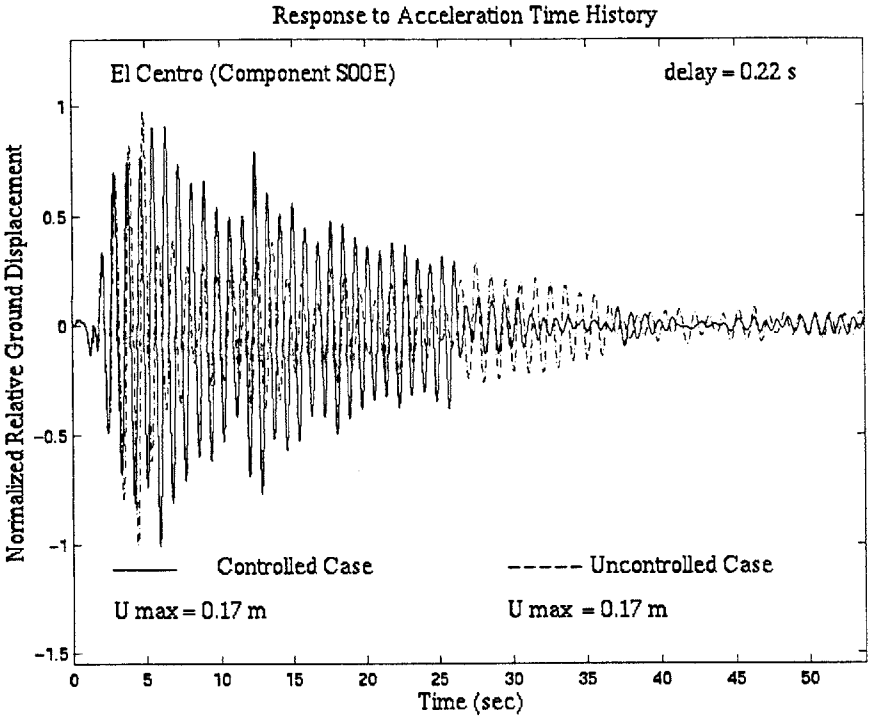

Figure C5 – Response to El Centro Time History, $t_d = 0.22$ sec

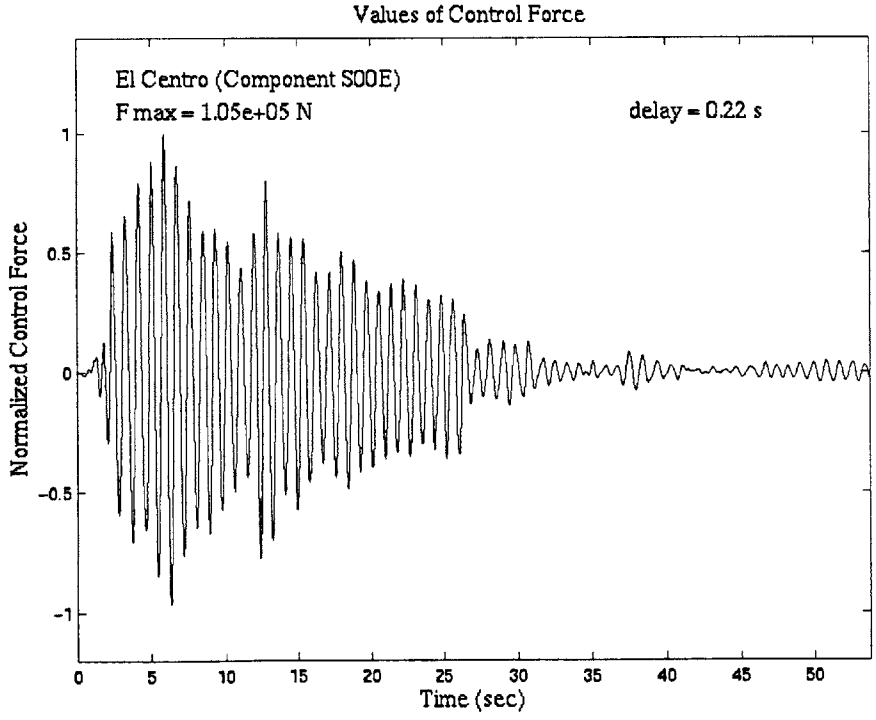

Figure C6 – Time History of Control Force for El Centro Excitation, $t_d = 0.22$ sec

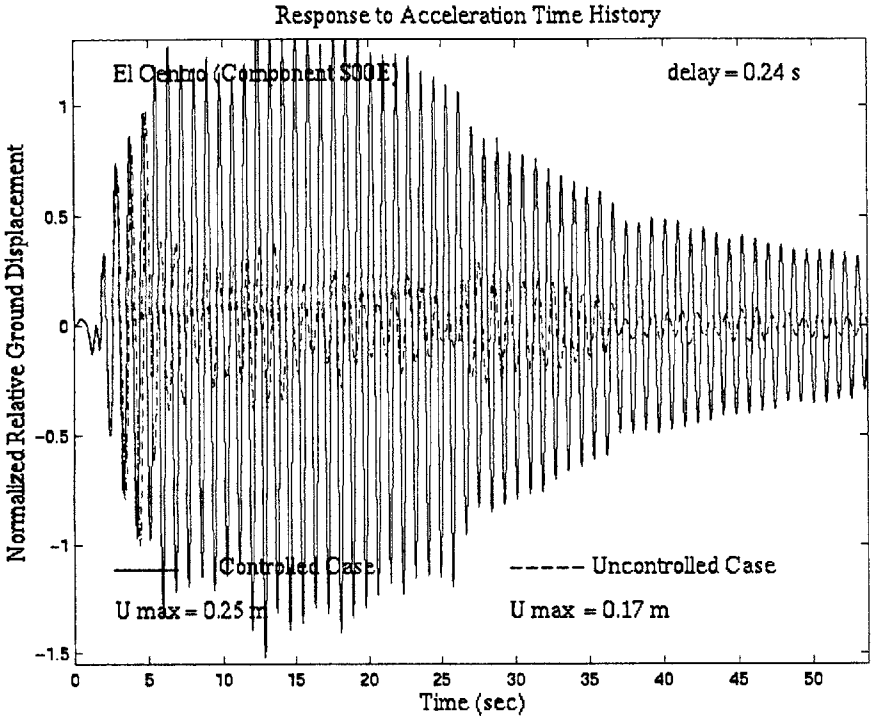

Figure C7 – Response to El Centro Time History, $t_d = 0.24$ sec

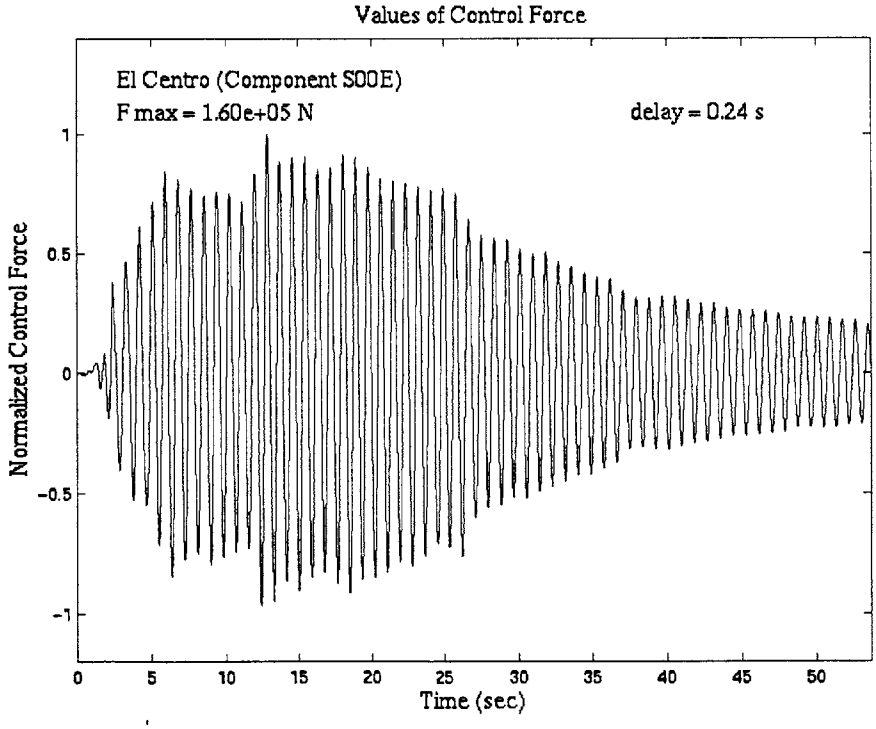

Figure C8 – Time History of Control Force for El Centro Excitation, $t_d = 0.24$ sec

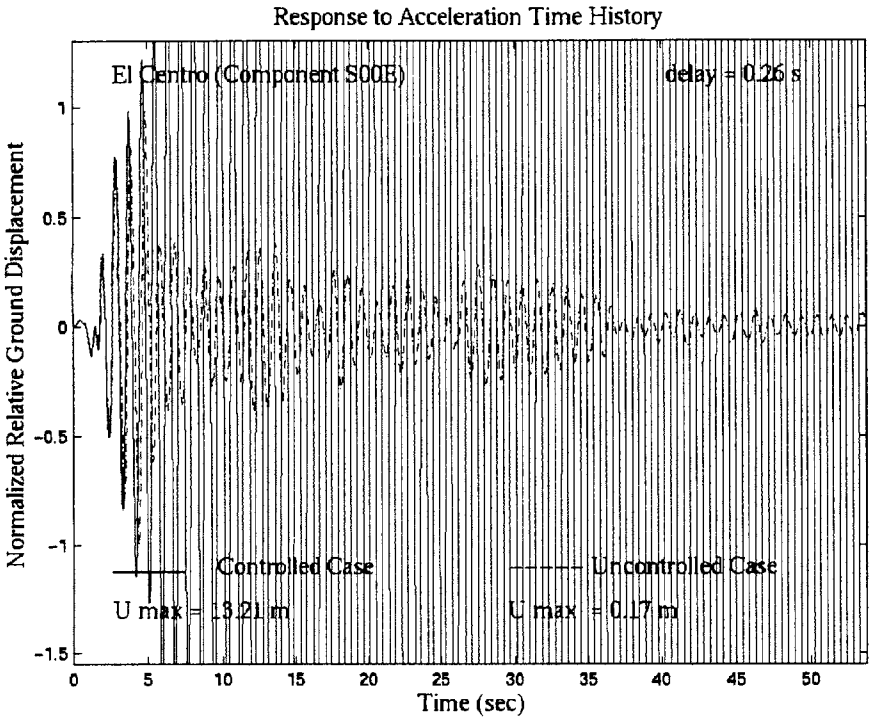

Figure C9 – Response to El Centro Time History, $t_d = 0.26$ sec

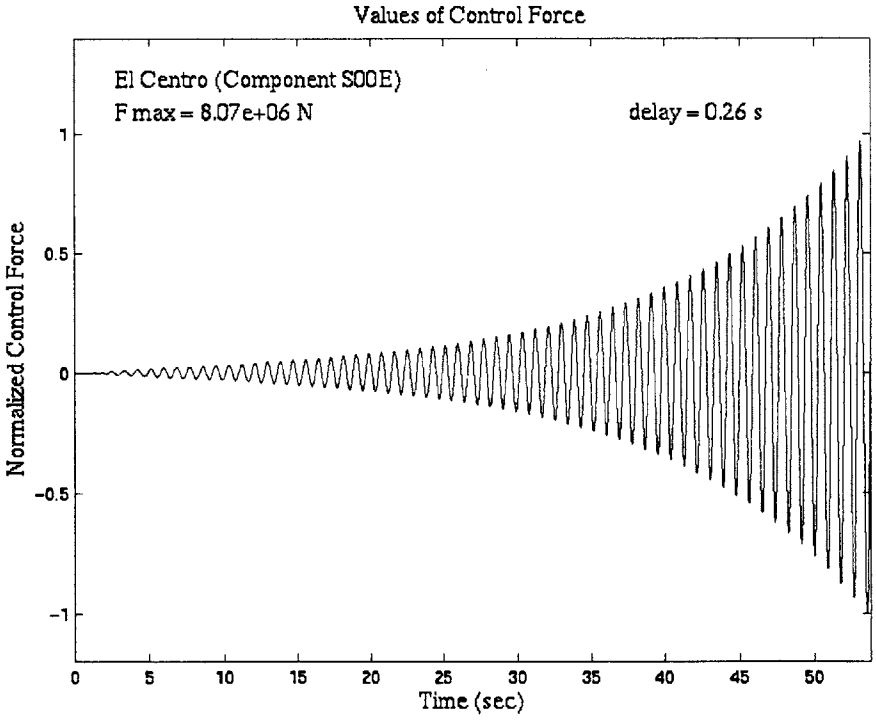

Figure C10 – Time History of Control Force for El Centro Time Excitation, $t_d = 0.26$ sec

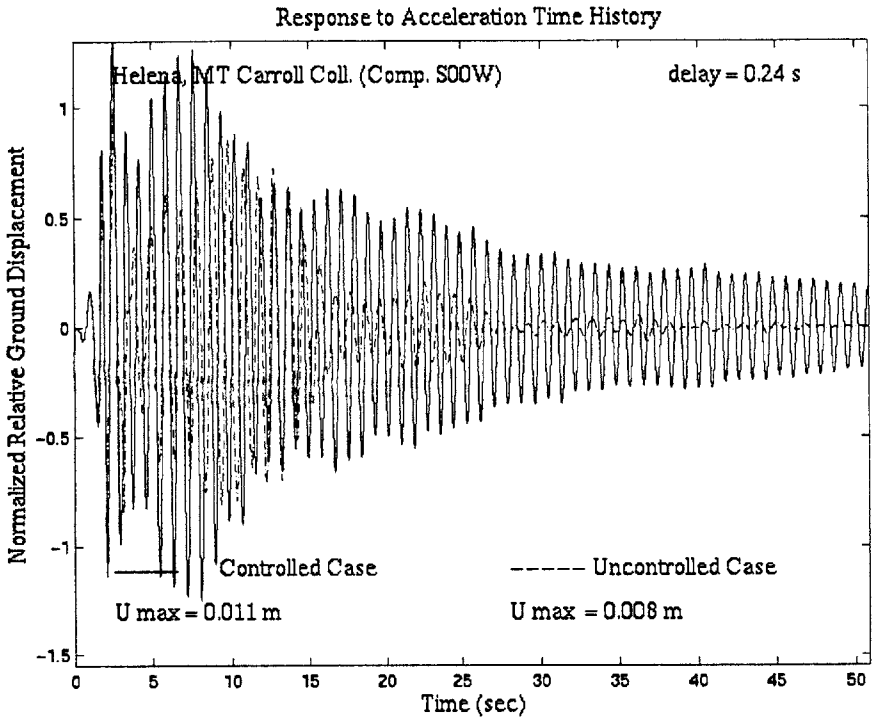

Figure C11 – Response to Helena, MT Carroll College Time History, t_d = 0.24 sec

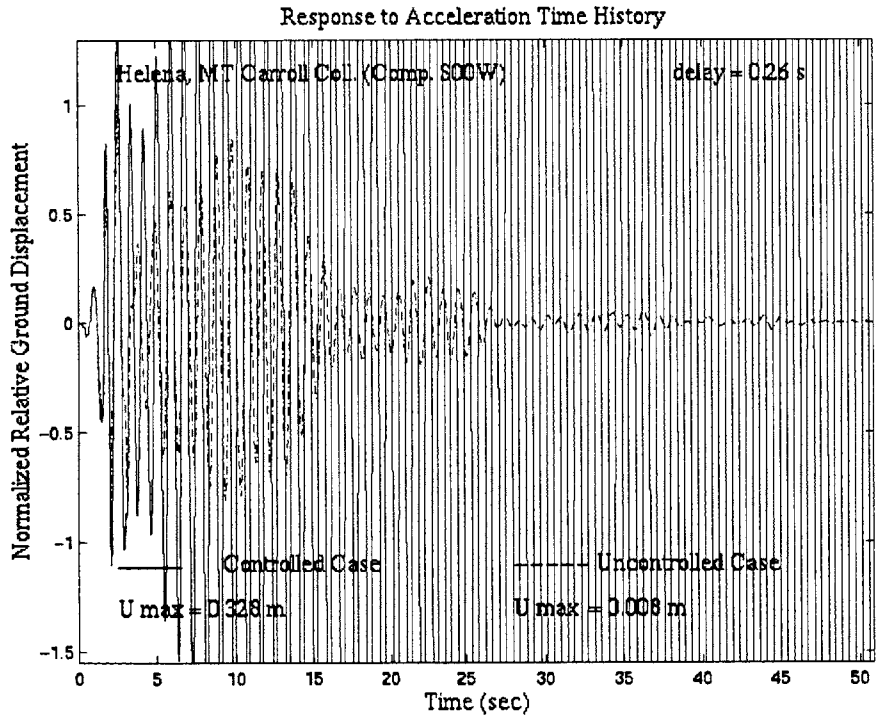

Figure C12 – Response to Helena, MT Carroll College Time History, t_d = 0.26 sec

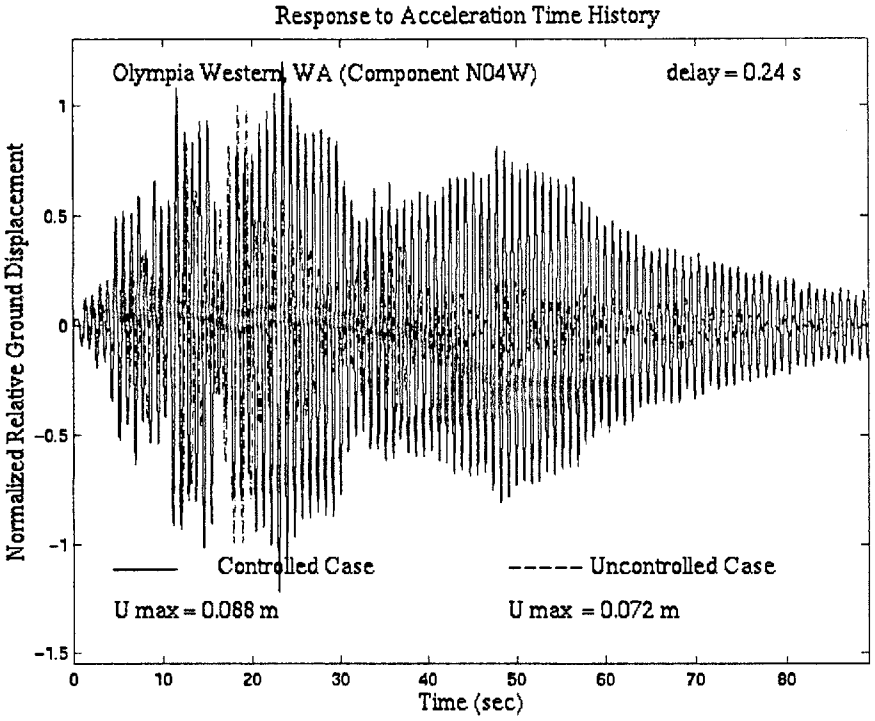

Figure C13 – Response to Olympia Western, WA Time History, t_d = 0.24 sec

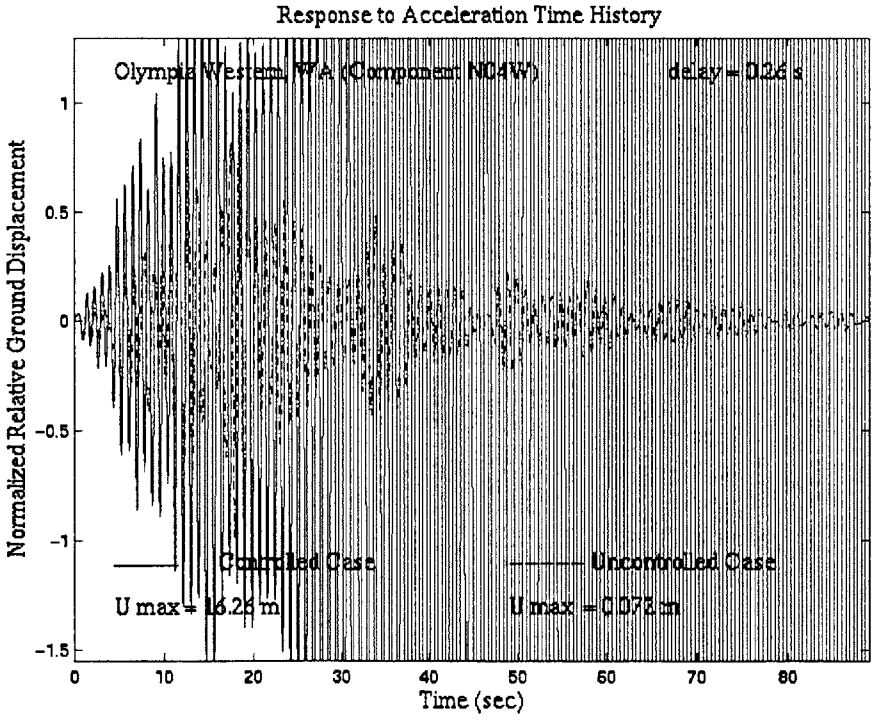

Figure C14 – Response to Olympia Western, WA Time History, t_d = 0.26 sec

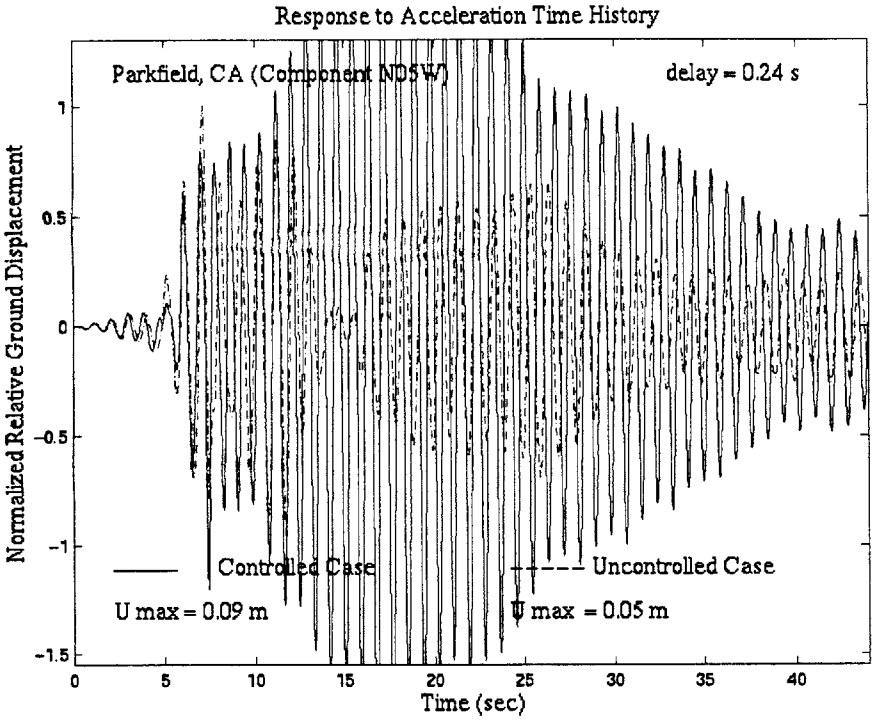

Figure C15 – Response to Parkfield, CA Time History, $t_d = 0.24$ sec

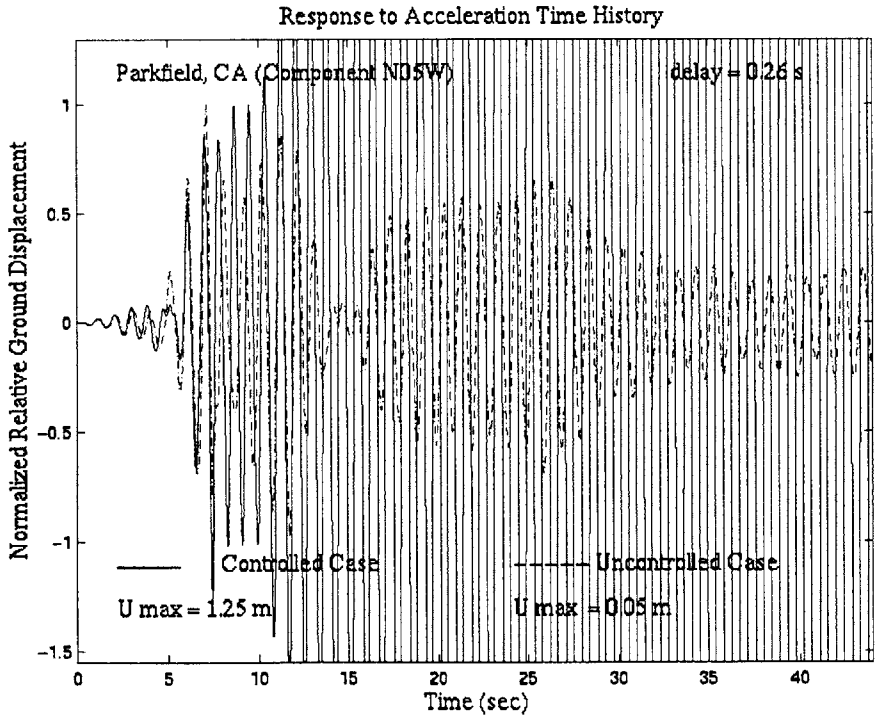

Figure C16 – Response to Parkfield, CA Time History, $t_d = 0.26$ sec

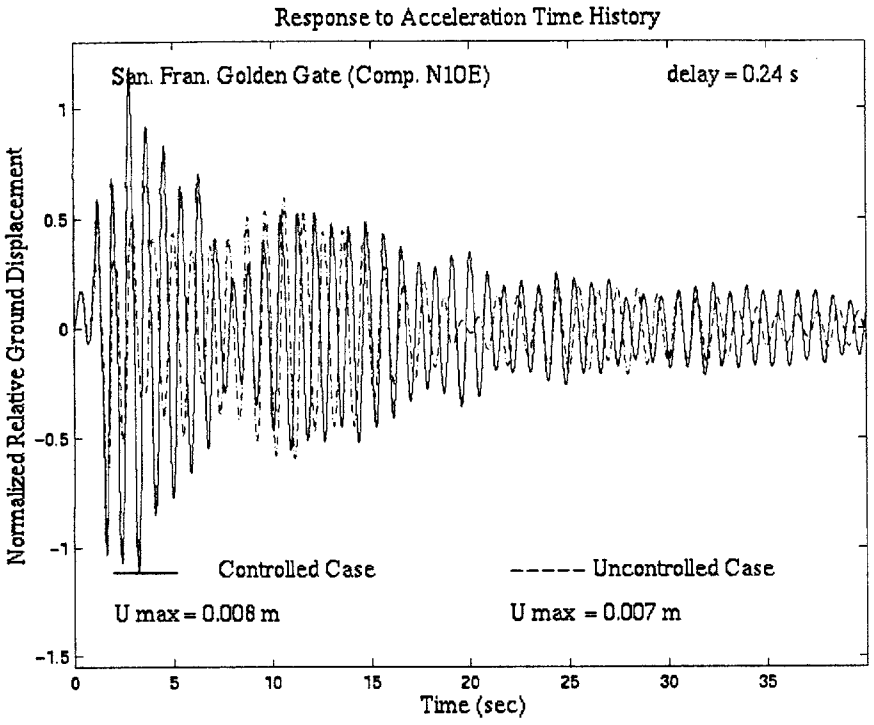

Figure C17 – Response to San Francisco Golden Gate Time History, t_d = 0.24 sec

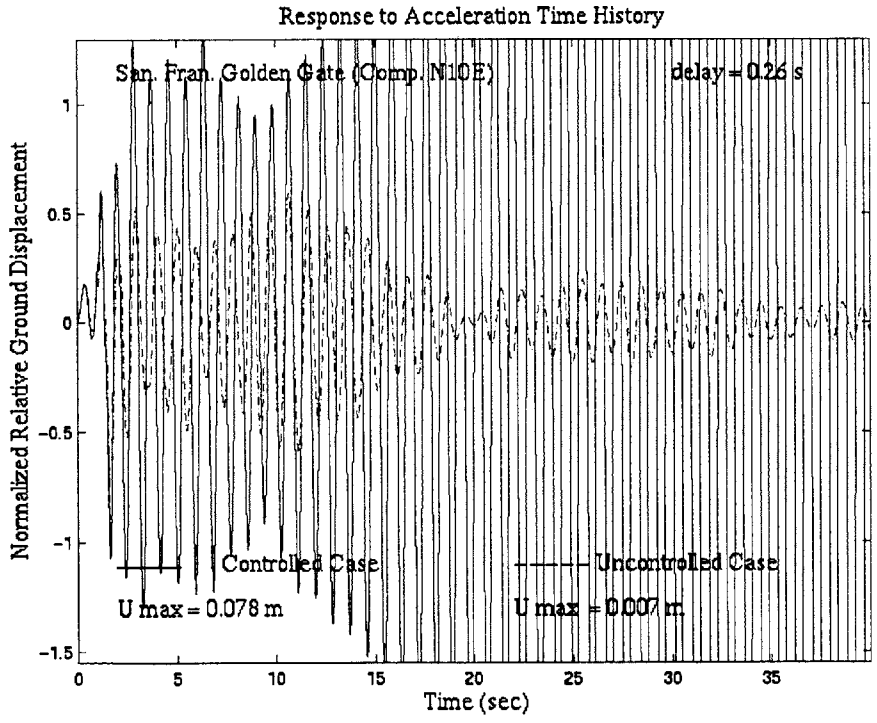

Figure C18 – Response to San Francisco Golden Gate Time History, t_d = 0.26 sec

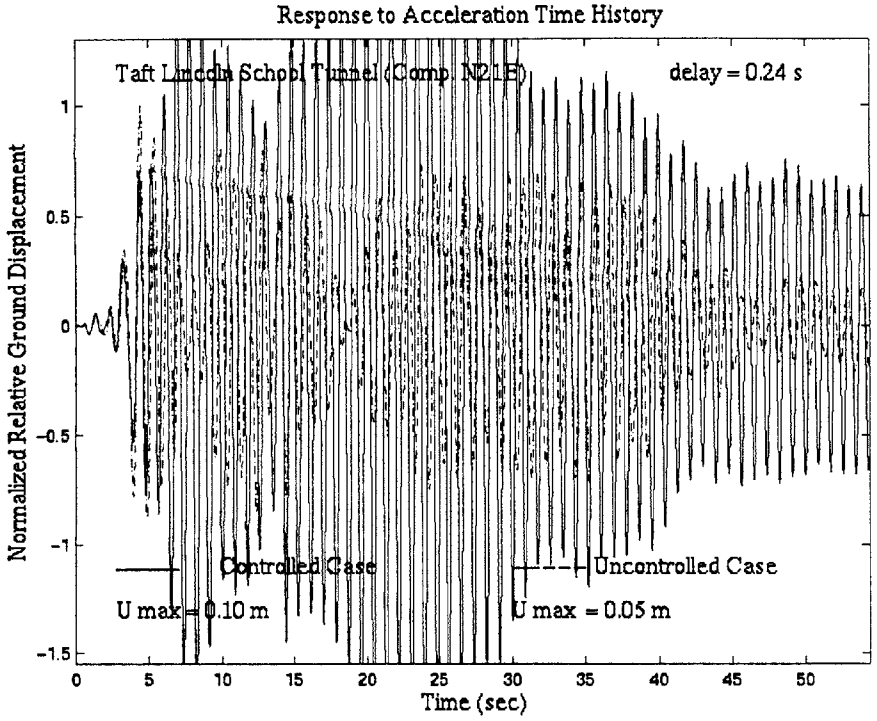

Figure C19 – Response to Taft Lincoln School Tunnel Time History, $t_d = 0.24$ sec

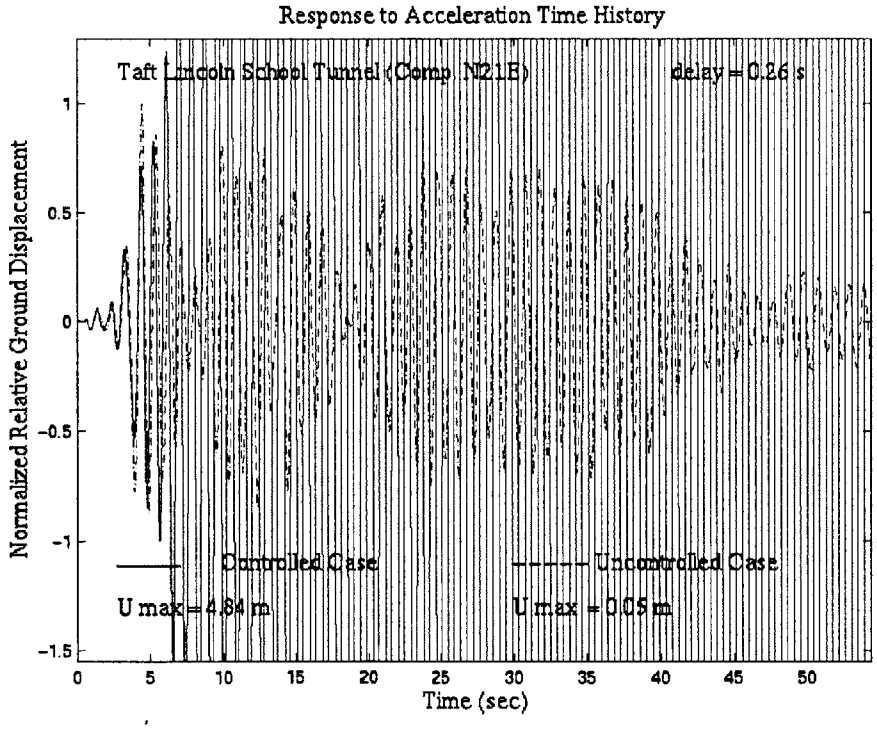

Figure C20 – Response to Taft Lincoln School Tunnel Time History, $t_d = 0.26$ sec

Appendix D

Adaptive Control for Earthquake Time Histories

```
%     Michael Cusack

%       var_damp_3a.m

%       input:                earthquake accleration time history
%       control alogrithm:    adaptive

%       Response Approximation Methods

%       controlled:     discrete time state equation
%       uncontrolled:   discrete time state equation (w/o control force)

syms i; syms m; syms c; syms delta_t; syms r; syms t; syms k;

m = 50000;              % (kg)     mass of structure
delta_t = 0.02;         % (sec)    time-step duration
r = 0;                  %           weighting/cost parameter
r_value = '\fontname{times}r = 0.0';
filename = 'El_Centro_Comp_S00E';
quake_title = '\fontname{times}El Centro (Component S00E)';
fid = fopen(filename);                      % time history of acceleration
accel_data = fscanf(fid,'%g %g',[2 inf]); % values
accel_data = accel_data';                   %
fclose(fid);                                %

num_trials = size(accel_data);
num_trials = num_trials(1) - 2;

Q = [0, 0; 0, 1];               %  weighting/cost parameter
R = r;                          %  weighting/cost parameter

U_i_c = [0; 0];            % initial conditions for controlled case
U_i_u = [0; 0];            % initial conditions for uncontrolled case

x=(0:num_trials)';                          % time step values
U_controlled = zeros(num_trials+1,1);       % controlled response values
U_uncontrolled = zeros(num_trials+1,1);     % uncontroled response values
F_control = zeros(num_trials+1,1);          % control force values
C_control = zeros(num_trials+1,1);          % viscous damping parameter
values
K_control = zeros(num_trials+1,1);          % variable stiffness values
Modulus_1 =   zeros(num_trials+1,1);

% ***   Uncontrolled case   ************************************** %

k_u = 2000000;              % (N/m)    initial stiffness of structure
c_u = 12500;                % (kg/s)   initial damping coefficient
w_n_u = (k_u/m)^(1/2);      % (rad/s)  initial natural frequency of
                            %          structure
zeta_u = c_u/(2*w_n_u*m);   % initial damping fraction of structure

A_u = [0, 1; -k_u/m, -c_u/m];      %  coefficient matrix
Abar_u = expm(A_u*delta_t);        % A_u integrated over time step
B = [0; 1/m];                      % coefficient matrix
D = [0; 1/m];                      % coefficient matrix
Bbar_u = eval(int(expm(A_u*t),t,0,delta_t)*B);
                                   % B integrated over time step
```

```
Dbar_u = Bbar_u;                    % D integrated over time step

% ***   Adaptively controlled case - initial values   ********** %

k_c = 0;                    % (N/m)    variable stiffness of structure
c_c = 0;                    % (kg/s)   variable damping coefficient
k_t = k_c + k_u;            % (N/m)    total stiffness of structure
c_t = c_c + c_u;            % (kg/s)   total damping coefficient
w_n_c = (k_t/m)^(1/2);      % (rad/s)  controlled  natural frequency of
                            % structure
zeta_c = c_t/(2*w_n_c*m);
                        % controlled total damping fraction of structure

A_c = [0, 1; -k_t/m, -c_t/m];
Abar_c = expm(A_c*delta_t);                 % A_c integrated over time step
Bbar_c = eval(int(expm(A_c*t),t,0,delta_t)*B);
                                            % B integrated over time step
Dbar_c = Bbar_c;                            % D integrated over time step

% ********************************************************************** %

for i = 0 : 1 : num_trials

      time = i*delta_t;
      a_ground_i = accel_data(i+1, 2);
      F_ground_i = -m*a_ground_i;

      % Uncontrolled case:

      U_i1_u = Abar_u*U_i_u + Dbar_u*F_ground_i;
      U_i_u = U_i1_u;

      % Adaptively controlled case:

      [X,L,G,RR] = dare(Abar_c, Bbar_c, Q, R);
      F_control_i1 = -[0, G(2)]*U_i_c;    %  control force at time i+1

      if(U_i_c(1) ~= 0)
        k_c = -F_control_i1 / U_i_c(1);
        else
        k_c = 0;
      end
      if(k_c > k_u)
        k_c = k_u;
      elseif(k_c < (-k_u))
        k_c = -0.9999*k_u;  %  k_c cannot be set exactly to -k_u because
      end                   %     it will lead to division by zero

      F_control_i1 = F_control_i1 + k_c*U_i_c(1);

      if(U_i_c(2) ~= 0)
        c_c = -F_control_i1 / U_i_c(2);
      else
        c_c = 0;
      end

      if(c_c > c_u)
        c_c = c_u;
      end

      F_actuator_i1 = F_control_i1 + c_c*U_i_c(2);

      k_t = k_c + k_u;
```

```
      w_n_c = (k_t/m)^(1/2);
      zeta_c = c_t/(2*w_n_c*m);

      A_c = [0, 1; -k_t/m, -c_t/m];

      Abar_c = [1 - k_t/(2*m)*delta_t^2, delta_t - c_t/(2*m)*delta_t^2;
      -k_t/m*delta_t - c_t*k_t/(2*m^2)*delta_t^2, 1 - c_t/m*delta_t -
      k_t/(2*m)*delta_t^2 + c_t^2/(2*m^2)*delta_t^2];

      Bbar_c = [delta_t^2/(2*m); delta_t/m - c_t*delta_t^2/(2*m^2)];

      Dbar_c = Bbar_c;

      U_i1_c = Abar_c*U_i_c + Bbar_c*F_actuator_i1 + Dbar_c*F_ground_i;
      U_i_c = U_i1_c;

      x(i+1) = time;
      U_controlled(i+1) = U_i1_c(1);
      U_uncontrolled(i+1) = U_i1_u(1);
      F_control(i+1) = F_actuator_i1;
      C_control(i+1) = c_c;
      K_control(i+1) = k_c;

      control_eig = eig(Abar_c - Bbar_c*[0, G(2)]);
      real_c = real(control_eig);
      real_c = real_c(1);
      imag_c = imag(control_eig);
      imag_c = imag_c(1);
      modulus = (real_c^2 + imag_c^2)^(1/2);

      Modulus_1(i+1) = modulus;

end

% ********************************************************************** %

j = size(U_uncontrolled);
j = j(1) - 1;
U_max_u = 0;
U_max_c = 0;

for i = 1 : 1 : j
      if(abs(U_uncontrolled(i)) > U_max_u & U_uncontrolled(i) ~= Inf)
        U_max_u = abs(U_uncontrolled(i));
      end
      if(abs(U_controlled(i)) > U_max_c & U_controlled(i) ~= Inf)
        U_max_c = abs(U_controlled(i));
      end
end

for i = 1 : 1 : j
      U_controlled(i) = U_controlled(i) / U_max_u;
      U_uncontrolled(i) = U_uncontrolled(i) / U_max_u;
end


K_max = 0;

for i = 1 : 1 : j
      if(abs(K_control(i)) > K_max & K_control(i) ~= Inf)
        K_max = abs(K_control(i));
      end
end
```

```
for i = 1 : 1 : j
        K_control(i) = K_control(i) / K_max;
end

C_max = 0;

for i = 1 : 1 : j
        if(abs(C_control(i)) > C_max & C_control(i) ~= Inf)
        C_max = abs(C_control(i));
      end
end

for i = 1 : 1 : j
        C_control(i) = C_control(i) / C_max;
end

F_max = 0;

for i = 1 : 1 : j
        if(abs(F_control(i)) > F_max & F_control(i) ~= Inf)
        F_max = abs(F_control(i));
      end
end

for i = 1 : 1 : j
        F_control(i) = F_control(i) / F_max;
end

figure

whitebg('white');

plot(x, U_controlled, 'black',x, U_uncontrolled, '-.black');
xlabel('\fontname{times} Time (sec)','FontSize',14);
ylabel('\fontname{times}Normalized Relative Ground
Displacement','FontSize',14);
text(0.05*x(num_trials+1),1.15,quake_title,'FontSize',14);
text(0.8*x(num_trials+1),1.15,r_value,'FontSize',14);
text(0.05*x(num_trials+1),-1.06,'____','FontSize',14);
text(0.18*x(num_trials+1),-1.1,'\fontname{times}Controlled
Case','FontSize',14);
text(0.05*x(num_trials+1),-1.3,'\fontname{times}U max = 0.16
m','FontSize',14);
text(0.55*x(num_trials+1),-1.1,'\fontname{times}----- Uncontrolled
Case','FontSize',14);
text(0.55*x(num_trials+1),-1.3,'\fontname{times}U max = 0.17
m','FontSize',14);
title('\fontname{times}Response to Acceleration Time
History','FontSize',14);
axis([0 x(num_trials+1) -1.55 1.3]);

figure

plot(x, K_control,'black');
xlabel('\fontname{times}Time (sec)','FontSize',14);
ylabel('\fontname{times}Normalized Values of Control
Stiffness','FontSize',14);
text(0.05*x(num_trials+1),1.15,quake_title,'FontSize',14);
text(0.8*x(num_trials+1),1.15,r_value,'FontSize',14);
text(0.55*x(num_trials+1),-1.3,'\fontname{times}k_c max = 2.00e+06
N/m','FontSize',14);
title('\fontname{times}Variable Stiffness Control of Acceleration Time
History','FontSize',14);
axis([0 x(num_trials+1) -1.55 1.3]);
```

```
figure

plot(x, C_control,'black');
xlabel('\fontname{times}Time (sec)','FontSize',14);
ylabel('\fontname{times}Normalized Values of Control
Damping','FontSize',14);
text(0.05*x(num_trials+1),1.2,quake_title,'FontSize',14);
text(0.8*x(num_trials+1),1.2,r_value,'FontSize',14);
text(0.55*x(num_trials+1),-0.2,'\fontname{times}c_c max = 1.25e+04
kg/sec','FontSize',14);
title('\fontname{times}Variable Damping Control of Acceleration Time
History','FontSize',14);
axis([0 x(num_trials+1) -0.3 1.3]);

figure

plot(x, F_control,'black');
xlabel('\fontname{times}Time (sec)','FontSize',14);
ylabel('\fontname{times}Normalized Values of Control
Force','FontSize',14);
text(0.05*x(num_trials+1),1.15,quake_title,'FontSize',14);
text(0.8*x(num_trials+1),1.15,r_value,'FontSize',14);
text(0.55*x(num_trials+1),-1.3,'\fontname{times}F max = 1.51e+05
N','FontSize',14);
title('\fontname{times}Variable Actuator Force Control of Acceleration
Time History','FontSize',14);
axis([0 x(num_trials+1) -1.55 1.3]);

figure

plot(x, Modulus_1,'black');
xlabel('\fontname{times}Time (sec)','FontSize',14);
ylabel('\fontname{times}Modulus of Abar - Bbar*K_f','FontSize',14);
text(0.05*x(num_trials+1),1.0003,quake_title,'FontSize',14);
text(0.8*x(num_trials+1),1.0003,r_value,'FontSize',14);
title('\fontname{times}Stability of Adaptive Control
Algorithm','FontSize',14);
axis([0 x(num_trials+1) 0.9965 1.0005]);
```

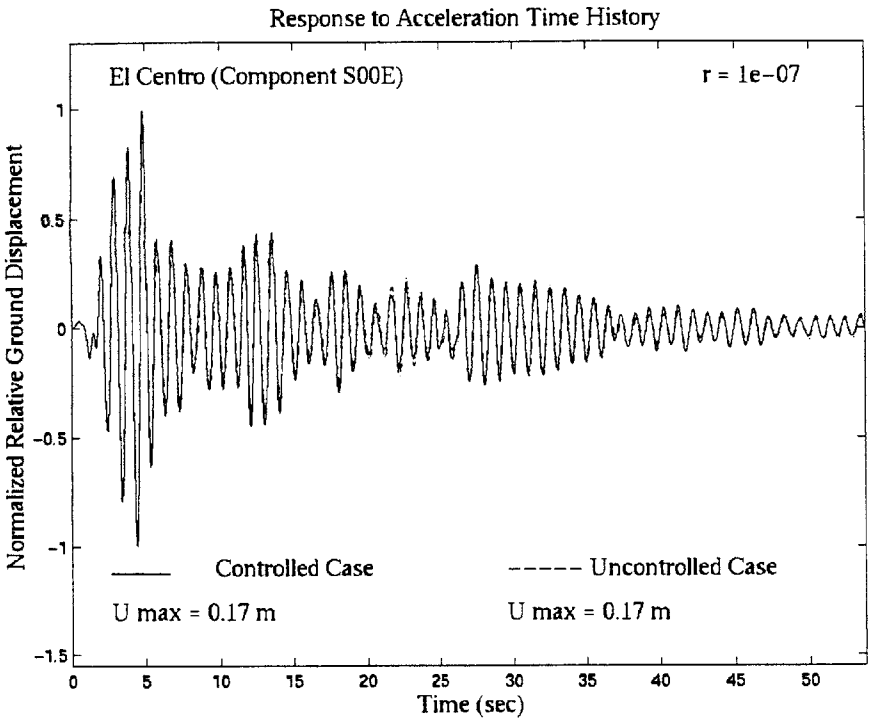

Figure D1 – Response to El Centro Time History, r = 1 x 10^{-7}

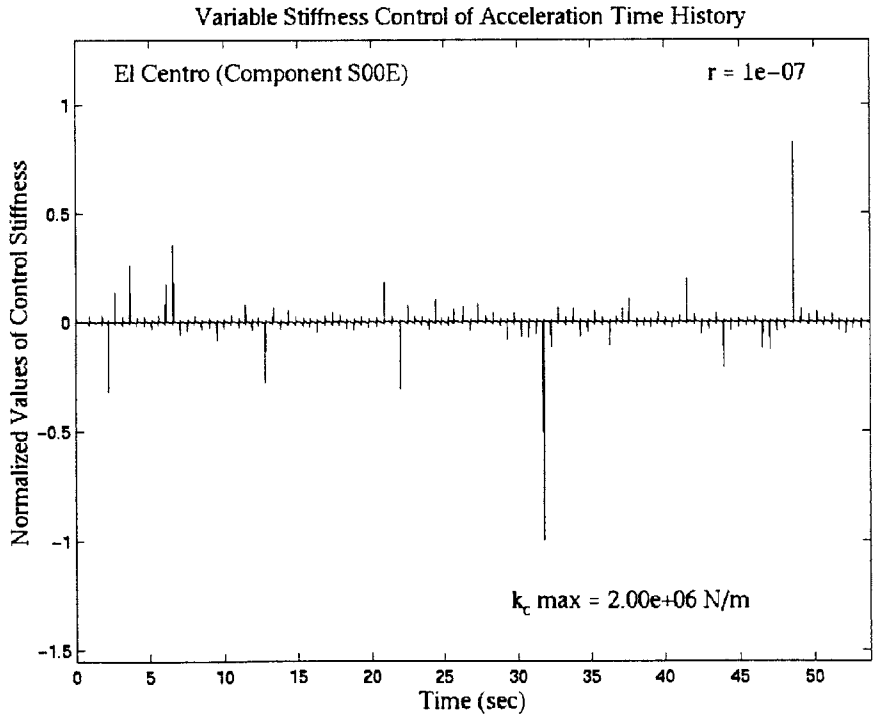

Figure D2 – Time History of Variable Stiffness for El Centro Excitation, r = 1 x 10^{-7}

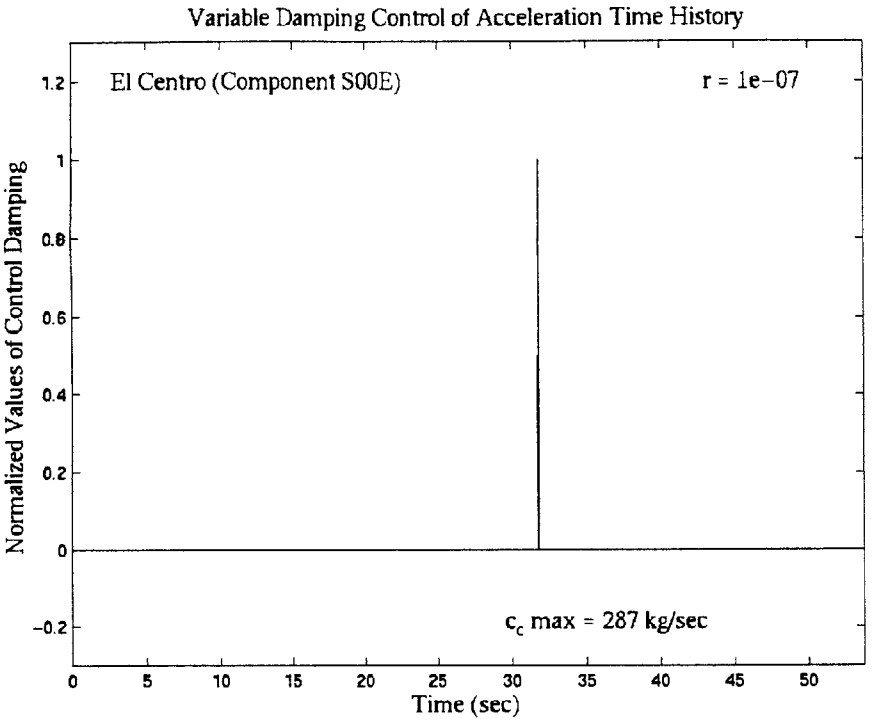

Figure D3 – Time History of Variable Damping for El Centro Excitation, r = 1 x10^{-7}

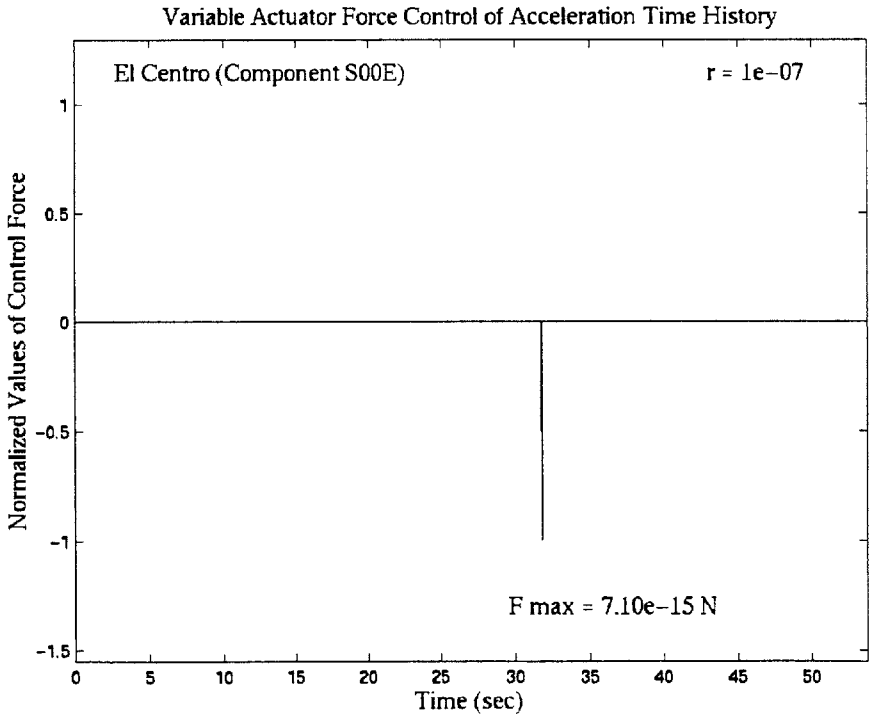

Figure D4 – Time History of Control Force for El Centro Excitation, r = 1 x10^{-7}

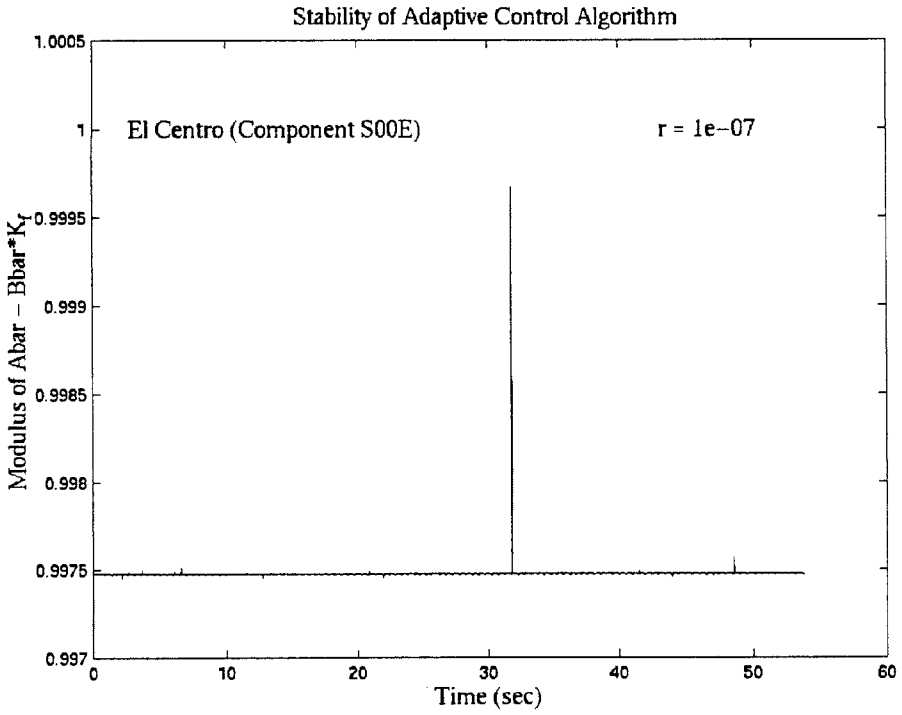

Figure D5 – Stability Check of Adaptive Control Algorithm for El Centro Excitation

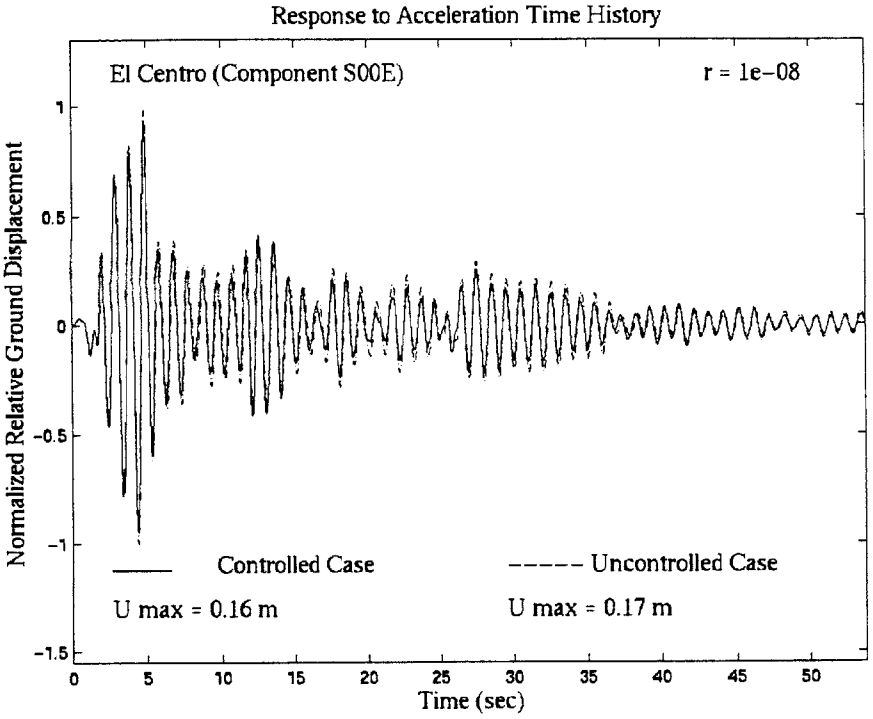

Figure D6 – Response to El Centro Time History, r = 1 x 10^{-8}

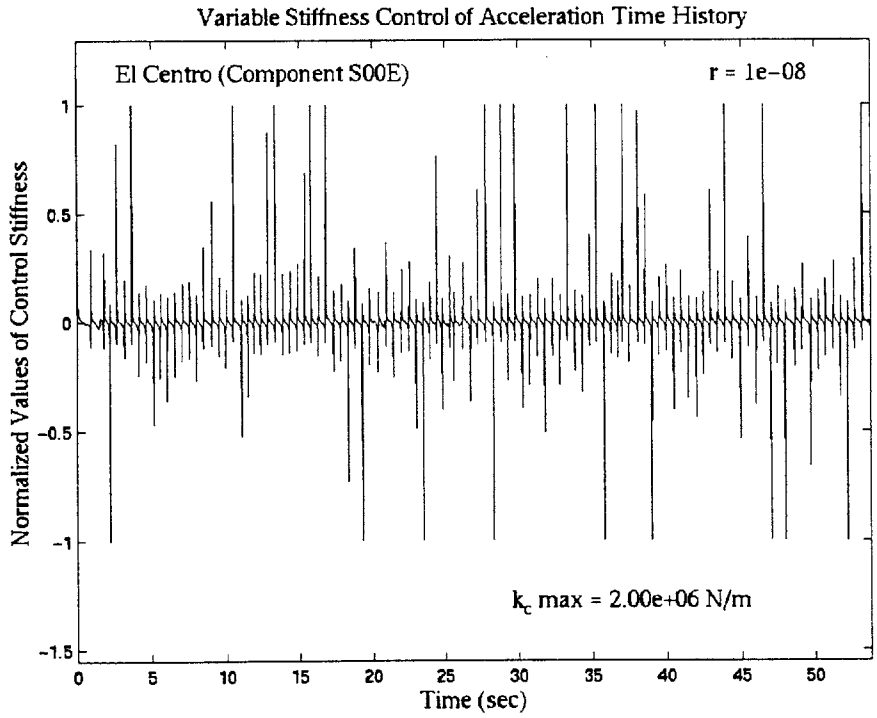

Figure D7 – Time History of Variable Stiffness for El Centro Excitation, r = 1 x 10^{-8}

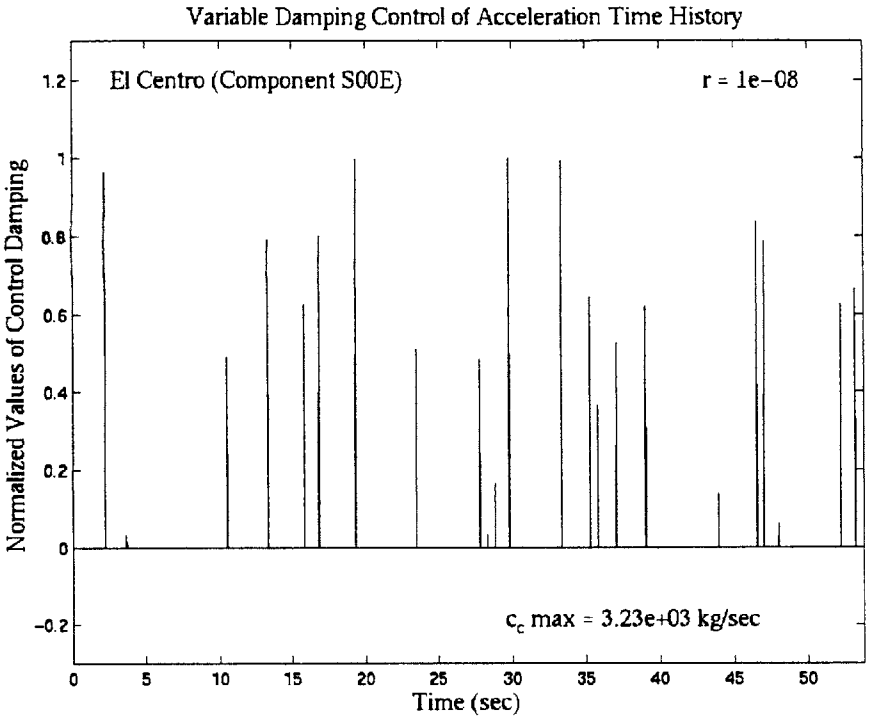

Figure D8 – Time History of Variable Damping for El Centro Excitation, r = 1 x10^{-8}

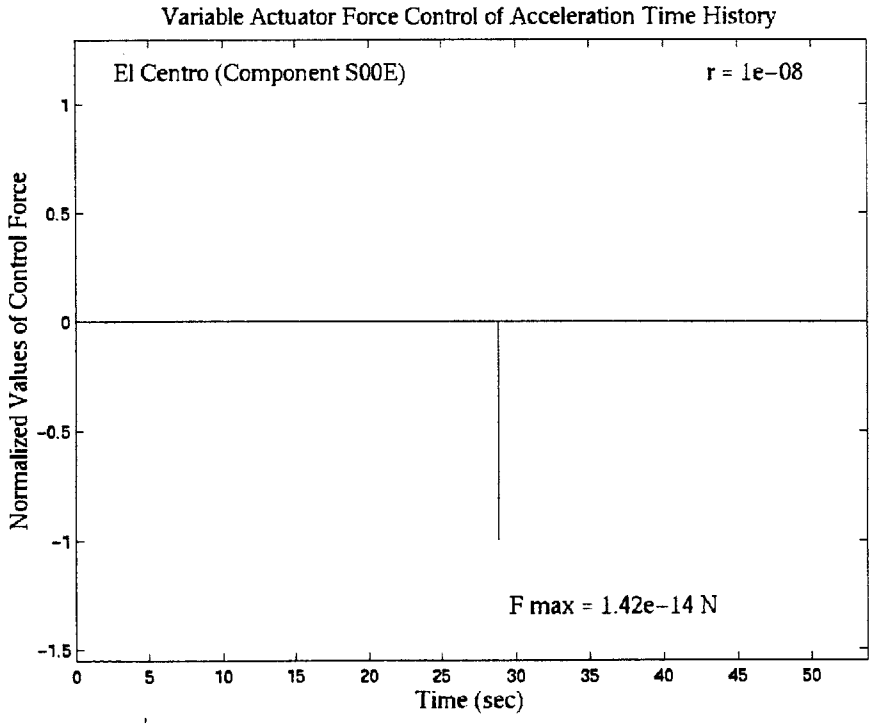

Figure D9 – Time History of Control Force for El Centro Excitation, r = 1 x10^{-8}

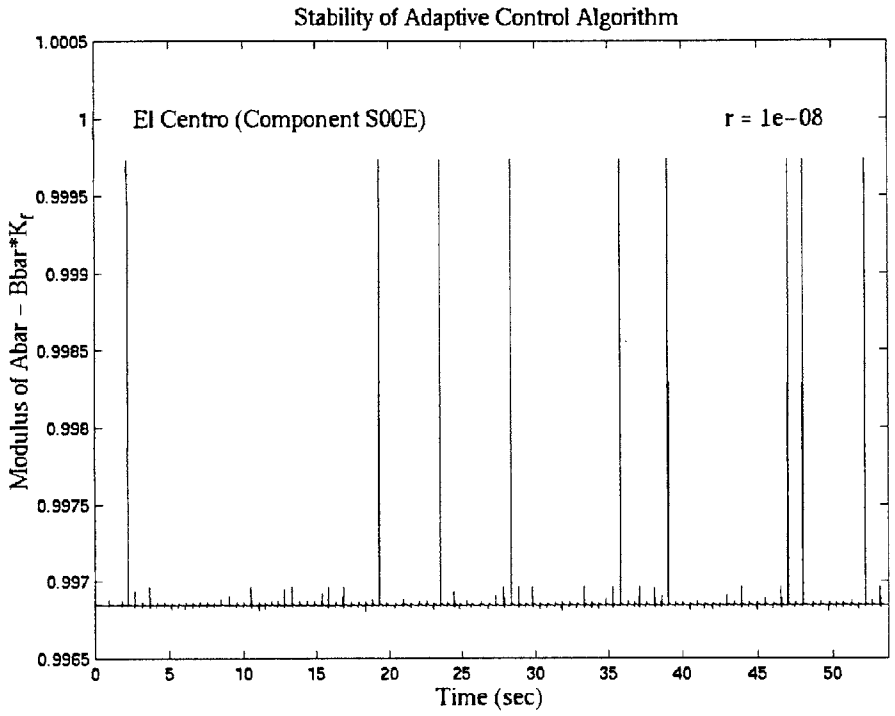

Figure D10 – Stability Check of Adaptive Control Algorithm for El Centro Excitation

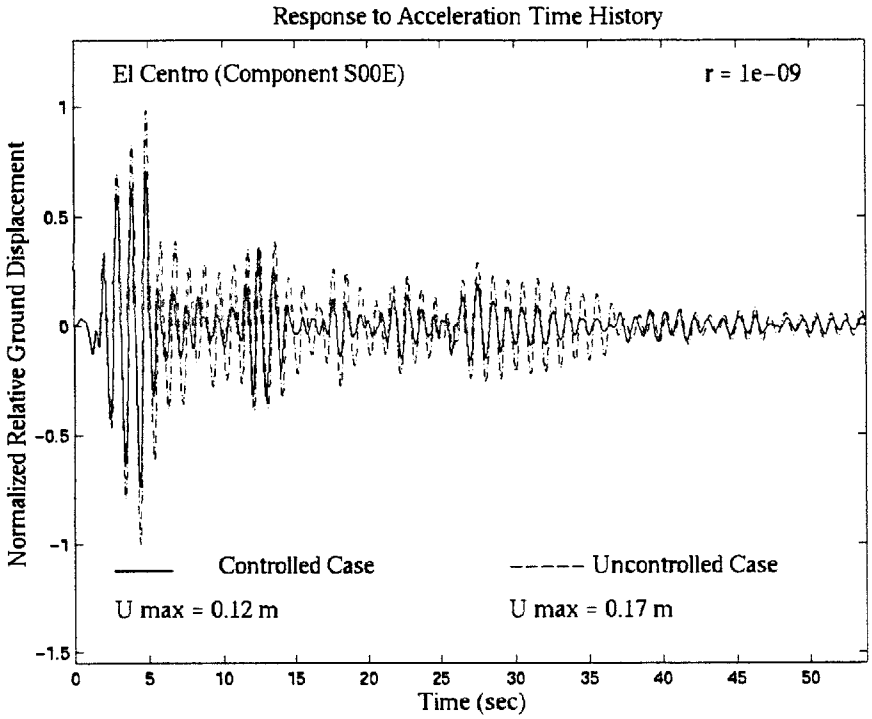

Figure D11 – Response to El Centro Time History, r = 1 x 10^{-9}

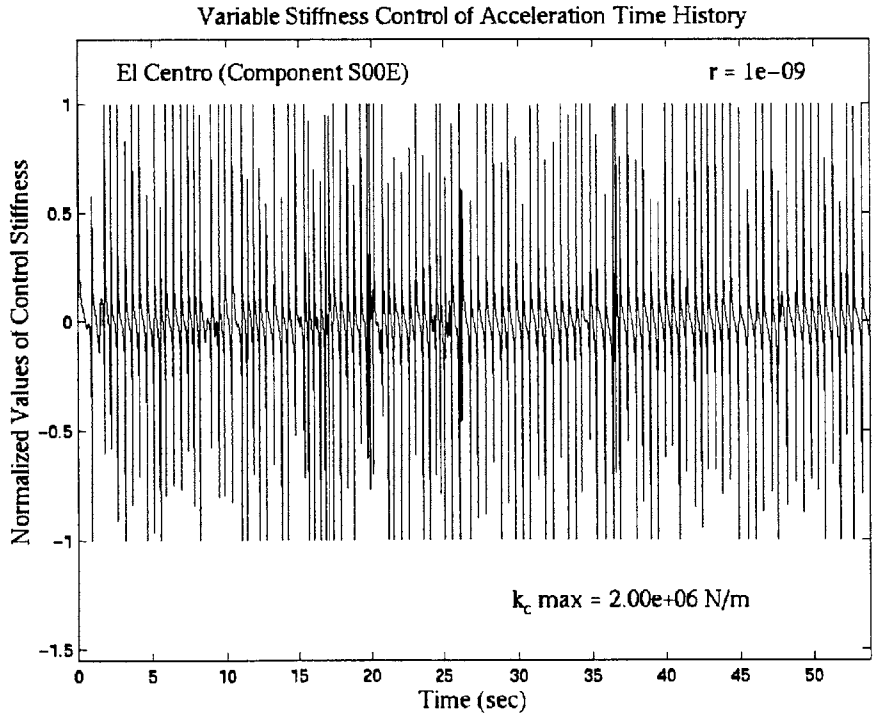

Figure D12 – Time History of Variable Stiffness for El Centro Excitation, r = 1 x 10^{-9}

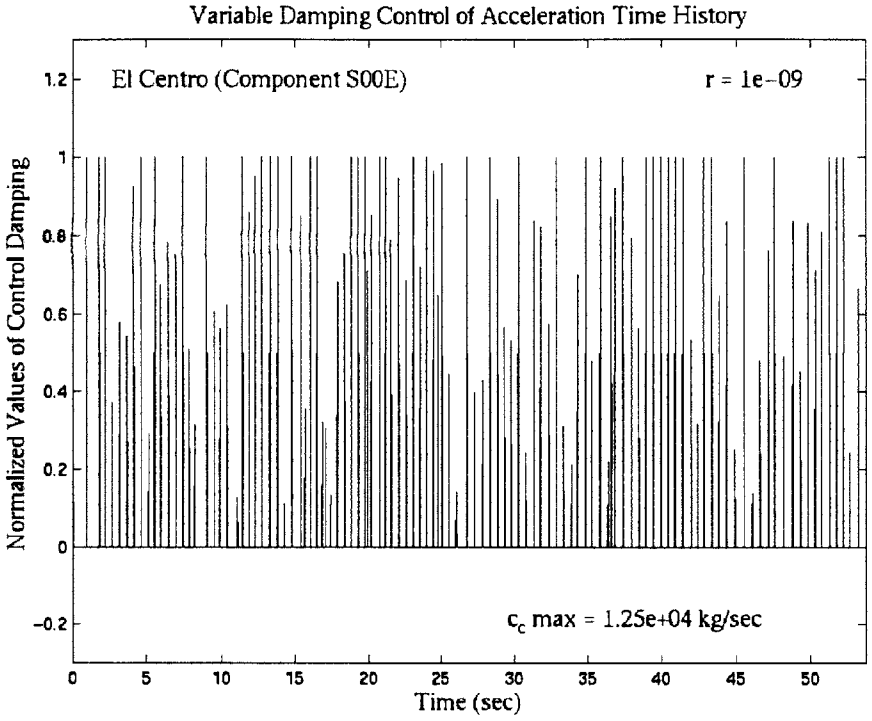

Figure D13 – Time History of Variable Damping for El Centro Excitation, r = 1 x10^{-9}

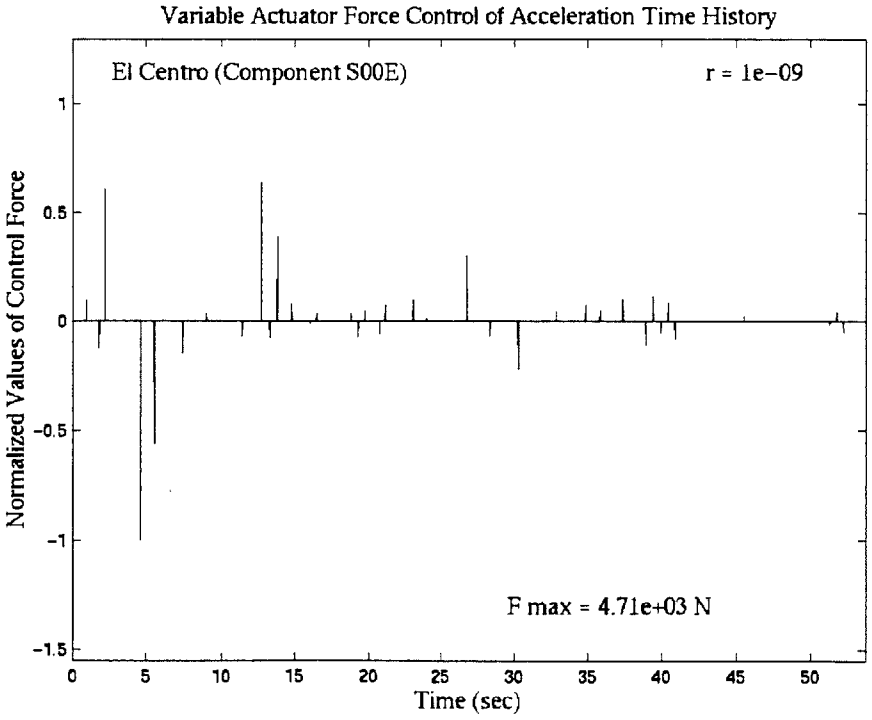

Figure D14 – Time History of Control Force for El Centro Excitation, r = 1 x10^{-9}

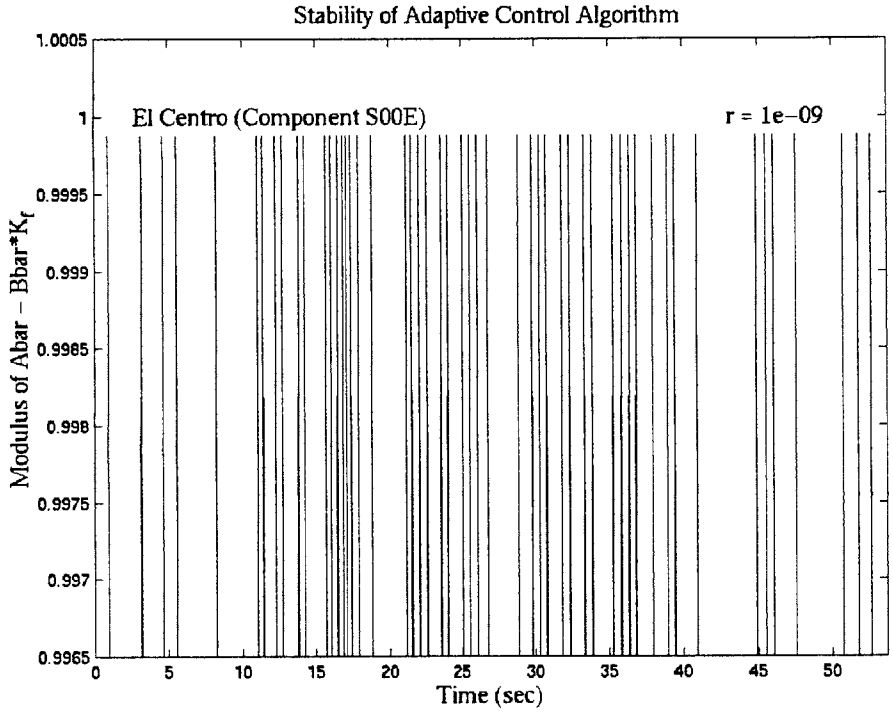

Figure D15 – Stability Check of Adaptive Control Algorithm for El Centro Excitation

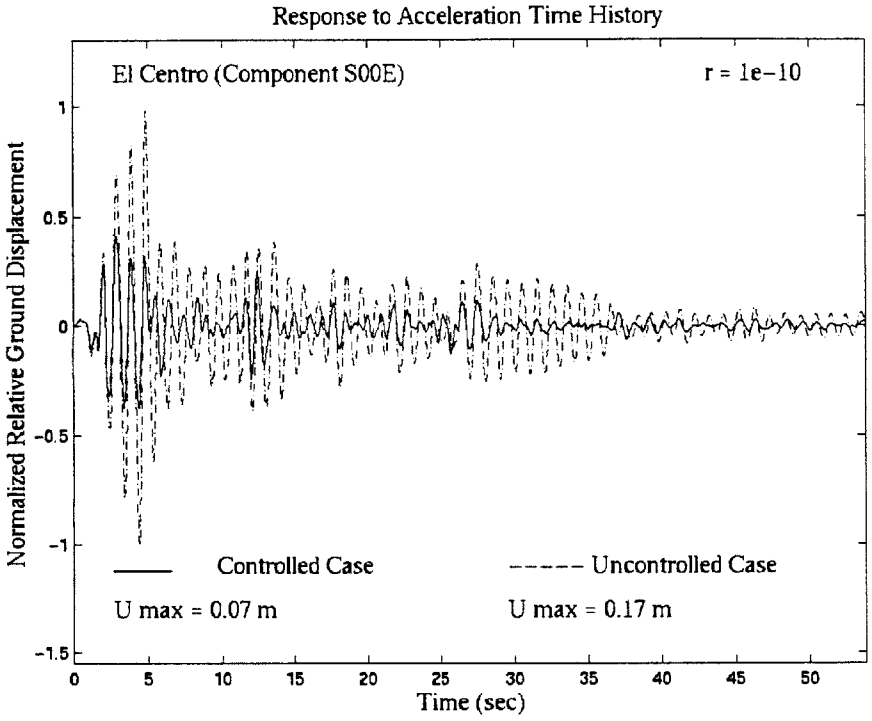

Figure D16 – Response to El Centro Time History, r = 1 x 10^{-10}

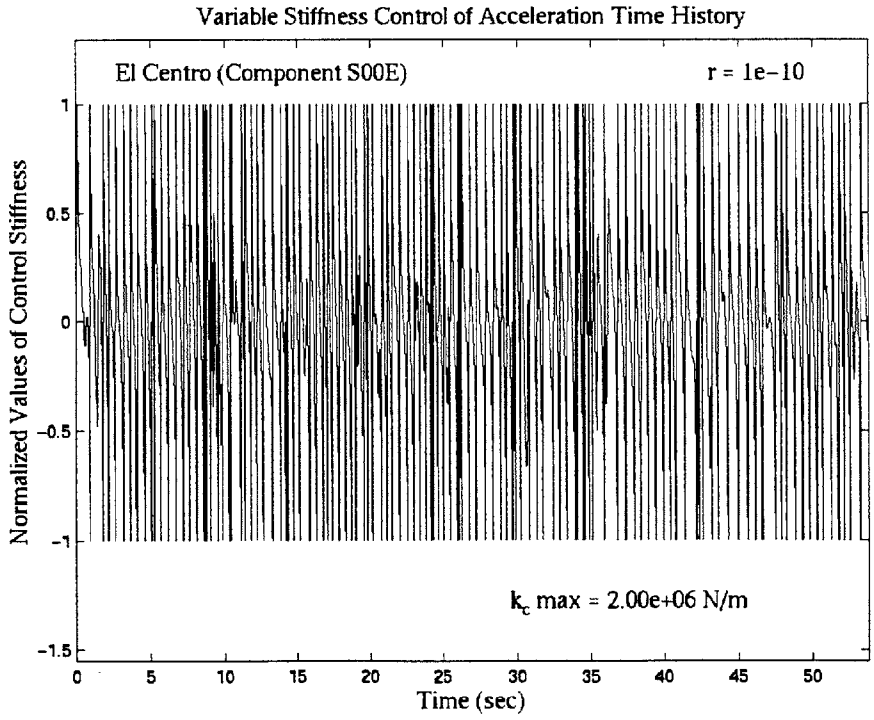

Figure D17 – Time History of Variable Stiffness for El Centro Excitation, r = 1 x 10^{-10}

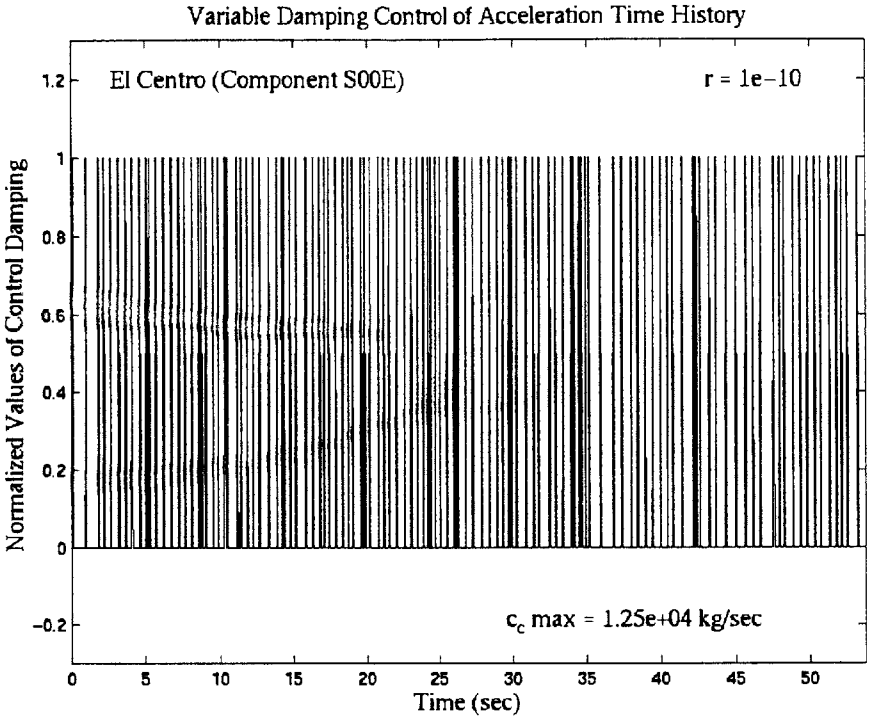

Figure D18 – Time History of Variable Damping for El Centro Excitation, r = 1 x10^{-10}

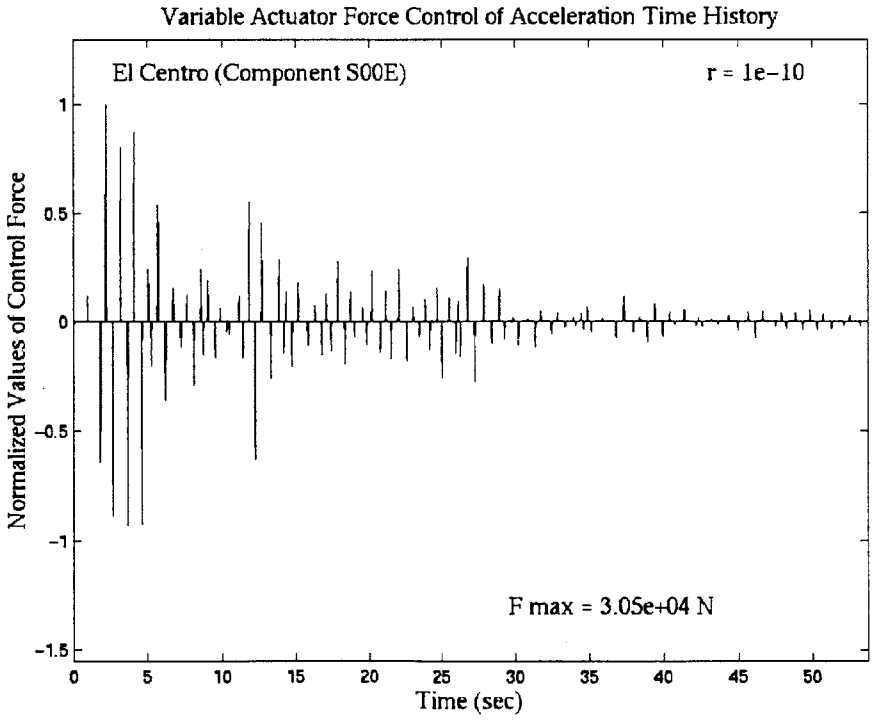

Figure D19 – Time History of Control Force for El Centro Excitation, r = 1 x10^{-10}

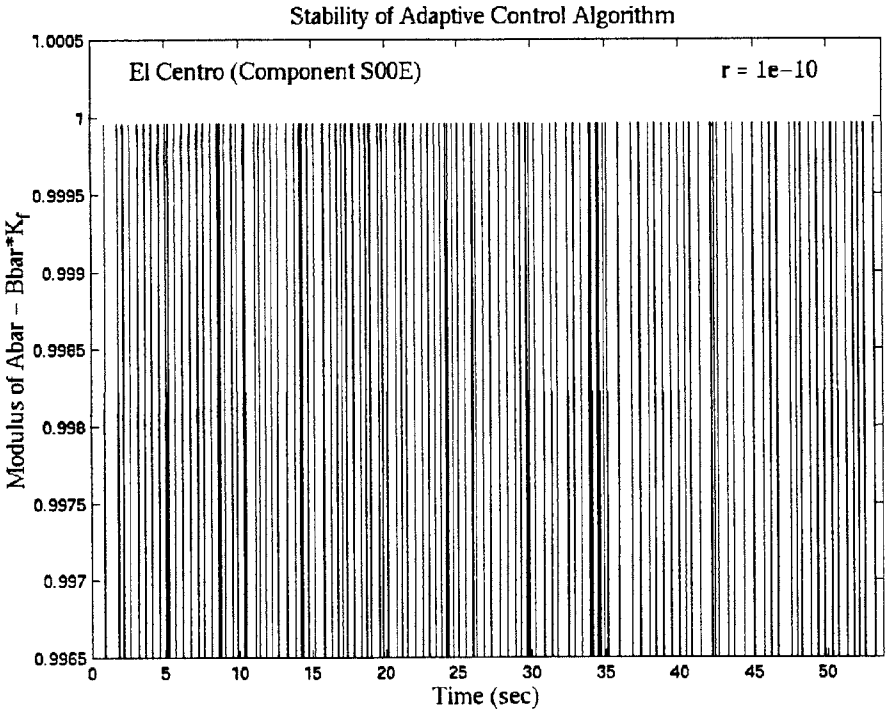

Figure D20 – Stability Check of Adaptive Control Algorithm for El Centro Excitation

Appendix E

Adaptive Control with Time Delay

```
%     Michael Cusack

%       var_damp_3b.m

%       input:                earthquake accleration time history
%       control alogrithm:    adaptive

%       Response Approximation Methods

%       controlled:     discrete time state equation
%       uncontrolled:   discrete time state equation (w/o control force)

% **********************  TIME DELAY EFFECTS  ****************************

syms i; syms m; syms c; syms delta_t; syms r; syms t; syms k;

m = 50000;              % (kg)     mass of structure
delta_t = 0.02;         % (sec)    time-step duration
r = 0;                  %           weighting/cost parameter
r_value = '\fontname{times}delay = 0.26 s';
filename = 'El_Centro_Comp_S00E';
quake_title = '\fontname{times}El Centro (Component S00E)';
fid = fopen(filename);                          % time history of acceleration
accel_data = fscanf(fid,'%g %g',[2 inf]); % values
accel_data = accel_data';                       %
fclose(fid);                                    %

num_trials = size(accel_data);
num_trials = num_trials(1) - 2;

Q = [0, 0; 0, 1];               %  weighting/cost parameter
R = r;                          %  weighting/cost parameter

U_i_c = [0; 0];             % initial conditions for controlled case
U_i_u = [0; 0];             % initial conditions for uncontrolled case

x=(0:num_trials)';                          % time step values
U_controlled = zeros(num_trials+1,1);       % controlled response values
U_uncontrolled = zeros(num_trials+1,1);     % uncontroled response values
F_control = zeros(num_trials+1,1);          % control force values
C_control = zeros(num_trials+1,1);      % viscous damping parameter values
K_control = zeros(num_trials+1,1);          % variable stiffness values
Modulus_1 =   zeros(num_trials+1,1);

% ***   Uncontrolled case   ****************************************** %

k_u = 2000000;              % (N/m)     initial stiffness of structure
c_u = 12500;                % (kg/s)    initial damping coefficient
w_n_u = (k_u/m)^(1/2);      % (rad/s)   initial natural frequency of
structure
zeta_u = c_u/(2*w_n_u*m);   %           initial damping fraction of
structure

A_u = [0, 1; -k_u/m, -c_u/m];    %  coefficient matrix
Abar_u = expm(A_u*delta_t);      % A_u integrated over time step
B = [0; 1/m];                                   % coefficient matrix
D = [0; 1/m];                                   % coefficient matrix
```

```
Bbar_u = eval(int(expm(A_u*t),t,0,delta_t)*B);
                                        % B integrated over time step
Dbar_u = eval(int(expm(A_u*t),t,0,delta_t)*D);
                                        % D integrated over time step

% ***   Adaptively controlled case - initial values   *************** %

k_c = 0;                    % (N/m)    variable stiffness of structure
c_c = 0;                    % (kg/s)   variable damping coefficient
k_t = k_c + k_u;            % (N/m)    total stiffness of structure
c_t = c_c + c_u;            % (kg/s)   total damping coefficient
w_n_c = (k_t/m)^(1/2);
                % (rad/s)  controlled  natural frequency of structure
zeta_c = c_t/(2*w_n_c*m);
                % controlled total damping fraction of structure

A_c = [0, 1; -k_t/m, -c_t/m];
Abar_c = expm(A_c*delta_t);  % A_c integrated over time step
Bbar_c = eval(int(expm(A_c*t),t,0,delta_t)*B);
                                          % B integrated over time step
Dbar_c = eval(int(expm(A_c*t),t,0,delta_t)*D);
                                          % D integrated over time step

% ********************************************************************** %

num_delays = 2;
time_delay = num_delays*delta_t;
F_control_i1 = zeros(num_delays,1);

for i = 0 : 1 : num_trials
      i
      time = i*delta_t;
      a_ground_i = accel_data(i+1, 2);
      F_ground_i = -m*a_ground_i;

      % Uncontrolled case:

      U_i1_u = Abar_u*U_i_u + Dbar_u*F_ground_i;
      U_i_u = U_i1_u;

      % Adaptively controlled case:

      [X,L,G,RR] = dare(Abar_c, Bbar_c, Q, R);
      F_control_i1(num_delays) = -[0, G(2)]*U_i_c;
                                          %  control force at time i+1

      if(U_i_c(1) ~= 0)
        k_c = -F_control_i1(1) / U_i_c(1);
        else
        k_c = 0;
      end
      if(k_c > k_u)
        k_c = k_u;
      elseif(k_c < (-k_u))
        k_c = -0.9999*k_u;  %  k_c cannot be set exactly to -k_u because
      end                   %     it will lead to division by zero

      F_control_i1(1) = F_control_i1(1) + k_c*U_i_c(1);

      if(U_i_c(2) ~= 0)
        c_c = -F_control_i1(1) / U_i_c(2);
      else
        c_c = 0;
      end
```

```
      if(c_c > c_u)
        c_c = c_u;
      elseif(c_c < 0)
        c_c = 0;
      end

      F_actuator_i1 = F_control_i1(1) + c_c*U_i_c(2);

      k_t = k_c + k_u;
      w_n_c = (k_t/m)^(1/2);
      zeta_c = c_t/(2*w_n_c*m);

      A_c = [0, 1; -k_t/m, -c_t/m];

      Abar_c = [1 - k_t/(2*m)*delta_t^2, delta_t - c_t/(2*m)*delta_t^2;
               -k_t/m*delta_t - c_t*k_t/(2*m^2)*delta_t^2, 1 -
               c_t/m*delta_t - k_t/(2*m)*delta_t^2 +
               c_t^2/(2*m^2)*delta_t^2];

      Bbar_c = [delta_t^2/(2*m); delta_t/m - c_t*delta_t^2/(2*m^2)];

      Dbar_c = Bbar_c;

      U_i1_c = Abar_c*U_i_c + Bbar_c*F_actuator_i1 + Dbar_c*F_ground_i;
      U_i_c = U_i1_c;

      for j = 1 : 1 : num_delays-1
        F_control_i1(j) = F_control_i1(j+1);
      end

      x(i+1) = time;
      U_controlled(i+1) = U_i1_c(1);
      U_uncontrolled(i+1) = U_i1_u(1);
      F_control(i+1) = F_actuator_i1;
      C_control(i+1) = c_c;
      K_control(i+1) = k_c;

      control_eig = eig(Abar_c - Bbar_c*[0, G(2)]);
      real_c = real(control_eig);
      real_c = real_c(1);
      imag_c = imag(control_eig);
      imag_c = imag_c(1);
      modulus = (real_c^2 + imag_c^2)^(1/2);

        Modulus_1(i+1) = modulus;

end

% ********************************************************************** %

j = size(U_uncontrolled);
j = j(1) - 1;
U_max_u = 0;
U_max_c = 0;

for i = 1 : 1 : j
      if(abs(U_uncontrolled(i)) > U_max_u & U_uncontrolled(i) ~= Inf)
        U_max_u = abs(U_uncontrolled(i));
      end
      if(abs(U_controlled(i)) > U_max_c & U_controlled(i) ~= Inf)
        U_max_c = abs(U_controlled(i));
      end
end
```

```
for i = 1 : 1 : j
        U_controlled(i) = U_controlled(i) / U_max_u;
        U_uncontrolled(i) = U_uncontrolled(i) / U_max_u;
end


K_max = 0;

for i = 1 : 1 : j
        if(abs(K_control(i)) > K_max & K_control(i) ~= Inf)
        K_max = abs(K_control(i));
      end
end

for i = 1 : 1 : j
        K_control(i) = K_control(i) / K_max;
end

C_max = 0;

for i = 1 : 1 : j
        if(abs(C_control(i)) > C_max & C_control(i) ~= Inf)
        C_max = abs(C_control(i));
      end
end

for i = 1 : 1 : j
        C_control(i) = C_control(i) / C_max;
end

F_max = 0;

for i = 1 : 1 : j
        if(abs(F_control(i)) > F_max & F_control(i) ~= Inf)
        F_max = abs(F_control(i));
      end
end

for i = 1 : 1 : j
        F_control(i) = F_control(i) / F_max;
end

figure

whitebg('white');

plot(x, U_controlled, 'black',x, U_uncontrolled, '-.black');
xlabel('\fontname{times} Time (sec)','FontSize',14);
ylabel('\fontname{times}Normalized Relative Ground
Displacement','FontSize',14);
text(0.05*x(num_trials+1),1.15,quake_title,'FontSize',14);
text(0.8*x(num_trials+1),1.15,r_value,'FontSize',14);
text(0.05*x(num_trials+1),-1.06,'____','FontSize',14);
text(0.18*x(num_trials+1),-1.1,'\fontname{times}Controlled
Case','FontSize',14);
text(0.05*x(num_trials+1),-1.3,'\fontname{times}U max = 0.014
m','FontSize',14);
text(0.55*x(num_trials+1),-1.1,'\fontname{times}----- Uncontrolled
Case','FontSize',14);
text(0.55*x(num_trials+1),-1.3,'\fontname{times}U max = 0.007
m','FontSize',14);
title('\fontname{times}Response to Acceleration Time
History','FontSize',14);
```

```
axis([0 x(num_trials+1) -1.55 1.3]);

figure

plot(x, K_control,'black');
xlabel('\fontname{times}Time (sec)','FontSize',14);
ylabel('\fontname{times}Normalized Values of Control
Stiffness','FontSize',14);
text(0.05*x(num_trials+1),1.15,quake_title,'FontSize',14);
text(0.8*x(num_trials+1),1.15,r_value,'FontSize',14);
text(0.55*x(num_trials+1),-1.3,'\fontname{times}k_c max = 2.00e+06
N/m','FontSize',14);
title('\fontname{times}Variable Stiffness Control of Acceleration Time
History','FontSize',14);
axis([0 x(num_trials+1) -1.55 1.3]);

figure

plot(x, C_control,'black');
xlabel('\fontname{times}Time (sec)','FontSize',14);
ylabel('\fontname{times}Normalized Values of Control
Damping','FontSize',14);
text(0.05*x(num_trials+1),1.2,quake_title,'FontSize',14);
text(0.8*x(num_trials+1),1.2,r_value,'FontSize',14);
text(0.55*x(num_trials+1),-0.2,'\fontname{times}c_c max = 1.25e+04
kg/sec','FontSize',14);
title('\fontname{times}Variable Damping Control of Acceleration Time
History','FontSize',14);
axis([0 x(num_trials+1) -0.3 1.3]);

figure

plot(x, F_control,'black');
xlabel('\fontname{times}Time (sec)','FontSize',14);
ylabel('\fontname{times}Normalized Values of Control
Force','FontSize',14);
text(0.05*x(num_trials+1),1.15,quake_title,'FontSize',14);
text(0.8*x(num_trials+1),1.15,r_value,'FontSize',14);
text(0.55*x(num_trials+1),-1.3,'\fontname{times}F max = 1.65e+04
N','FontSize',14);
title('\fontname{times}Variable Actuator Force Control of Acceleration
Time History','FontSize',14);
axis([0 x(num_trials+1) -1.55 1.3]);

figure

plot(x, Modulus_1,'black');
```

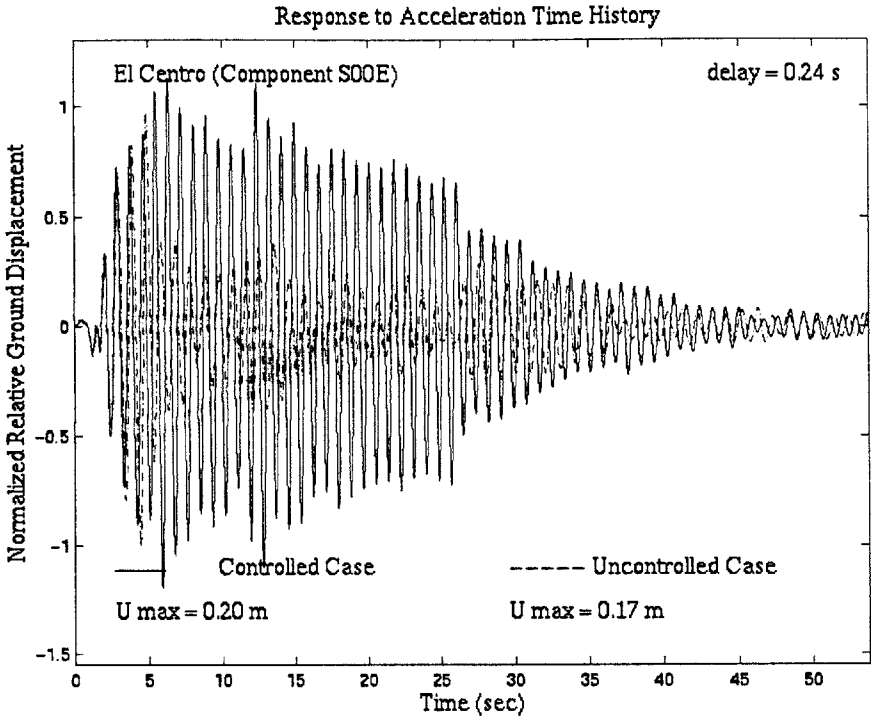

Figure E1 – Response to El Centro Time History, $t_d = 0.24$ sec

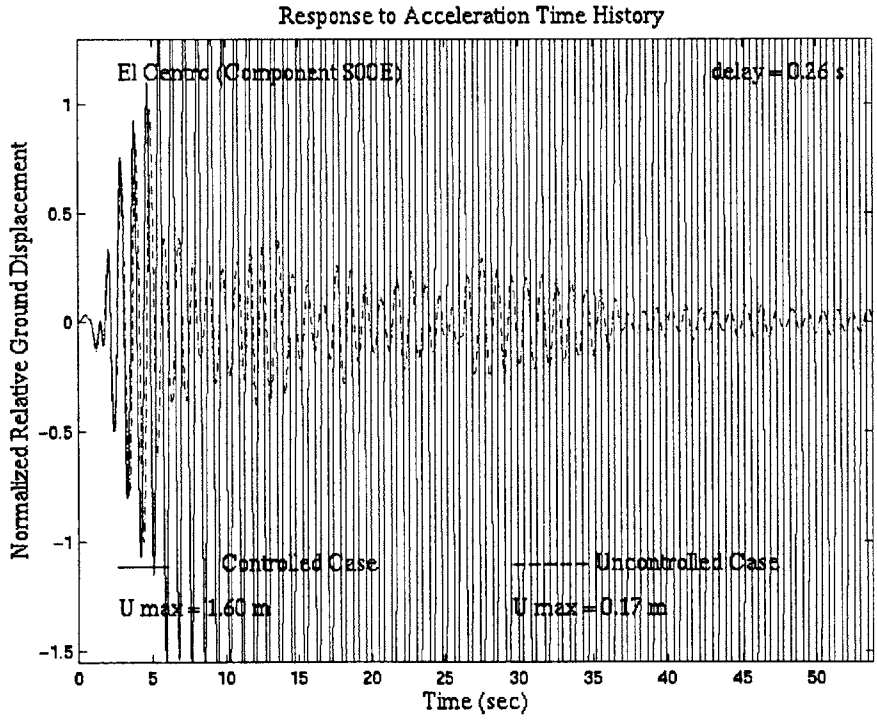

Figure E2 – Response to El Centro Time History, $t_d = 0.26$ sec

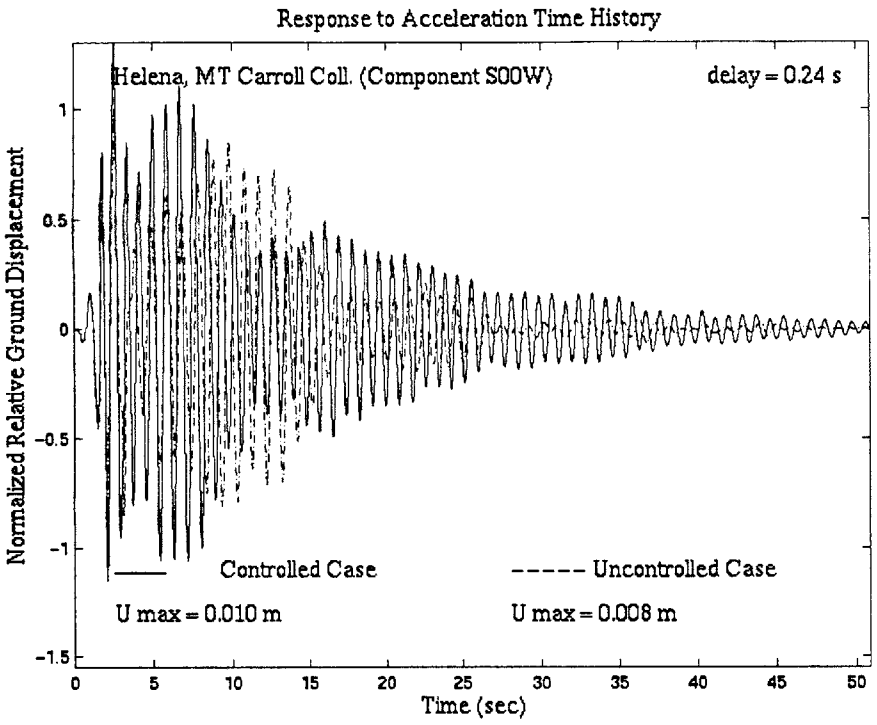

Figure E3 – Response to Helena, MT Carroll College Time History, $t_d = 0.24$ sec

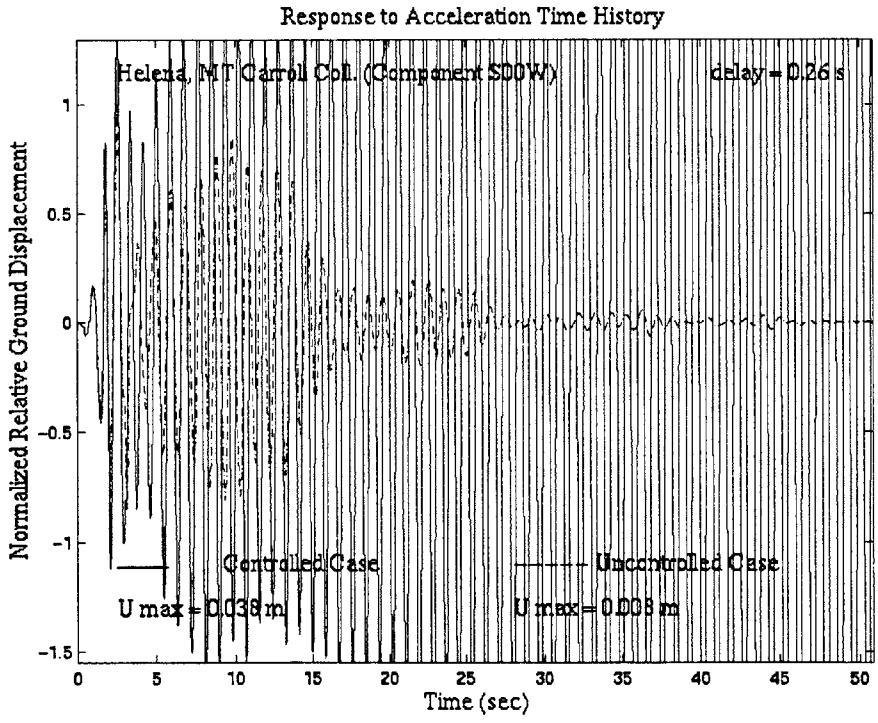

Figure E4 – Response to Helena, MT Carroll College Time History, $t_d = 0.26$ sec

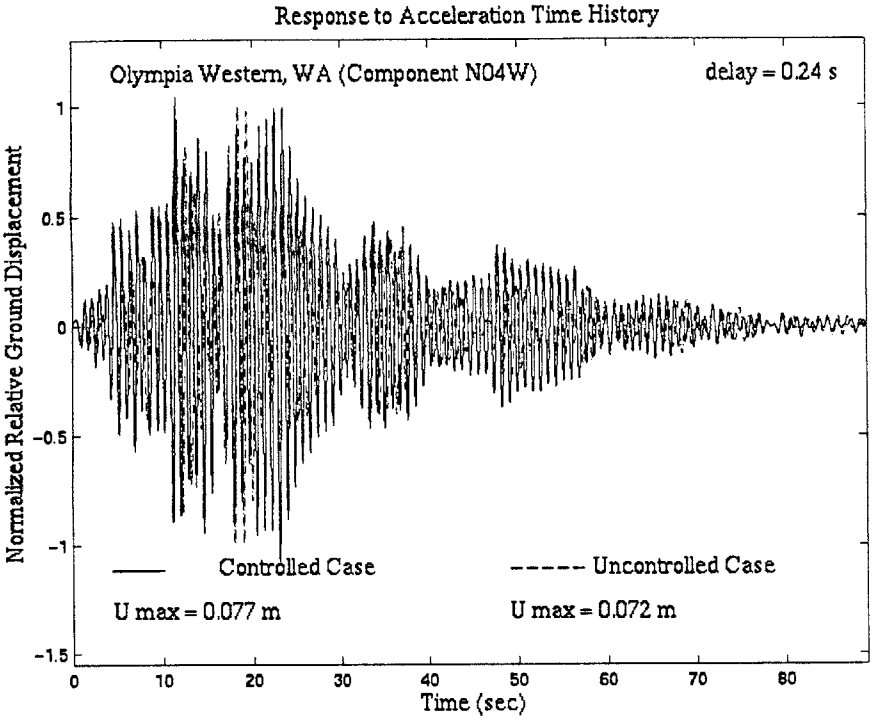

Figure E5 – Response to Olympia Western, WA Time History, t_d = 0.24 sec

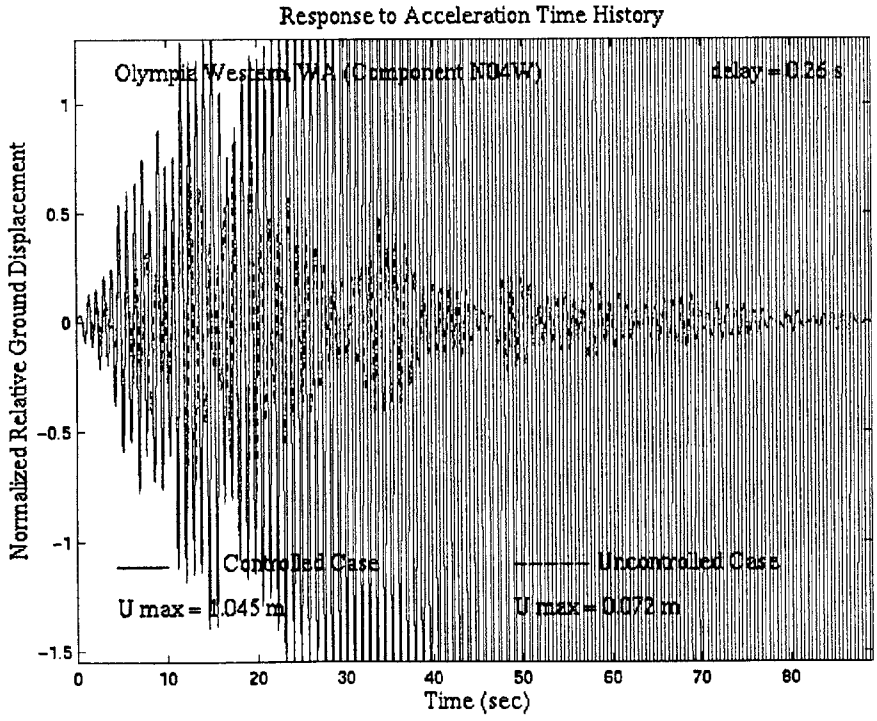

Figure E6 – Response to Olympia Western, WA Time History, t_d = 0.26 sec

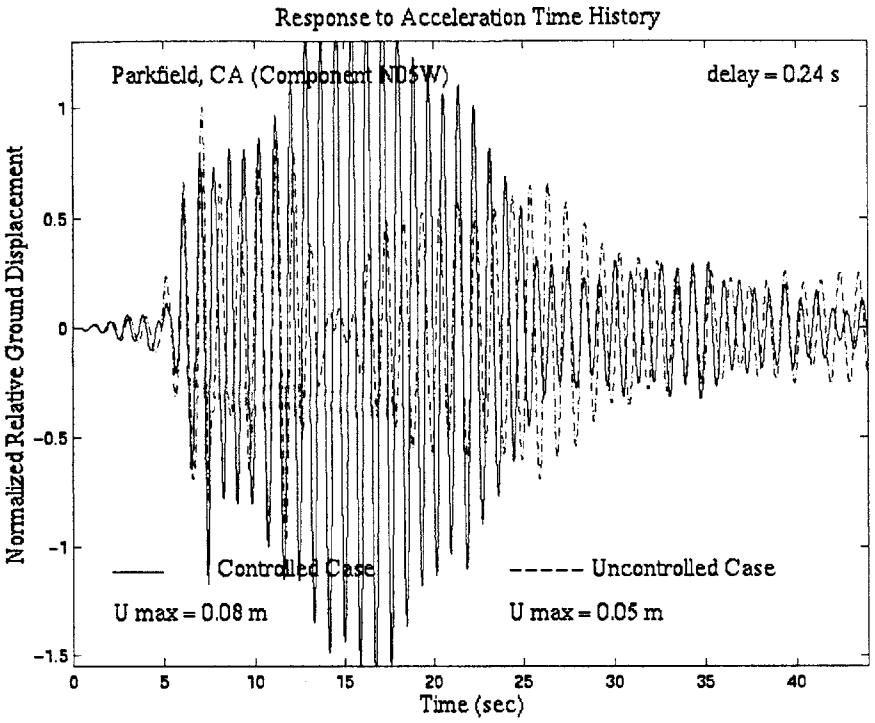

Figure E7 – Response to Parkfield, CA Time History, $t_d = 0.24$ sec

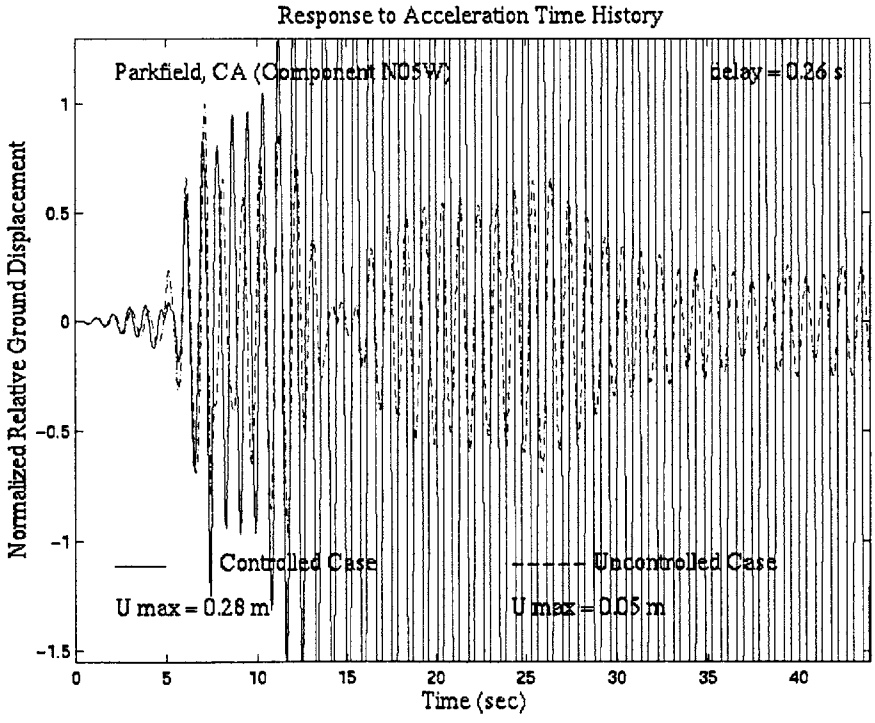

Figure E8 – Response to Parkfield, CA Time History, $t_d = 0.26$ sec

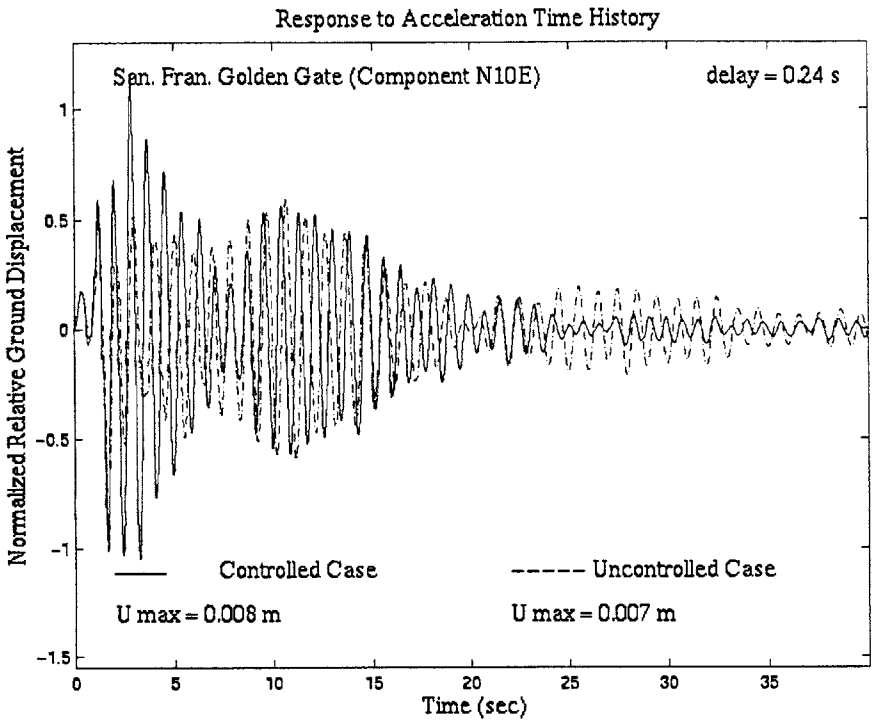

Figure E9 – Response to San Francisco Golden Gate Time History, $t_d = 0.24$ sec

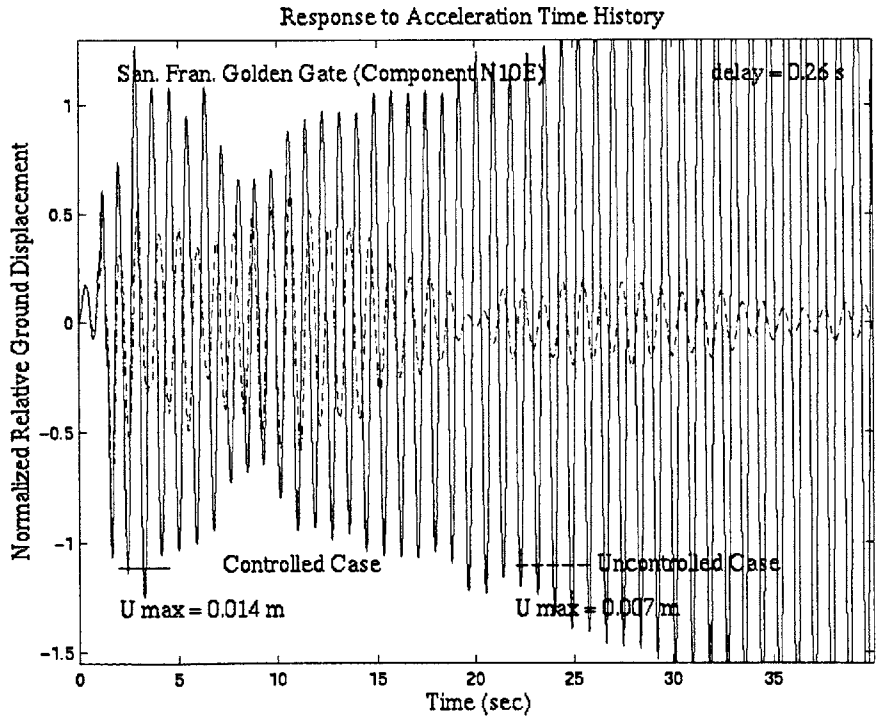

Figure E10 – Response to San Francisco Golden Gate Time History, $t_d = 0.26$ sec

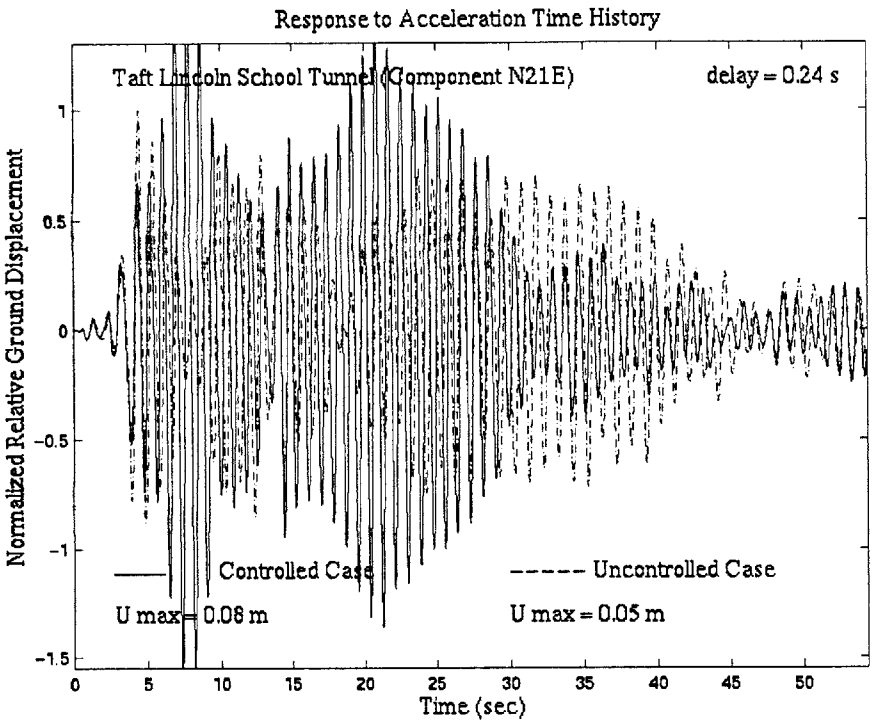

Figure E11 – Response to Taft Lincoln School Tunnel Time History, $t_d = 0.24$ sec

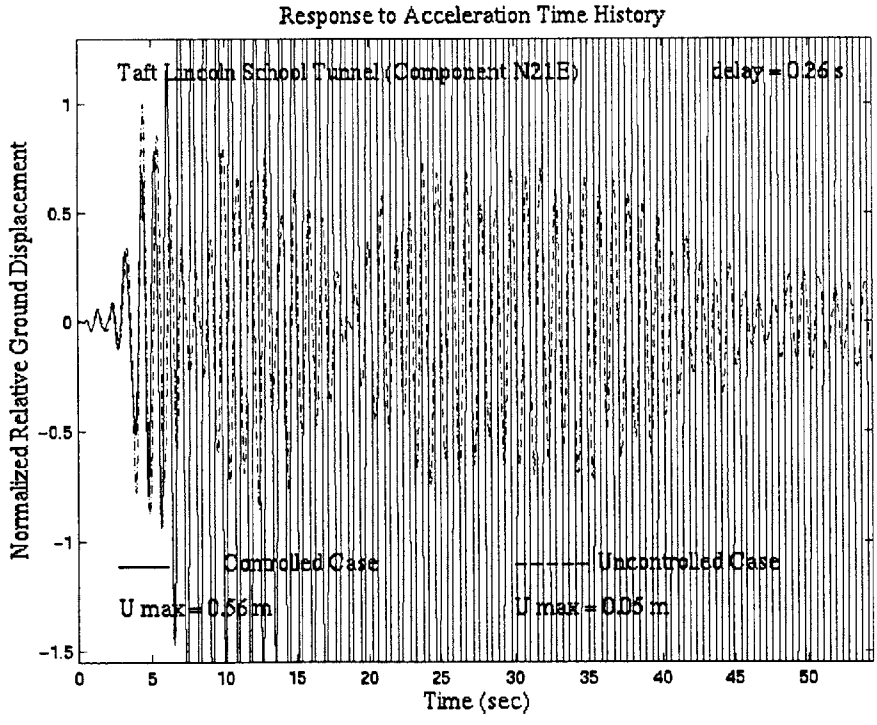

Figure E12 – Response to Taft Lincoln School Tunnel Time History, $t_d = 0.26$ sec

Appendix F

System Parameter Effects on Maximum Allowable Time Delay

```
%       Michael Cusack

%       test1.m

syms t;

m = 50000;
k = 2000000;
c = 12500;
delta_t = 0.02;
r = 1e-09;

delta_t = 0.002*i;

A = [0, 1; -k/m, -c/m];
B = [0; 1/m];
Abar = expm(A*delta_t);
Bbar = eval(int(expm(A*t),t,0,delta_t)*B);
Abar_tr = Abar';

[V,D] = eig(Abar);
[W,D] = eig(Abar_tr);

Q = [0, 0; 0, 1];
R = r;

[X,L,G,RR] = dare(Abar, Bbar, Q, R);
K_f = [0, G(2)];

lambda_1 = D(1,1);
W_1 = [(W(1,2)); (W(2,2))]/W(1,2);
V_1 = [(V(1,2)); (V(2,2))]/V(1,2);

g_zz = W_1'*Bbar*K_f*V_1;
g_zz= real(g_zz);
lambda_real = real(lambda_1);
lambda_imag = imag(lambda_1);

K = (lambda_real^2 + lambda_imag^2 + g_zz^2 - 1)/(2*g_zz);

v_theta = 2*atan((-lambda_imag + (lambda_imag^2 - (K^2 - ...
                              lambda_real^2))^(1/2))/(K + lambda_real));

cos_theta = lambda_real - g_zz*cos(v_theta);
sin_theta = lambda_imag + g_zz*sin(v_theta);

rho = (cos_theta^2 + sin_theta^2)^(1/2);
theta = acos(cos_theta);
v = v_theta / theta;
```

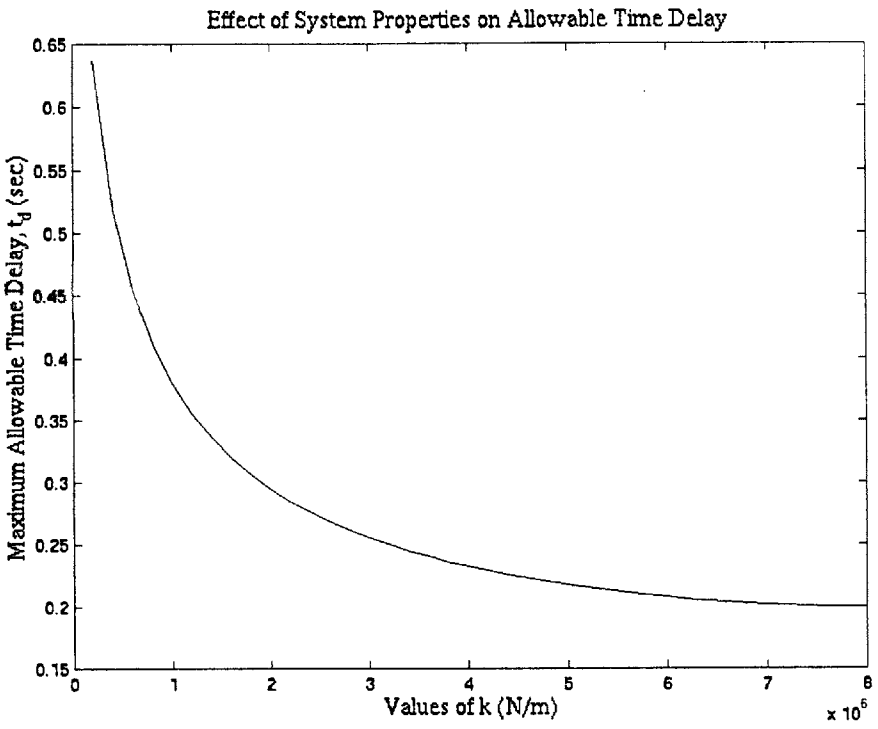

Figure F1 – Change in Maximum Allowable Time Delay with Varying Stiffness

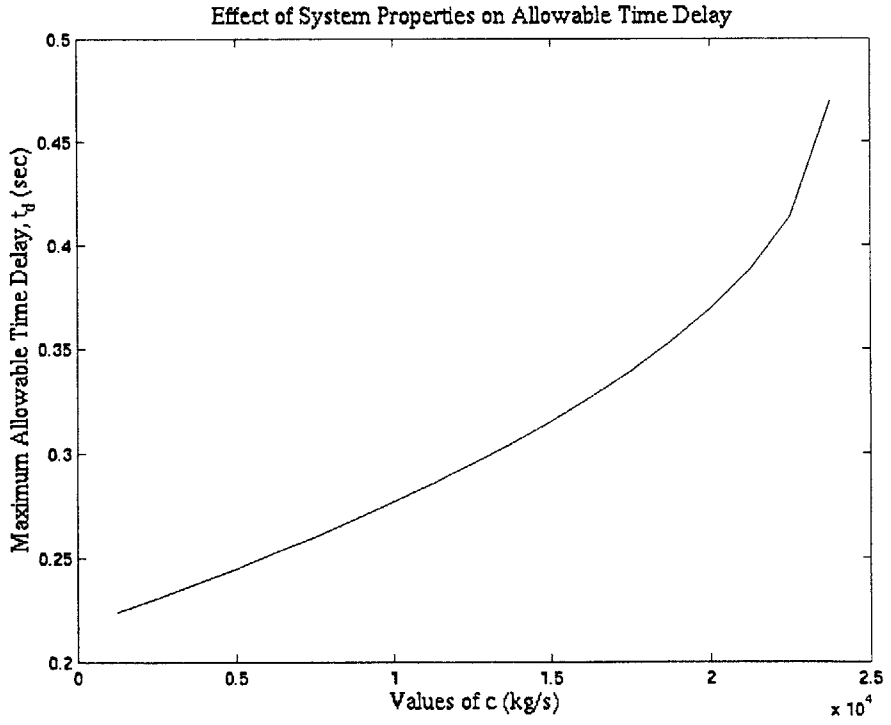

Figure F2 – Change in Maximum Allowable Time Delay with Varying Damping

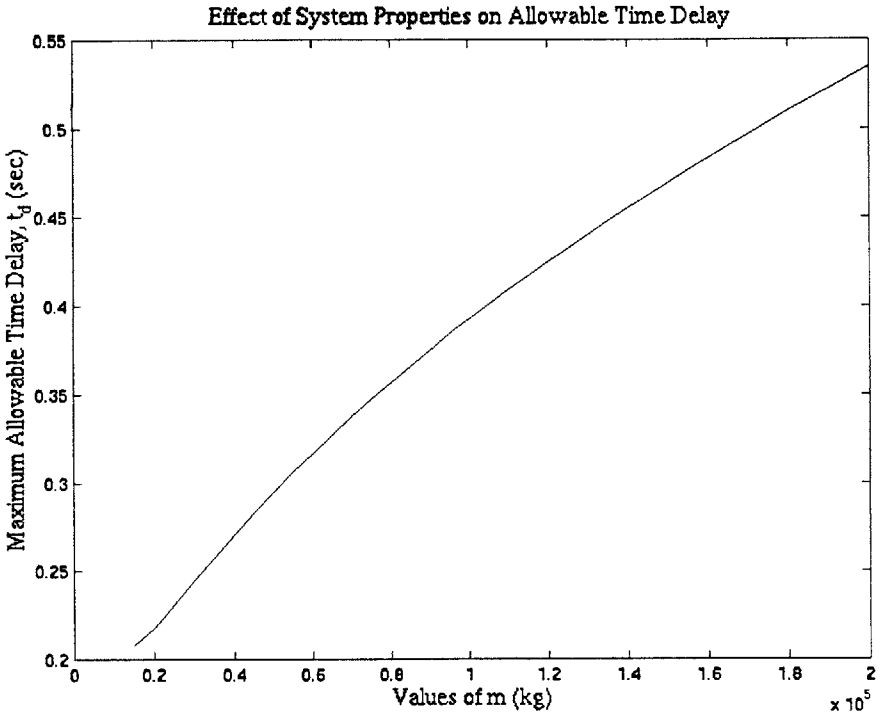

Figure F3 – Change in Maximum Allowable Time Delay with Varying Mass

References

[1] J. Fujie. (1989). Current Status of Maglev Transportation Systems in the World. *11th International Conference on Maglev Technology*, pp. 9-17.

[2] S. Yamamura and H. Yamaguchi. Electromagnetic Levitation System by Means of Salient-Pole Type Magnets Coupled with Laminated Slotless Rails. *1986 IEEE International Conference on Maglev & Linear Drives*, pp. 229-230.

[3] K. Sawada. (July 1996). Development of Magnetically Levitated High Speed Transport System in Japan. *IEEE Transactions on Magnetics*, Vol. 32, No. 4, pp. 2230-2235.

[4] G. R. Slemon. The Canadian MAGLEV Project. In E.R. Laithwaite, editor, *Transport Without Wheels*. Elek Science, London, 1977.

[5] Y. Kyotani. (1988). Recent Progress by JNR on Maglev. *IEEE Transactions on Magnetics*, Vol. 24, No. 2, pp. 804-807.

[6] Maglev Systems Development Department Home Page, http://www.rtri.or.jp/rd/maglev/html/english/maglev_frame_E.html, 2 July 1999.

[7] H. Nakashima. (July 1994). The Superconducting Magnet for the Maglev Transport System. *IEEE Transactions on Magnetics*, Vol. 30, No. 4, pp. 1572-1578.

[8] L. Dye. (2 June 1999). Research gives lift to 'maglev': Team's breakthrough may help get technology on track. *Boston Globe*.

[9] N. Kurata, T. Kobori, M. Takahashi, N. Niwa & H. Kurino. (1994). Shaking Table Experiment of Active Variable Damping System. *Proceedings of the First World Conference on Structural Control*, Los Angeles, California.

[10] J. Connor and B. Klink. Introduction to Structural Motion Control.

[11] M. Yamamoto and S. Aizawa. (1994). Control Effects of Active Mass Damper System Installed on Actual Buildings. *Proceedings of the First World Conference on Structural Control*, Los Angeles, California.

[12] M. Sakamoto, T. Kobori, T. Yamada & M. Takahashi. (1994). Practical Applications of Active and Hybrid Response Control Systems and Their Verifications by Earthquake and Strong Wind Observations. *Proceedings of the First World Conference on Structural Control*, Los Angeles, California.

[13] 1-561 Home Page, http://moment.mit.edu/documentLibrary/Duox/doux.html, 2 July 1999.

[14] Y. Koike, T. Murata, K. Tanida, M. Mutaguchi, T. Kobori, K. Ishii, Y. Takenaka & T. Arita. (1994). Development of V-Shaped Hybrid Mass Damper and Its Application to High-Rise Buildings. *Proceedings of the First World Conference on Structural Control*, Los Angeles, California.

[15] T. Kobori, M. Takahashi, T. Nasu and N. Niwa. (1993). Seismic Response Controlled Structure with Active Variable Stiffness System. *Earthquake Engineering and Structural Dynamics*. Vol. 22, pp. 925-941.

[16] M. Takahashi, T. Kobori, T. Nasu, N. Niwa & N. Kurata. (1998). Active Response Control of Buildings for Large Earthquakes- Seismic Response Control System with Variable Structural Characteristics. *Smart Mater. Struct.* **7**, pp. 522-529.

[17] F. Gordaninejad, A. Ray and R. Bindu. Vibration Control of Structures Using Hybrid ER/Viscous Fluid Dampers. *Proceedings of the First World Conference on Structural Control*, Los Angeles, California.

[18] Rheonetic Systems, http://www.mrfluid.com/technology.html, 2 July 1999.

[19] B. F. Spencer Jr., G. Yang, J. D. Carlson and M.K. Sain. (1998). "Smart" Dampers for Seismic Protection of Structures: A Full-Scale Study. *Second World Conference on Structural Control*, Kyoto, Japan. Proceedings, in press.

[20] S.J. Dyke, B.F. Spencer Jr., M.K. Sain and J.D. Carlson. An Experimental Study of MR Dampers for Seismic Protection. *Smart Materials and Structures: Special Issue on Large Civil Structures*. In print.